Laporan Akhir Projek Penyelidikan Jangka Pendek

Development of SN-9ZN-Based Solder Alloy With High Corrosion Resistance to Alkaline Electrolyte

by
Assoc. Prof. Dr. Ahmad Azmin Mohamad
Dr. Projjal Basu

2012

UNIVERSITI SAINS MALAYSIA

Final Report

For Research University (Individual) Grant

Development of Sn-9zn-Based Solder Alloy with High Corrosion Resistance to Alkaline Electrolyte

by

Assoc. Prof. Dr. Ahmad Azmin Mohamad

Muhammad Firdaus Mohd Nazeri

Muhammad Ghaddafy Affendy

Contents

List of publications

1. Muhammad Firdaus Mohd Nazeri, Muhammad Ghaddafy Affendy and Ahmad Azmin Mohamad, Corrosion study of Sn-9Zn lead free solder in 6 M KOH electrolytes, Int. J. Electrochem. Sci., 7 (2012) 4182 – 4191.
2. Muhammad Firdaus Mohd Nazeri and Ahmad Azmin Mohamad, Polarisation study of Sn-9Zn lead free solders in 6 M KOH electrolyte, Journal of Electronic Materials, revision 2013.
3. Muhammad Firdaus Mohd Nazeri and Ahmad Azmin Mohamad, Effect of Zn content on the corrosion properties of Sn-Zn lead-free solders in 6 M KOH solution, Submitted to Metall. Mater. Trans. A, 2013.
4. Muhammad Firdaus Mohd Nazeri and Ahmad Azmin Mohamad, Effect of In additions to the corrosion properties of Sn-9Zn solder in 6 M KOH, in manuscript 2013.
5. Muhammad Firdaus Mohd Nazeri and Ahmad Azmin Mohamad, Cross-sectional characterizations of Sn-9Zn solder after polarization in 6 M KOH, In manuscript 2013.
6. Liu Mei Lee, Habsah Haliman and Ahmad Azmin Mohamad, Interfacial reaction of Sn-3.0Ag-0.5Cu thin film during solder reflowing, Soldering & Surface Mount Technology, 2013, in press.
7. Liu Mei Lee, Habsah Haliman and Ahmad Azmin Mohamad, Corrosion of Sn3.0Ag0.5Cu Thin Film in 6 M Potassium Hydroxide Solution, Submitted to Soldering & Surface Mount Technology, 2013.
8. Liu Mei Lee and Ahmad Azmin Mohamad, Interfacial Reaction of Sn-Ag-Cu Lead-Free Solder Alloy on Cu: A Review, Advances in Materials Science and Engineering, revision 2013.

9. Liu Mei Lee and Ahmad Azmin Mohamad, Corrosion Characterization of Sn-Ag-Cu Lead-free Solder Alloy in Corrosive Solutions: A Review, in manuscript.
10. Muhammad Ghaddafy Affendy and Ahmad Azmin Mohamad, Effect of corrosion on the shear strength of Cu/Sn-9Zn/Cu lap joints in 3.5 wt. % NaCl solution, Int. J. Electrochem. Sci., 7 (2012) 4951 – 4958.
11. Muhammad Ghaddafy Affendy and Ahmad Azmin Mohamad, Corrosion and mechanical studies of Cu/Sn-9Zn/Cu lap joints in 3.5 wt. % NaCl solution, in manuscript 2013.
12. Muhammad Ghaddafy Affendy and Ahmad Azmin Mohamad, Effect of crosshead speed on the shear strength of Cu/Sn-9Zn/Cu lap joints, 2013, in manuscript.
13. Mui Chee Liew, Ibrahym Ahmad, Liu Mei Lee, Muhammad Firdaus Mohd Nazeri, Habsah Haliman and Ahmad Azmin Mohamad, Corrosion behavior of Sn-3.0Ag-0.5Cu lead free solder in potassium hydroxide electrolyte, Metall. Mater. Trans. A, 43 (2012) 3742-3747.
14. Kausar Harun and Ahmad Azmin Mohamad, Effect of Corrosion on Tensile Properties of Cu/SAC/Cu butt joints, 2013, in manuscript 2013.

Chapter 1: Introduction

1.1 Introduction

Global electronic industries have widely utilized the lead-bearing solder. The use has had a long history due to the good combination of cost, excellent properties, and ease of processing. Since then, the technology of soldering using the lead-bearing solder, especially the tin-lead (Sn-Pb) alloy, has reached its level of maturity and can be considered as fully developed. Among the well-known Sn-Pb alloys are the eutectic Sn-37Pb and the near eutectic Sn-40Pb [1-2, 6-8].

However, in the past decade, health concerns especially in relation to the toxicity of materials have emerged. The Environmental Protection Agency (EPA) has cited lead (Pb) and lead compounds to be 2 of the top 17 chemicals that pose the greatest threat to humans and the environment. In the electronics industry, occupational exposure to Pb waste as derived from the manufacturing process has been cited. The possible inhalation of Pb vapors or dust during soldering operations can cause health and environmental problems. This resulted to the banning of lead-containing solders in all applications [1-2, 6-8].

As a result, the search for the new lead-free solder has become a major issue because there are strict performance requirements that should be fulfilled by new solder alloys in order to fully replace the Sn-Pb alloy. Among these requirements are as follows: (1) the alloys must meet the expected levels of electrical and mechanical performance, and (2) they must have the desired melting point. However, the most important criterion is the assurance that the replacement solder is comparable to or better than Sn-Pb alloys [1-2].

A vast number of lead-free solder alloys have been proposed so far, and among them, tin-based solders such as tin-zinc (Sn-Zn), and tin-silver-copper (Sn-Ag-Cu; SAC) have been

extensively studied [1]. Most of these alloys have been used as "drop-in" replacements for Sn-Pb alloys and have been employed for special applications [1]. The acceptable melting points of these solders appear to be an attractive option for many researchers [2, 6-7, 9-12, 14-15, 33-38]. These solders also considered as of one of the promising candidates as a replacement for Sn-Pb solder because its combination of low cost and good mechanical properties closely resembles the good characteristics of the eutectic Sn-Pb solder [6-7].

1.2 Problem Statement

A solder serves as a die-bonding material that provides the electrical and mechanical connection in an electronic circuit. The range of solder applications is very wide, comprising of high-end electronic products such as integrated circuits of computers and cell phones, to simpler electrical devices such as calculator and toys. The selection of the solder as a joining material is based on its high input-output signal that allows a high number of terminals to be made at a given area, as well as its ease of application [1].

In small electronic devices, batteries are used to supply the power. Alkaline-based batteries use potassium hydroxide (KOH) as the electrolyte. Normally, 6 M KOH is utilized as the electrolyte due to its high ionic conductivity that allows for better transfer of charges [23-28]. However, KOH is a very corrosive electrolyte [21-22]. For a battery with poor or defective packaging which leads to cracks during high pressure operation, the electrolyte will leak and wet the circuit board.

If the Sn-9Zn and SAC solders are used in the circuit, there is always a possibility that this corrosive electrolyte will damage the solder or the joining material in the circuit. The

corrosive attack of KOH on the solder can cause the deterioration of the solder, resulting in the loss of mechanical integrity and thus operation failure. As a result, the solder will not function properly. Furthermore, the existence of the electrolyte on the circuit board will induce short-circuiting that may interfere with the functionality of the electronic device. To date, the corrosion properties of Sn-9Zn and SAC in alkaline-based batteries electrolyte have not been studied yet.

1.3 Project Objectives

This work has three objectives:

- To investigate the effect of potassium hydroxide (KOH) solution to the corrosion properties of Sn-9Zn and SAC lead-free solder;
- To study the effect 6 M KOH solution to the corrosion properties of SAC thin film; and
- To investigate the effect 6 M KOH solution to the corrosion properties of bulk SAC solder

Chapter 2: Literature Review

2.1 Interfacial Reaction of Sn-Ag-Cu Lead-Free Solder Alloy on Cu: A Review

2.2 Introduction

Among various alloy systems that are considered as lead-free solder candidates, Sn-Ag-Cu alloys have been recognized as the most promising because of their relatively low melting temperature (compared with the Sn-Ag binary eutectic lead free solder), superior mechanical properties, and good compatibility with other components [1-3]. Sn-Ag-Cu alloys are widely used as lead-free solutions for ball-grid-array (BGA) interconnection in the microelectronic packaging industry as solder balls and pastes [4].

Among bumping materials, a family of solder alloys based on the ternary Sn-Ag-Cu eutectic (217 °C) composition has the most potential for broad use in the industry [5]. The eutectic composition is favorable to be chosen because it behaves as an independent homogenous phase and has a unique metallographic structure and a distinct melting point [6]. Sn-Ag-Cu solders can promote enhanced joint strength as well as creep and thermal fatigue resistance, and can permit increased operating temperatures for the fabrication of advanced electronic systems and devices [7, 8]. The International Printed Circuit Association has suggested that 96.5Sn–3.0Ag–0.5Cu (SAC305) and Sn–3.9Ag–0.6Cu (two near-eutectic alloys) will be the most widely used alloys in the future [7]. This prediction is attributed to their good mechanical properties, acceptable wetting properties, and suitable melting points [2, 3, 9-11].

Lead-free solder joints have been reported to have fine and stable microstructures because of the formation of small-dispersed particles. Thus, these joints have higher shear strengths [12, 13]. Sn-Ag-Cu solders require a higher reflow temperature because of its higher

melting point. For instance, the melting point of Sn-3.8Ag-0.7Cu is 219 °C, and that of SAC305 is 217 °C. The high melting temperature not only requires a new reflow profile, but also increases the component stability concerns that accompany a higher temperature. Several components may not survive at a high reflow temperature.

2.3 Lead free solder and its applications

Soldering is a well-recognized metallurgical joining method to bond solder to as a base material (usually metal) at a melting point below 425 °C [14]. Let us take **Figure 1** as an example. During the soldering process, the SAC305 solder wire (**Figure 1a**) melts and gets into contact with Cu substrate base metal (**Figure 1b**). Moreover, the Sn in the molten solder reacts with Cu to form intermetallic compound (IMC) on the interface. It is this IMC layer that bonds the solder and Cu together [15-20].

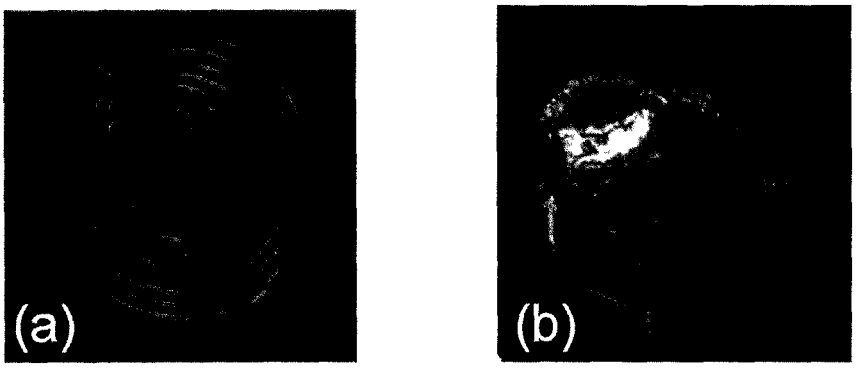

Figure 1: Appearance change of (a) a coiled SAC305 solder wire into (b) a solid SAC305 solder on the Cu substrate during solder reflowing.

Generally, the soldering process is portrayed in **Figure 2**. The soldering process can be divided into three stages [21]:

(a) spreading,

(b) base metal dissolution, and

(c) formation of an IMC layer.

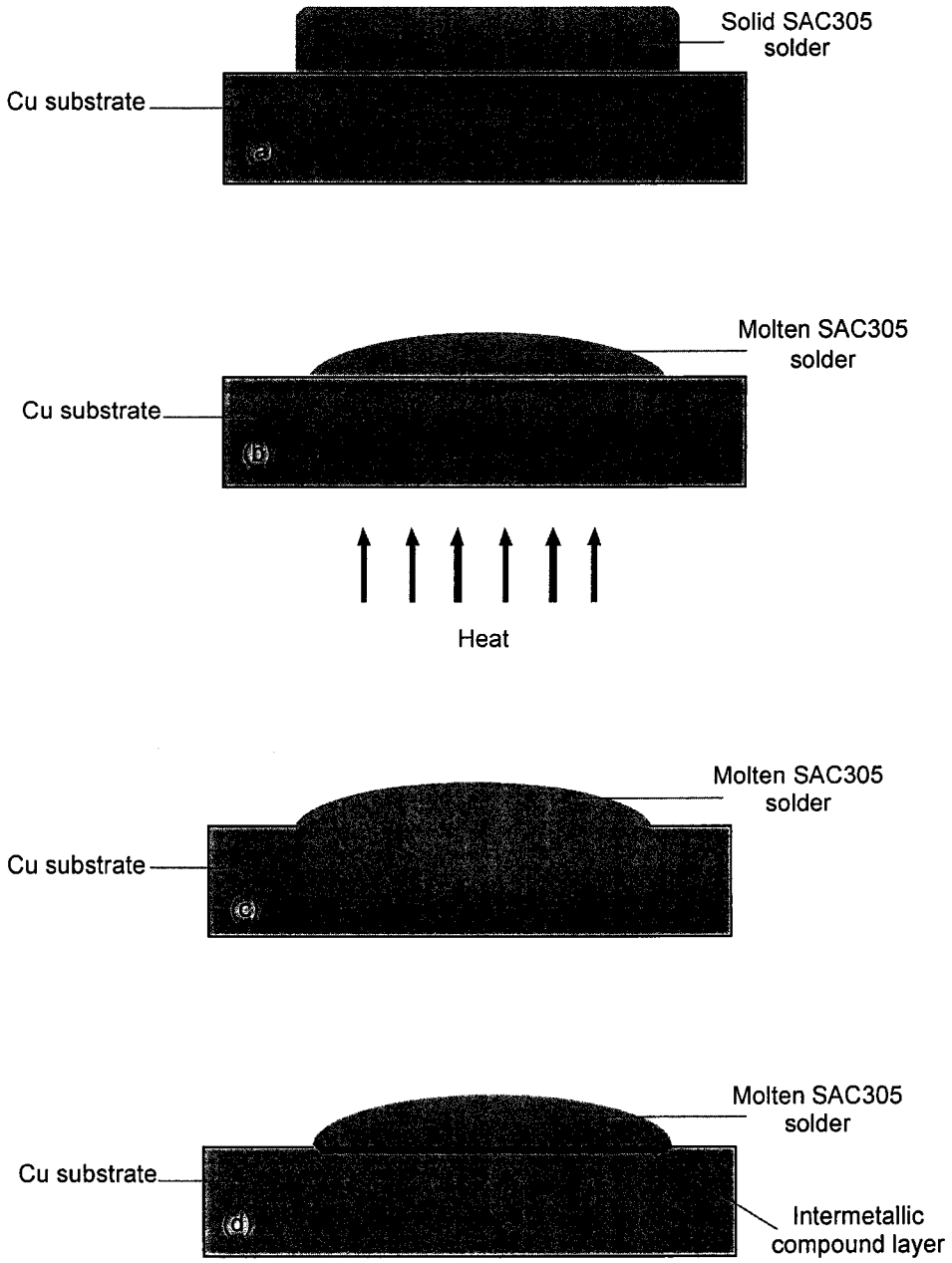

Figure 2: Solder wetting process: (a) SAC305 solder on the Cu substrate, (b) liquid solder spreading over the Cu substrate during soldering, (c) Cu diffuse in the liquid solder, and (d) Cu reacting with the liquid solder to form an intermetallic compound layer.

The Cu substrate did not melt or change its microstructure during soldering. The liquid phase then transformed to various solid phases when the joints were cooled down. The different kinds and relative amounts of the solid phases formed during solidification are important for solder joint properties.

Solders are usually low melting point alloys because soldering is conducted when the solders are completely molten [22]. The products are used at their solid phases at relatively high operation temperatures. Hence, diffusivity is an important property for most solders. In addition, good wetting is required for good solders; thus, interfacial reactions with substrates are usually important not only at the liquid/solid contacts, but also at the solid/solid contacts at high operation temperatures [22].

The solder joint strength is controlled by the land pattern design and a good metallurgical bond between the component and the board. A reliable solder connection must have a solderable surface to form a good metallurgical bond between the solder and the components being joined. Interfacial reactions at the solder joints are key factors in the fabrication of electronic products.

2.4 Intermetallic Compound of Sn-Ag-Cu Solders with Cu Substrate

In electronic products, all common base materials, coatings, and metallizations, such as Cu, Ni, Ag, Ag–Pd, and Au, form IMCs with Sn. Therefore, chemical reactions occur between solders and conductor metals during soldering (i.e., component metallizations, board surface finishes, and underlying conductors), and IMCs nucleate and grow at the solder/conductor interfaces.

The presence of IMCs between solders and conductor metals is desirable because it results in good metallurgical bonding. A thin, continuous, and uniform IMC layer is an essential

requirement for good bonding. Without IMCs, the solder/conductor joint is weak because no metallurgical interaction occurs in the bonding, which is disastrous to electronic packaging. However, a thick IMC layer at the solder/conductor metal interface may degrade the reliability of the solder joints because of their inherent brittle nature and their tendency to generate structural defects caused by mismatches of the physical properties (such as elastic modulus and coefficient of thermal expansion) [23]. A thick IMC layer should be avoided during the process. Thus, knowledge of the solder/conductor metal interactions and phase evolution in the solder interconnections is important to understand the reliability of solder interconnections from a metallurgical viewpoint and to optimize the soldering process [17].

The intermetallic reaction layers are formed in three consecutive stages [17]:

(a) dissolution,

(b) chemical reaction, and

(c) solidification.

During the soldering of the Sn-Ag-Cu solder on the Cu substrate, the Cu starts to dissolve instantaneously to the molten solder after the flux removed the oxides and permitted metallurgical contact between the solder and contacted Cu. The initial rate of dissolution is very high. The dissolution is a non-equilibrium process, and a very high concentration of Cu could be locally found in the Cu/liquid interface. After a short duration of time, the layer of molten solder adjacent to the contacted Cu becomes supersaturated with the dissolved Cu throughout the interface.

From a thermodynamics viewpoint, the solid IMC starts to form in the layer of the solder adjacent to the contacted metal at the local equilibrium solubility. Cu_6Sn_5 crystallites are formed because a large driving force for the chemical reaction between Cu and Sn atoms exists at the

metastable composition. Scallop-type Cu_6Sn_5 first formed at the Sn/Cu interface during soldering, and its rate of formation is very fast. Cu_6Sn_5 was formed by the dissolution of Cu, followed by a chemical reaction. If contact with the molten solder is long enough, Cu_3Sn formed between Cu_6Sn_5 and Cu. Cu_3Sn was formed by diffusion and by reaction type growth [24].

Figure 3 briefly illustrates the interfacial reaction of SAC305/Cu during solder reflow. When heat is applied, the solid SAC305 solder melts, and the contacted Cu substrate starts to dissolve to the molten SAC305 solder (**Figure 3a**). The layer of molten SAC305 solder near the SAC305/Cu interface becomes supersaturated with the dissolved Cu (**Figure 3b**). The solid IMC begins to form at the interfacial zone. Cu_6Sn_5 with a scallop structure was first formed (**Figure 3c**), followed by thin layer-like Cu_3Sn (**Figure 3d**).

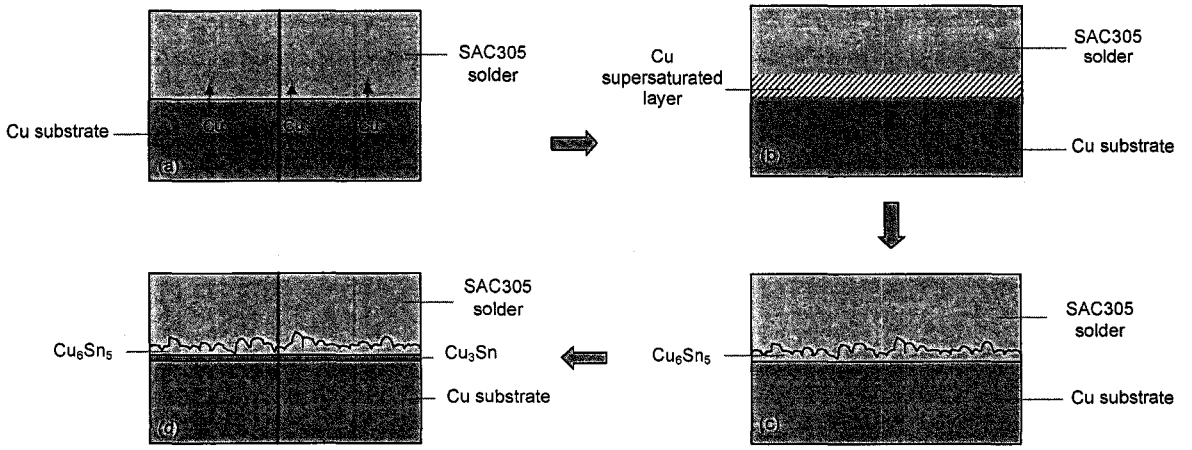

Figure 3: Scheme of the interfacial reaction of SAC305/Cu during solder reflow; (a) dissolution of the Cu substrate, (b) supersaturation of the molten solder layer with Cu, (c) formation of the scallop-type Cu_6Sn_5 at the interface, and (d) Cu_3Sn emerges between Cu_6Sn_5/Cu with prolonged soldering.

2.5 Structural phases of IMCs in Sn-Ag-Cu/Cu

Cu is the most frequently used conductor metal, and it is utilized in contact with solders because of its good solderability characteristic and excellent thermal conductivity performance [25]. Liu et al. [26] investigated the interfacial reactions between a SAC305 solder paste and a polycrystalline Cu substrate at 250 °C and 300 °C from 30 s to 1800 s. They found that some nano-sized Ag_3Sn particles were adsorbed on the SAC305/Cu interface after soldering. The authors explained that Ag atoms first reacted with Sn to form an Ag_3Sn phase in the liquid solder. During solidification, the Ag_3Sn phase precipitated near the IMCs and were prone to be "captured" by the IMCs. Moreover, Wang et al. [27] performed X-ray diffraction (XRD) analysis on interfacial SAC305/Cu to examine the phase structure of IMC during soldering at 260 °C for 20 s. The XRD pattern indicates that the crystal structure of IMCs for SAC305/Cu is Cu_6Sn_5. However, no Ag_3Sn phase was detected in this case.

The XRD patterns of SAC305 in various solder forms are shown in **Figure 4**. The overall intensity of the SAC305 solder wire was much lower than that of the as-deposited SAC305 thin film and of the as-reflowed SAC305/Cu. The as-deposited SAC305 thin film exhibited β-Sn, ή-Cu_6Sn_5, and Ag_3Sn reflections. Heating the SAC305 solder wire did not result in phase changes, except in its relative intensity. The peaks of Cu_6Sn_5 and Ag_3Sn were too low to be seen in the XRD pattern of the SAC305 solder wire (**Figure 4a**), which had lower intensity than that of the as-deposited SAC305 thin film (**Figure 4b**). After solder reflow at 230 °C, most β-Sn phases diminished (**Figure 4c**). By contrast, the diffraction peaks of ή-Cu_6Sn_5 and Ag_3Sn became more evident. New phases of IMCs formed and were confirmed as η-Cu_6Sn_5, ε-Cu_3Sn, and SnO.

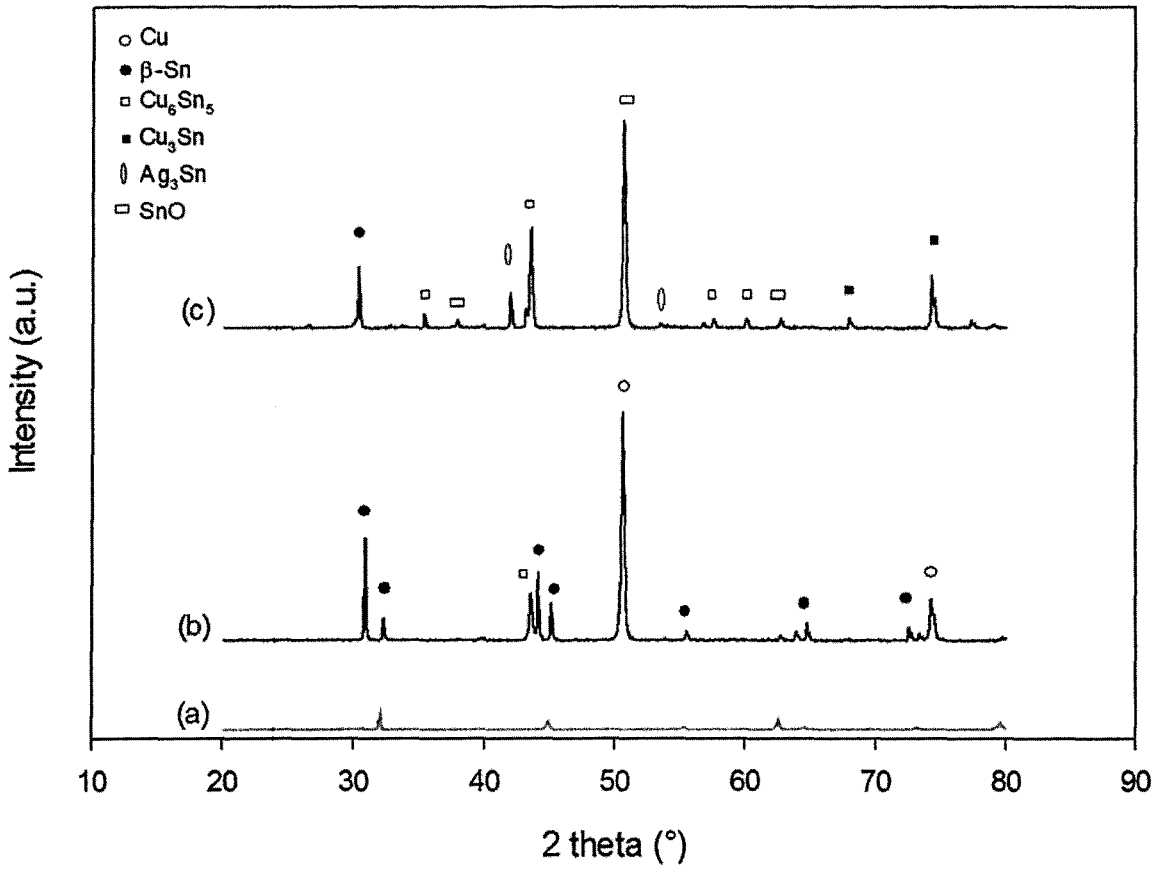

Figure 4: XRD patterns from the top surface of (a) SAC305 solder wire, (b) as-deposited SAC305 thin film, and (c) as-reflowed SAC305/Cu.

2.6 Morphology evolution of IMCs in Sn-Ag-Cu/Cu

Kar et al. [28] evaluated the microstructure of a transition joint consisting of an Sn–Ag–Cu solder alloy and a Cu substrate in a reflowed condition at 230 °C for 120 s. They confirmed the presence of Cu_6Sn_5, Cu_3Sn, and Ag_3Sn intermetallic phases at the interfacial reaction layer (IRL). The presence of Ag in the IRL was minimal and did not take part in the formation of IMCs at the interface. Gao et al. [29], assumed that a significant quantity of Ag was entangled with Sn to form Ag_3Sn within the solder alloy. Thus, the extent of diffusion of Sn towards the IRL was reduced.

One of the characteristics of IMC is the formation of a scallop-type morphology. Scallop-type Cu_6Sn_5 IMCs were formed at SAC305/Cu interfaces, whereas the solder was in the molten state during the reflow at 270 °C for 120 s [30]. This result also correspond to the study done by Kim et al. [1] on the effect of IMC on a SAC305 solder alloy (in the form of pastes and balls) with a Cu substrate joint after reflow treatment at 260 °C. Yoon and Jung [31] also investigated the interfacial reaction of Cu/Sn-3.5Ag-0.7Cu/Cu sandwich solder joints. Typical scallop-type Cu_6Sn_5 IMC layers were formed at both Sn–3.5Ag–0.7Cu/Cu interfaces after reflow. The layers had a composition of approximately 54.8 at.% Cu and 45.2 at.% Sn.

Figure 5 displays the cross-sectional FESEM micrograph of the as-reflowed SAC305/Cu sample. The reaction layer on the Cu substrate is the scallop Cu_6Sn_5 phase, which was formed during the reflow treatment. Long Cu_6Sn_5 IMCs were observed at the top of the interfacial Cu_6Sn_5 scallops, and the growth is attributed to the Cu flux from the Cu substrate to the scallops [32]. However, relatively large Cu_6Sn_5 IMCs were formed in the solder matrix because of the dissolution of the Cu pad. Some Cu pads were dissolved in the molten SAC305 solder during reflow, and the dissolved Cu was precipitated as large Cu_6Sn_5 IMCs in the solder matrix. In other words, the solidification of a eutectic SAC305 solder produced a mixture of β-Sn matrix, fine Ag_3Sn, and Cu_6Sn_5 IMC particles.

Moreover, Ag_3Sn IMC was uniformly dispersed in the solder after reflow [33]. A microstructural analysis on SAC solder alloys with different Ag contents was performed to understand the microstructure details and to evaluate the formation of intermetallic compounds. Elongated plates of the ε-Ag_3Sn phase were observed in the eutectic matrix of Sn-1.0Ag-0.5Cu (SAC105), Sn-2.0Ag-0.5Cu (SAC205), and SAC305 solder alloys. On the other hand, large ε-

Ag_3Sn intermetallics plates and elongated plates of the ε-Ag_3Sn phase were clearly seen in the Sn-4.0Ag-0.5Cu (SAC405) solder alloy.

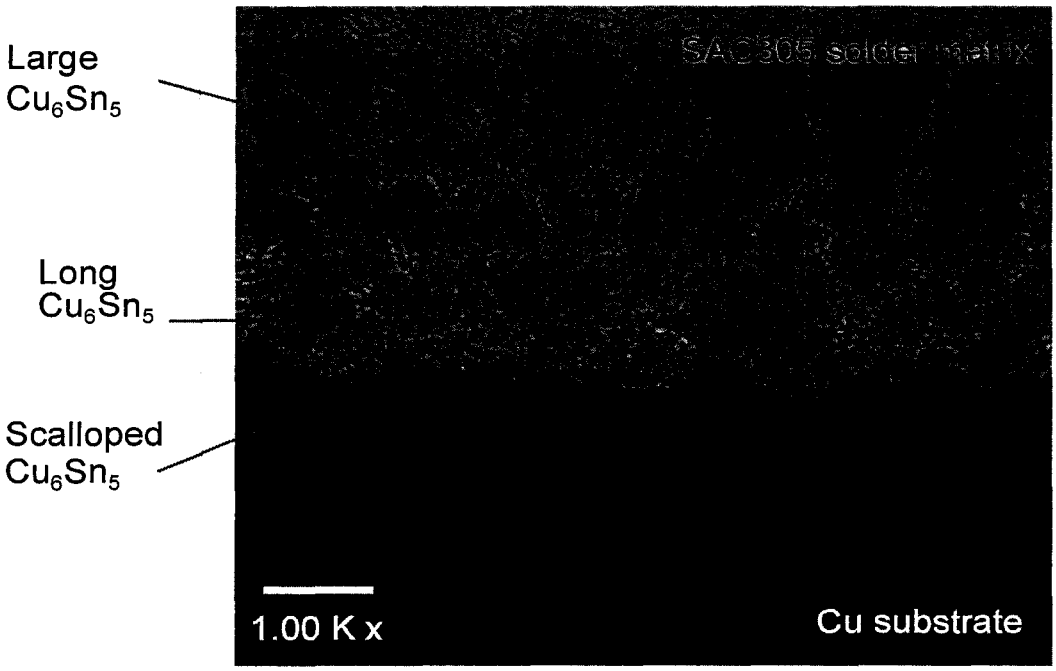

Figure 5: FESEM image of SAC305 solder joints with the Cu substrate.

Figure 6 illustrates the morphologies of Ag_3Sn IMCs in the solder matrix, which can be changed by varying the Ag content. Ag_3Sn IMCs of elongated-plate-like structure exist when the Ag content is between 1.0 and 3.0 wt% (**Figure 6a**). A higher Ag composition of 4.0 wt% results in the formation of large Ag_3Sn IMCs, as in **Figure 6b**.

The overall reliability can be greatly affected by the amount and size of ε-Ag_3Sn IMCs in the microstructure. Large ε-Ag_3Sn IMCs are generally believed to be detrimental in both crack initiation and propagation, and numerous studies have attributed the failure of SAC305 solders to large plate-like ε-Ag_3Sn IMCs under impact and thermal cycling stimuli [1, 34, 35]. In addition,

the formation of large plate-like ε-Ag_3Sn IMCs cause solid dissolution and precipitation hardening, which in turn decrease the matrix strength [36, 37].

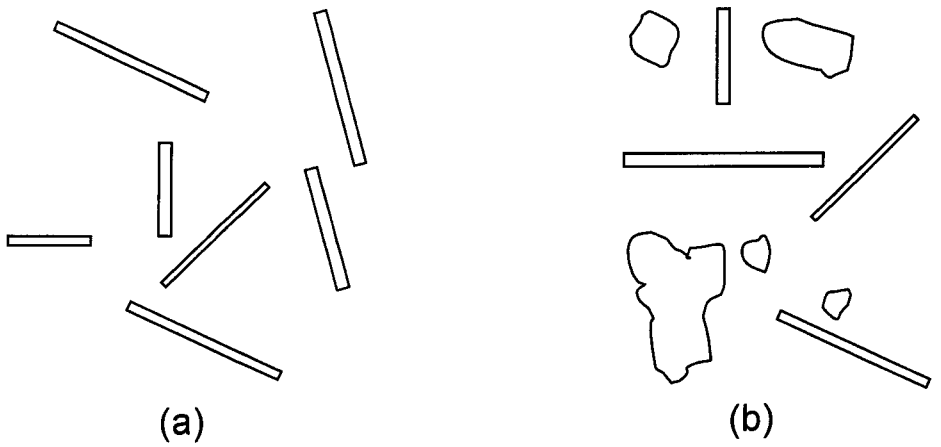

Figure 6: Morphologies of Ag_3Sn compound at varying Ag concentrations with (a) 1.0 Ag to 3.0 Ag alloying and (b) 4.0 Ag alloying.

Figure 7 shows the interfacial reaction of the SAC305 thin film deposited by the thermal evaporation technique. The thin film was subsequently reflowed at 230 °C for 30 s. The top white layer is the SAC305 solid layer, which comprised loose SAC305 particles that were physically adsorbed on the Cu substrate (**Figure 7a**). After solder reflow, interfacial reaction occurred. As shown in **Figures 7b**, two layers of IMCs were formed. The top region is Cu_6Sn_5, and the layer beneath is Cu_3Sn. Cu_6Sn_5 was thick and irregular in thickness, whereas Cu_3Sn was very thin and had a more uniform thickness and a layer-like morphology. However, the thin layer followed the topography of the adjacent Cu_6Sn_5 phase layer to a particular extent. No spalling or flaking of the IMCs was observed, which indicates that the Sn concentration in the thin film was low. The thin film SAC305 solder completely reacted with excess Cu substrate to form Cu_6Sn_5

during reflow. The Cu_3Sn intermetallic layer consistently increased with increasing temperature, whereas Cu_6Sn_5 gradually decreased with increasing reflow temperatures.

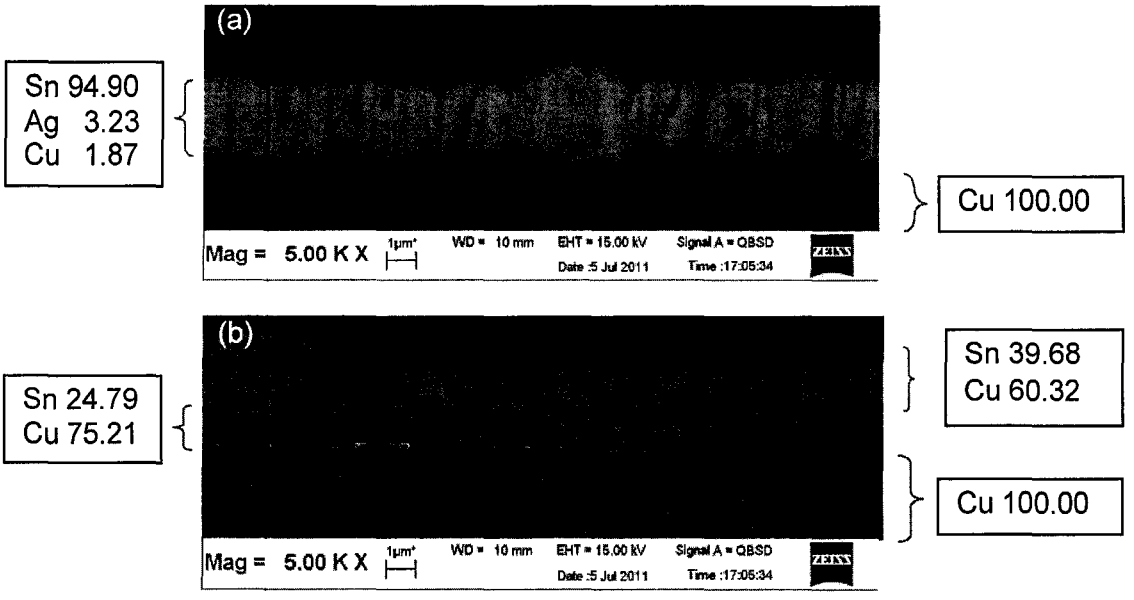

Figure 7: FESEM micrographs of the cross-sectional surface of (a) as-deposited SAC305 thin film and (b) as-reflowed SAC305/Cu at 230 °C for 30 s.

2.7 Formation and growth kinetics of interfacial IMCs

The formation of scallop Cu_6Sn_5 has been observed in wetting reactions between eutectic Sn-Pb and Cu [38-40], eutectic Sn-Ag and Cu [39], and eutectic Sn-Bi and Cu [39]. The scallop is a common growth mode, which grows bigger but fewer with time. This behavior indicates that a non-conservative ripening reaction occur among scallop-type grains. Furthermore, the scallop-type morphology is stable as long as unreacted Cu is present.

In a Cu-Sn system, Cu_6Sn_5 and Cu_3Sn IMCs form at solder/substrate interfaces [1, 39, 41-47]. The actual formation sequence of these phases is determined by local thermodynamic conditions at the Cu/Sn interface. The Cu_6Sn_5 phase precipitates during the earliest stages of

solder/substrate interactions, which correspond to a higher driving force for precipitation than that of the Cu_3Sn phase [48, 49]. The Cu_6Sn_5 phase has been experimentally confirmed to precipitate in a random fashion along the solder/substrate interface.

The formation and growth of interfacial Cu-Sn IMCs is illustrated in Figure 8. During the initial stage (**Figure 8a**), individual Cu_6Sn_5 grains appear at random locations along the solid/liquid interface within a few milliseconds. After the Cu_6Sn_5 grains appear, they began to spread along the interface without much growth perpendicular to the solder/substrate interface until they encounter other spreading grains, which resulted in the formation of a relatively uniform IMC layer of Cu_6Sn_5 (**Figure 8b**).

After the initial formation of the IMC layer, its thickness grows at the expense of the underlying substrate. The individual grains acquire a scallop-like morphology [50] that continues to grow perpendicularly to the interface (**Figure 8c**). The ripening process contributes to the formation of the scallop structure of IMCs, which result in the coarsening of the scallops as its number is decreasing (**Figure 8d**). This reaction is driven by the Gibbs–Thomson effect in the ripening process. Thus, smaller IMC grains are dissolved in the liquid solder, and the growth of neighboring grains are further promoted [39, 51, 52].

After the precipitation of the Cu_6Sn_5 phase, the precipitation of the Cu_3Sn phase at the Cu_6Sn_5/substrate interface becomes thermodynamically possible. This phenomenon is usually observed during the later stages of the soldering reactions. The thickness of Cu_3Sn is expected to be much smaller than that of Cu_6Sn_5 because Cu_3Sn was grown by solid state diffusion.

The evolution of Cu–Sn IMCs for Sn-Ag-Cu/Cu couples is based on the continuous growth of Cu_6Sn_5 via soldering and on the formation and growth of Cu_3Sn between Cu_6Sn_5 and

Cu. The formation of Cu_3Sn is governed by the phase stability according to the following reaction [53]:

$$Cu_6Sn_5 + 9Cu \rightarrow 5Cu_3Sn \quad (1)$$

Vianco et al. [54] found that the formation of Cu_6Sn_5 and Cu_3Sn at the interface between Cu and 95.5Sn-3.9Ag-0.6Cu. The authors concluded that Cu_6Sn_5 layer was formed during soldering and Cu_3Sn forms during solid state ageing between Cu_6Sn_5 and Cu substrate. The layer growth is diffusion-limited and sensitive to the copper concentration in the solder.

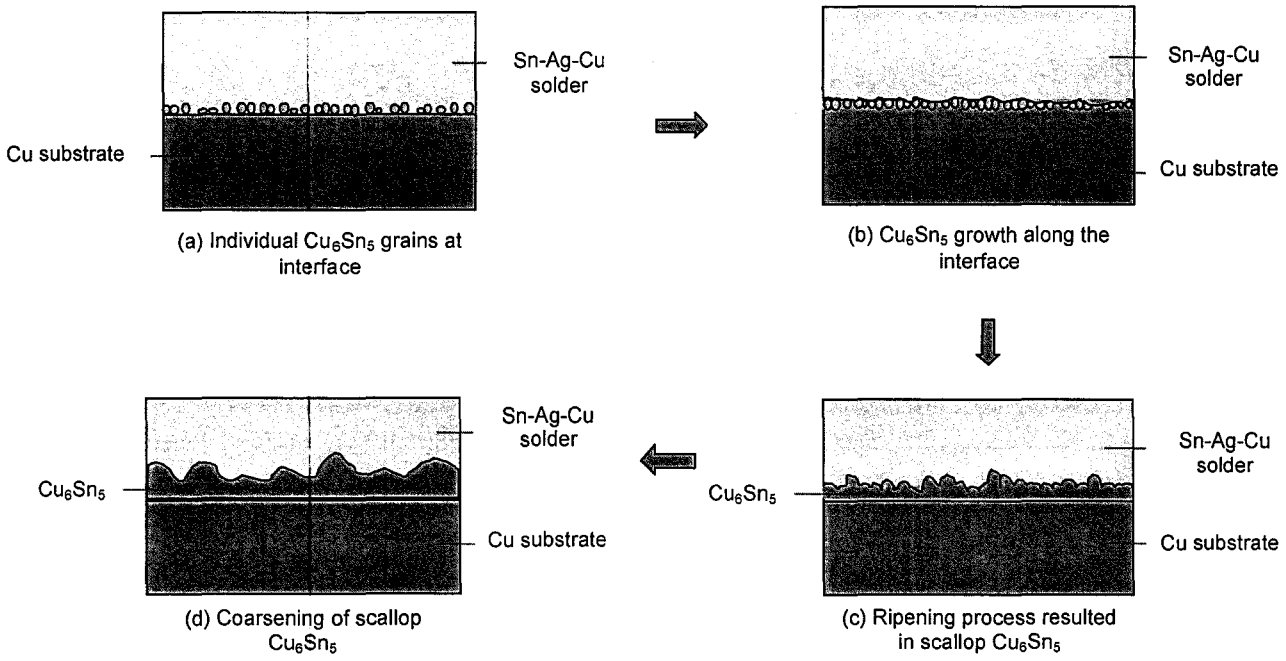

Figure 8: Schematic diagram of the growth mechanism of Cu_6Sn_5 at the Sn-Ag-Cu/Cu interface: (a) individual Cu_6Sn_5 grains at the interface, (b) Cu_6Sn_5 growth along the interface, (c) the ripening process resulted in scallop Cu_6Sn_5, and (d) coarsening of scallop Cu_6Sn_5.

The remaining amount of components, which are involved in the interfacial reaction, takes part in phase evolution after the formation of the first phase. In the Sn-Pb/Cu system, the Cu_6Sn_5 layer that first formed transforms into Cu_3Sn if the solder volume is very small compared with that of Cu [55, 56]. Conversely, the Cu_3Sn converts back to Cu_6Sn_5 if the thin film is Cu [57]. Cu_3Sn could dissolve itself to produce Cu_6Sn_5, and it also could react with Sn atoms to form Cu_6Sn_5 [3, 58]. The transformation equations from Cu_3Sn to Cu_6Sn_5 are shown in Equation 2 and Equation 3.

$$5Cu_3Sn \rightarrow 9Cu + Cu_6Sn_5 \quad (2)$$

$$2Cu_3Sn + 3Sn \rightarrow Cu_6Sn_5 \quad (3)$$

During cooling, the outer layer of Cu_3Sn that is in contact with the molten solder transforms back to Cu_6Sn_5 by the peritectic reaction

$$L + Cu_3Sn \rightarrow Cu_6Sn_5 \quad (4)$$

Many models exist to forecast the first phase formation of solid state interfacial reactions in thin films. The kinetics of growth of each layer can be diffusion- or interfacial-reaction-controlled. The largest product of the Gibbs free energy change and the rate of growth determines the formation of the first phase. In other words, the phase that has the largest flux of interdiffusion becomes the first phase that is formed.

The difference in IMC growth rates are attributed to various growth kinetics [59]. Diffusion rates control the IMC growth rate, whereas different solder/IMC interface energies control the coarsening of the IMC grains and nucleation kinetics. The IMC growth in solder joints is considered to be an ordinary diffusion growth and should be controlled by inter-

diffusion of elements of the substrates and of the solder. Interfacial IMCs layers continue to grow even at room temperature after the solder joints have completed solidification because of its low activation energy [60, 61].

If the IMC layer growth is a diffusion dominant process, the isothermal growth of the IMC layer should follow the square root time law. The thickness (d) of an IMC layer is directly observed with SEM together with the help of a powerful image processing system and can be expressed by parabolic equation [62];

$$d = d_0 + \sqrt{kt} \tag{5}$$

where d_O is the initial thickness (cm), t is the aging time (s) and k is the growth rate constant which is strongly related to the diffusion coefficient of atomic elements of the IMC (cm^2/s) and can be obtained from the linear regression line.

Re-written Equation (5) for experimental and plotting purposes;

$$d - d_0 = k^{1/2}\, t^{1/2} \tag{6}$$

The value of k for a particular temperature can be obtained from the slope of the linear regression of the average measured intermetallic thickness (d-d_o) versus $t^{1/2}$ plot.

Meanwhile, the activation energies for the intermetallic growth can be calculated using the Arrhenius relationship [63];

$$k = k_o exp\left(-\frac{Q}{RT}\right) \tag{7}$$

re-write Equation (7) for plotting;

$$\ln k = \ln k_o - \frac{Q}{RT} \tag{8}$$

where k_o is the layer-growth constant (cm^2/s), Q is the activation energy for layer growth

(kJ/mol), R is the ideal gas constant (8.314 J/mol K) and T is the absolute temperature (Kelvin). The Q for layer growth will be obtained from the slope of the *ln k* versus *1/T* plot multiplied by R.

2.8 Effects of Reflow Temperature and Time on Interfacial Intermetallic Compound

The thicknesses of the IMC layers are measured at multiple selected areas and then divided by the number of selected points to obtain the average value, as illustrated in **Figure 9**. The thickness of the IMC layers formed at the SAC305/Cu interface increases with increasing soldering temperature and time. Cu-Sn IMCs were formed at the interface of Sn–0.3Ag–0.7Cu and the Cu substrate by dip soldering in various soldering temperature and time [64]. Either Cu_3Sn or Cu_6Sn_5 intermetallic phase was found at the interfacial zone depending on the soldering condition. The authors concluded that the increase in intermetallic layer thickness in both cases is attributed to the diffusion growth of these intermetallic phases during the soldering process.

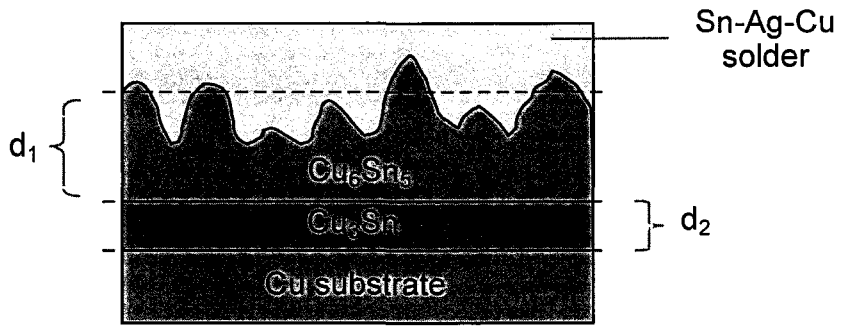

Figure 9: Schematic diagram of IMCs thickness measurements, with d_1 as the thickness of Cu_6Sn_5 and d_2 as the thickness of Cu_3Sn.

Additionally, Yu et al. [62] studied the formation and growth of IMC layer at the interface between Sn-3.5Ag lead-free solder and the Cu substrate during soldering and aging. The soldering was conducted at 250 °C using dipping method. A continuous IMC layer was formed in a short time and the dissolution of the IMC played an important role on the IMC growth. With the increasing of soldering time, both the growth rate and dissolution rate decreased. During aging at 70, 125 and 170 °C up to 1000 h, the initial scallop morphology of the IMC layer changed to that of a more planar type.

The increase in IMC thickness that resulted from increasing soldering time has also been reported by Yu et al. [3]. The authors soldered Sn–3.5Ag, Sn–3.5Ag–0.7Cu, Sn–3.5Ag–1.7Cu, and Sn–0.5Ag–4.0Cu lead-free solder alloys with a Cu substrate at 250 °C. The growth of the IMC layers is fast at a short soldering time. The thickness of the IMC layer gradually increases with increasing soldering time. However, the increasing rate of IMC thickness slows down when the soldering time exceeds 60 s. Thus, the authors concluded that the formation of IMC is initially controlled by reaction diffusion and by a high growth rate. After a specific thickness is reached, the growth is controlled by grain boundary diffusion mechanism. Hence, the growth of the IMC layer becomes slow, as shown in **Figure 10**.

The authors also concluded that Sn–0.5Ag–4.0Cu had the thinnest IMC layer when the soldering time is shorter than 90 s. After soldering for 600 s, the order of IMC thickness at the solder joints is: Sn–3.5Ag < Sn–3.5Ag–0.7Cu < Sn–3.5Ag–1.7Cu < Sn–0.5Ag–4.0Cu. Thus, the IMC thickness increased with increasing Cu content in the solder alloy. Moreover, the IMCs layer thickness quickly increased with increasing soldering time because of the precipitation effect of the Cu_6Sn_5 in the liquid solder. Both the Ag_3Sn phase and Cu_6Sn_5 compounds were

detected in the solder matrix of Sn–Ag–Cu/Cu after soldering for 30 s. The Cu_6Sn_5 became coarser with increasing Cu content.

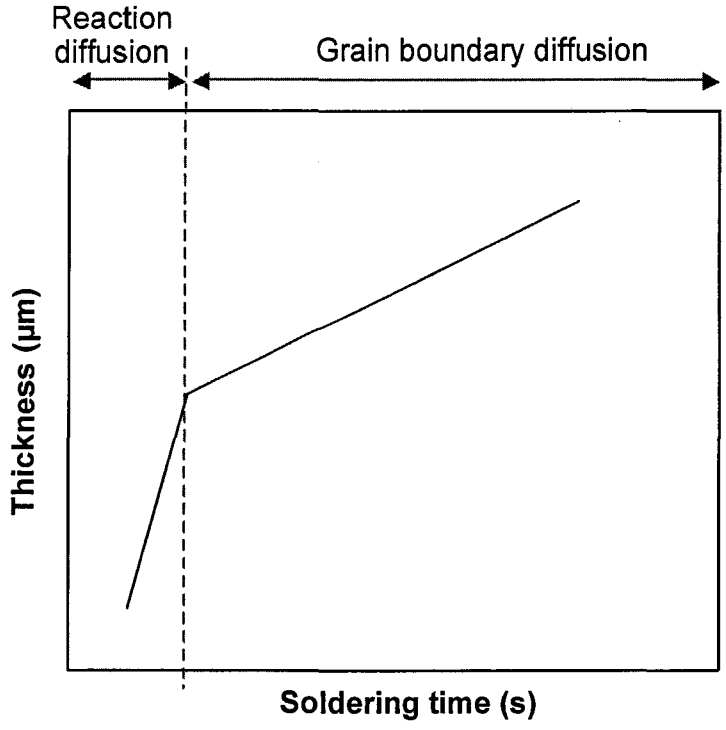

Figure 10: Growth mechanisms of IMC layer during soldering process.

After prolonged soldering for 180 s, a thin Cu_3Sn layer was formed between the Cu_6Sn_5 layer and Cu. Moreover, the IMC layers became thicker and the number of the IMC grains decreased when the samples underwent soldering for 600 s, which resulted in a scallop-like morphology.

Figure 11 demonstrates the growth of Cu-Sn IMCs at varying reflow times. **Figure 11a** shows the formation of a scallop-type structure at the interfacial layer of SAC305/Cu when the reflow time was 30 s. Ag_3Sn are present in the solder matrix. Furthermore, spalling of Cu_6Sn_5 spheroids were observed because the Sn concentration in SAC305 was high. The formation of the spheroids was assisted by the ripening reaction among the compound grains. When soldered

for 180 s, a thin band of Cu_3Sn was observed at the Cu_6Sn_5/Cu interface (**Figure 11b**). When soldered for 600 s, the IMC layers became thicker, and the number of scallop Cu_6Sn_5 decreased. Cu_3Sn maintained its continuous layer-like morphology with increasing thickness and reflow time (**Figure 11c**).

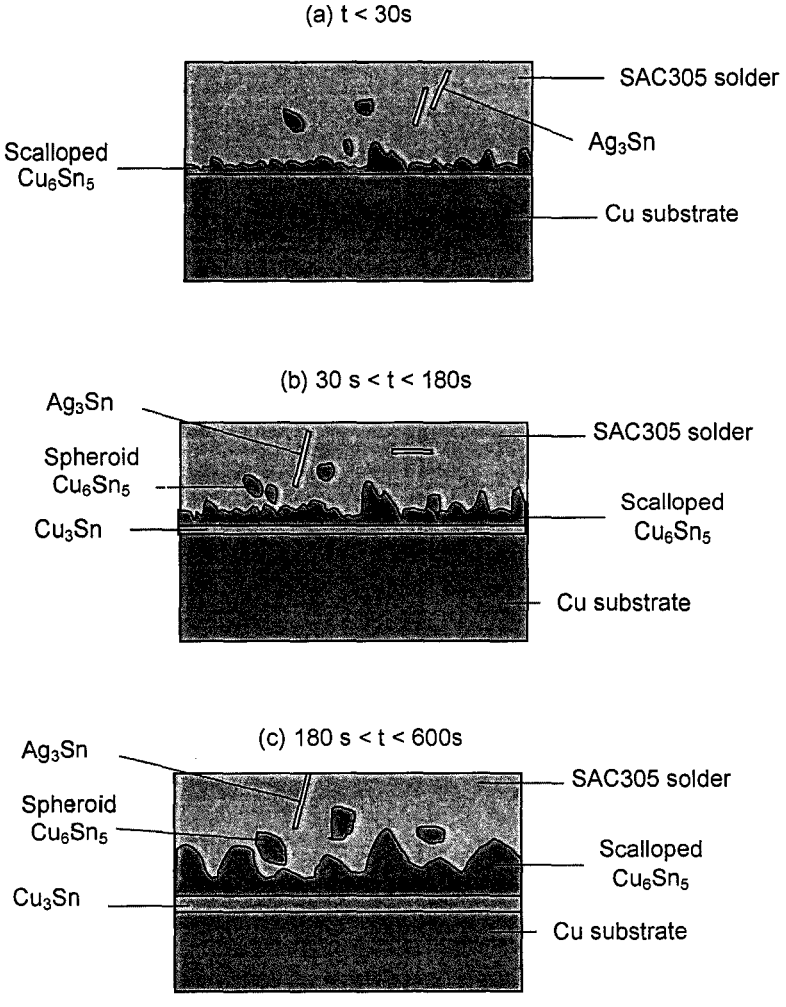

Figure 11: Growth mechanism of Cu-Sn IMCs at various reflow times: (a) formation of scallop Cu_6Sn_5 at the SAC305/Cu interfacial region, (b) appearance of Cu_3Sn between the Cu_6Sn_5/Cu interface, and (c) increase in both Cu-Sn IMCs thicknesses with increasing reflow times.

Li and Chen [65] also conducted an experiment on commercial lead-free solders, namely, Sn-3.5Ag and Sn-3.5Ag-0.7Cu, by using a standard infrared reflow oven at 250 °C for 2, 6, 15, 30, 60, 120, 240, and 360 s. Both Cu_6Sn_5 and Ag_3Sn were detected in the solder joint. The Ag_3Sn phase was detected because it was formed on top of the layer during the reflow process. However, a scallop-like layer of Cu_6Sn_5 IMC was located at the solder-Cu substrate interface. The authors added that Cu_3Sn phase was not observed in the as-solidified solder joint, although it may exist between Cu and the Cu_6Sn_5 phase.

Figure 12 compares the thicknesses of the IMC layers formed at the interfacial region as a function of reflow temperatures. The Cu_3Sn intermetallic layer consistently increased with increasing temperature (**Figure 12a**), whereas Cu_6Sn_5 gradually decreased with increasing reflow temperature (**Figure 12b**).

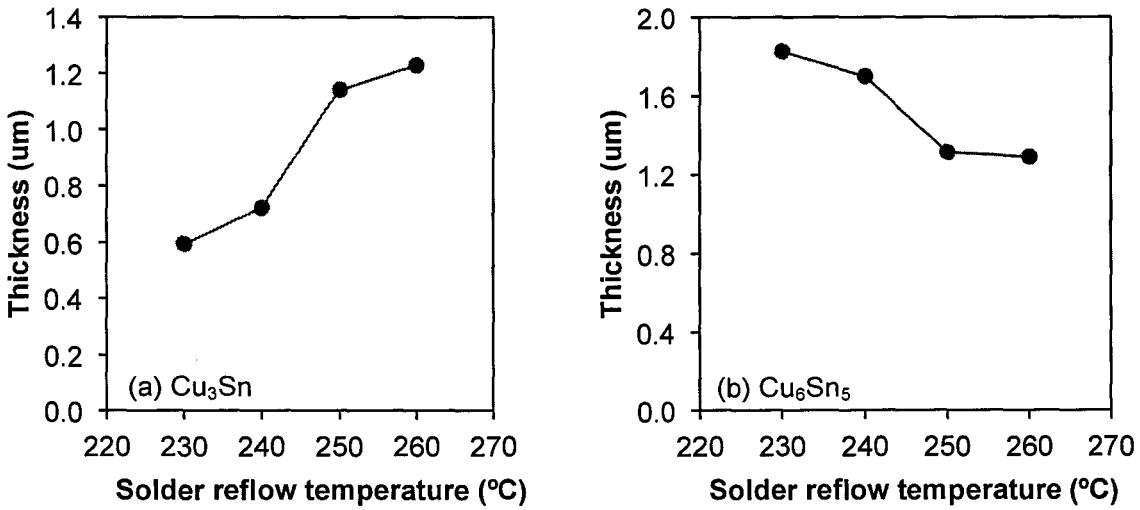

Figure 12: (a) Cu_3Sn and (b) Cu_6Sn_5 IMCs thickness as a function of reflow temperature at a reflow time of 30 s.

Figure 13 shows the relationship between the IMC layer thickness and the reflow time. Likewise, at a specific soldering temperature, the thickness of the IMC layers at the interfacial

zone increased with increasing soldering time. Based on the study done by Yu and Wang [3], the increase in soldering time enables the IMC layer to grow quickly because of the precipitation effect of Cu_6Sn_5. Cu_6Sn_5 could be recalled to develop into Cu_3Sn when the Sn supply is limited. Hence, the Cu_3Sn thickness increases with decreasing Cu_6Sn_5 thickness despite the fact that Cu_6Sn_5 generally grows with increasing solder time. These results provide evidence that the interfacial Cu_3Sn layer grows at the expense of Cu_6Sn_5 according to the reaction $Cu_6Sn_5 + 9Cu \rightarrow 5Cu_3Sn$ [53]. Moreover, the Cu_3Sn thickness growth follows a linear equation. According to material kinetics, a linear growth indicates that the formation of the interfacial Cu–Sn IMC layer is an interfacial reaction-controlled process [66].

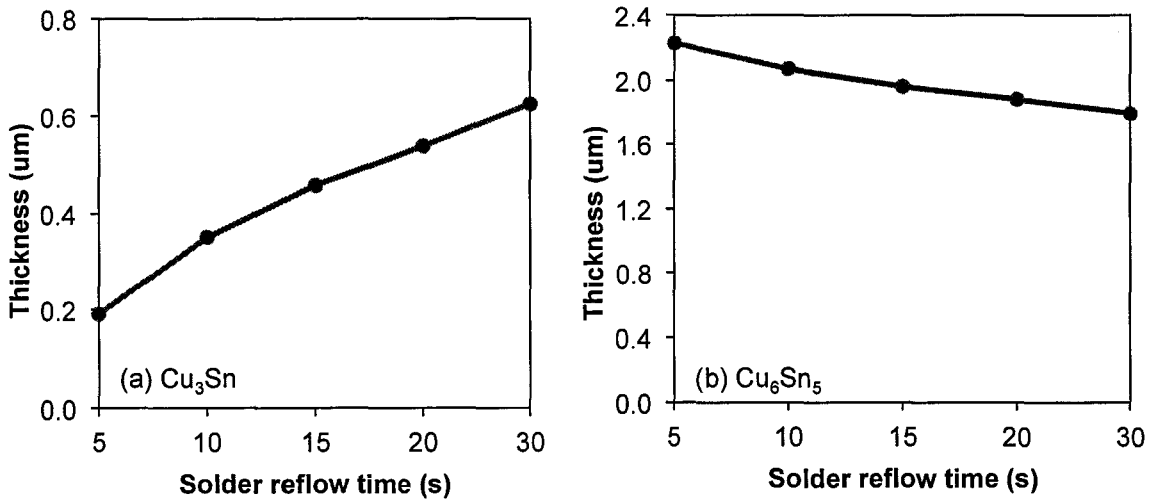

Figure 13: (a) Cu_3Sn and (b) Cu_6Sn_5 IMC layer thickness vs. reflow time at 230 °C.

The increase in the Cu_3Sn IMC layer results from the diffusion and reaction type growth during the soldering process [17]. The growth of Cu_3Sn consists of several steps: the dissolution of Cu from the Cu pad, the diffusion of Cu and Sn through the existing Cu_3Sn layer, and the conversion of Cu_6Sn_5 into Cu_3Sn at the Cu_6Sn_5/Cu_3Sn interface and the reaction of Sn with Cu at

the Cu/Cu_3Sn interface [67]. Conversely, Cu_6Sn_5 is formed by the dissolution of Cu, followed by a chemical reaction [17], and its growth is restricted by the Cu_3Sn layer because the amount of free Cu atoms that can diffuse to the Cu_6Sn_5 is very small. Therefore, Cu_3Sn grows rapidly with temperature, consuming Cu_6Sn_5 at the interface of Cu_3Sn/Cu_6Sn_5.

2.9 Summary

Sn-Ag-Cu is the leading candidate for the fabrication of eco-friendly products. Two intermetallic layers are commonly found at the interfacial zone of Sn-Ag-Cu and the Cu substrate, i.e., Cu_6Sn_5 and Cu_3Sn. Cu_6Sn_5 forms first and possesses a scallop-like structure, whereas Cu_3Sn emerges at the Cu_6Sn_5/Cu interface and has a layered structure. However, the thickness of Cu_3Sn is much smaller than that of Cu_6Sn_5, and its formation requires longer contact times. Morphological transformations could occur depending on the phase stability. Both Cu-Sn IMCs grow with increasing reflow temperature and time.

2.10 References

[1] K.S. Kim, S.H. Huh and K. Suganuma, "Effects of intermetallic compounds on properties of Sn–Ag–Cu lead-free soldered joints", *Journal of Alloys and Compounds*, vol. 352, no. 1-2, pp. 226-236, 2003.

[2] J.-W. Yoon, S.-W. Kim and S.-B. Jung, "IMC morphology, interfacial reaction and joint reliability of Pb-free Sn–Ag–Cu solder on electrolytic Ni BGA substrate", *Journal of Alloys and Compounds*, vol. 392, no. 1–2, pp. 247-252, 2005.

[3] D.Q. Yu and L. Wang, "The growth and roughness evolution of intermetallic compounds of Sn–Ag–Cu/Cu interface during soldering reaction", *Journal of Alloys and Compounds*, vol. 458, no. 1-2, pp. 542-547, 2008.

[4] M. Farooq, S. Ray, A. Sarkhel and C. Goldsmith, "Evaluation of Lead(Pb)-free Ceramic Ball Grid Array (CBGA): Wettability, Microstructure and Reliability", in *Proceedings. 51st Electronic Components and Technology Conference*, pp. 978-986, 2001.

[5] S. Kang, D. Leonard, D.-Y. Shih, L. Gignac, D. Henderson, S. Cho and J. Yu, "Interfacial reactions of Sn-Ag-Cu solders modified by minor Zn alloying addition", *Journal of Electronic Materials*, vol. 35, no. 3, pp. 479-485, 2006.

[6] H.H. Manko, "*Book Solders and Soldering: Materials, Design, Production, and Analysis for Reliable Bonding*", McGraw-Hill Companies, Inc., New York, 2001, pp. 1-141.

[7] C.M.L. Wu, D.Q. Yu, C.M.T. Law and L. Wang, "Properties of lead-free solder alloys with rare earth element additions", *Materials Science and Engineering: R: Reports*, vol. 44, no. 1, pp. 1-44, 2004.

[8] K.N. Subramanian, "*Book Lead-Free Electronic Solders: A Special Issue of the Journal of Materials Science: Materials in Electronics*", Springer, 2007,

[9] C.-h. Wang and S.-w. Chen, "Sn–0.7wt.%Cu/Ni interfacial reactions at 250 °C", *Acta Materialia*, vol. 54, no. 1, pp. 247-253, 2006.

[10] D. Li, C. Liu and P.P. Conway, "Characteristics of intermetallics and micromechanical properties during thermal ageing of Sn–Ag–Cu flip-chip solder interconnects", *Materials Science and Engineering: A*, vol. 391, no. 1–2, pp. 95-103, 2005.

[11] Y. Chan and D. Yang, "Failure mechanisms of solder interconnects under current stressing in advanced electronic packages", *Progress in Materials Science*, vol. 55, no. 5, pp. 428-475, 2010.

[12] Y. Li-Lei, L. Zonghe, J. Liu and A. Tholen, "Microstructural coarsening of lead free solder joints during thermal cycling", in *Proceedings. 50th Electronic Components & Technology Conference*, pp. 134-137, 2000.

[13] A.K. Gain, T. Fouzder, Y. Chan, A. Sharif, N. Wong and W.K.C. Yung, "The influence of addition of Al nano-particles on the microstructure and shear strength of eutectic Sn-Ag-Cu solder on Au/Ni metallized Cu pads", *Journal of alloys and compounds*, vol. 506, no. 1, pp. 216-223, 2010.

[14] H.H. Manko, "*Book Solder and soldering*", McGraw-Hill, New York, 1979,

[15] R.J.K. Wassink, "*Book Soldering in electronics*", Electrochemical Publications, Isle of Man, 1989,

[16] M. Abtew and G. Selvaduray, "Lead-free Solders in Microelectronics", *Materials Science and Engineering: R: Reports*, vol. 27, no. 5-6, pp. 95-141, 2000.

[17] T. Laurila, V. Vuorinen and J.K. Kivilahti, "Interfacial reactions between lead-free solders and common base materials", *Materials Science and Engineering: R: Reports*, vol. 49, no. 1-2, pp. 1-60, 2005.

[18] D.R. Frear, "*Book Solder mechanics: a states of the art assessment* ", Minerals, Metals & Materials Society, Warrendale, Pennsylvania, 1991,

[19] L.M. Lee, H. Haliman and A.A. Mohamad, "Interfacial reaction of a Sn-3.0 Ag-0.5 Cu thin film during solder reflow", *Soldering & Surface Mount Technology*, vol. 25, no. 1, pp. 15-23, 2013.

[20] M.C. Liew, I. Ahmad, L.M. Lee, M.F.M. Nazeri, H. Haliman and A.A. Mohamad, "Corrosion Behavior of Sn-3.0 Ag-0.5 Cu Lead-Free Solder in Potassium Hydroxide Electrolyte", *Metallurgical and Materials Transactions A*, vol. 43, no. 10, pp. 3742-3747, 2012.

[21] C. Lea, "*Book A Scientific Guide to Surface Mount Technology*", Electrochemical Publications Ltd, Ayrshire, Scotland, 1988,

[22] S.-W. Chen, C.-H. Wang, S.-K. Lin and C.-N. Chiu, "Phase Diagrams of Pb-Free Solders and their Related Materials Systems", *Journal of Materials Science: Materials in Electronics*, vol. 18, no. 1, pp. 19-37, 2007.

[23] S.M.L. Nai, J. Wei and M. Gupta, "Interfacial intermetallic growth and shear strength of lead-free composite solder joints", *Journal of Alloys and Compounds*, vol. 473, no. pp. 100-106, 2009.

[24] J. Kivilahti, "The Chemical Modeling of Electronic Materials and Interconnections", *JOM Journal of the Minerals, Metals and Materials Society*, vol. 54, no. 12, pp. 52-57, 2002.

[25] M.J. Rizvi, Y.C. Chan, C. Bailey, H. Lu and M.N. Islam, "Effect of adding 1 wt% Bi into the Sn–2.8Ag–0.5Cu solder alloy on the intermetallic formations with Cu-substrate during soldering and isothermal aging", *Journal of Alloys and Compounds*, vol. 407, no. 1-2, pp. 208-214, 2006.

[26] X. Liu, M. Huang, Y. Zhao, C.M.L. Wu and L. Wang, "The adsorption of Ag_3Sn nano-particles on Cu–Sn intermetallic compounds of Sn–3Ag–0.5Cu/Cu during soldering", *Journal of Alloys and Compounds*, vol. 492, no. 1-2, pp. 433-438, 2010.

[27] F.-J. Wang, Z.-S. Yu and K. Qi, "Intermetallic compound formation at Sn–3.0Ag–0.5Cu–1.0Zn lead-free solder alloy/Cu interface during as-soldered and as-aged conditions", *Journal of Alloys and Compounds*, vol. 438, no. 1–2, pp. 110-115, 2007.

[28] A. Kar, M. Ghosh, A.K. Ray and R.N. Ghosh, "Effect of copper addition on the microstructure and mechanical properties of lead free solder alloy", *Materials Science and Engineering: A*, vol. 459, no. 1-2, pp. 69-74, 2007.

[29] F. Gao, T. Takemoto and H. Nishikawa, "Effects of Co and Ni addition on reactive diffusion between Sn-3.5Ag solder and Cu during soldering and annealing", *Materials Science and Engineering: A*, vol. 420, no. 1-2, pp. 39-46, 2006.

[30] J.-W. Yoon, B.-I. Noh, B.-K. Kim, C.-C. Shur and S.-B. Jung, "Wettability and interfacial reactions of Sn–Ag–Cu/Cu and Sn–Ag–Ni/Cu solder joints", *Journal of Alloys and Compounds*, vol. 486, no. 1–2, pp. 142-147, 2009.

[31] J.-W. Yoon and S.-B. Jung, "Effect of surface finish on interfacial reactions of Cu/Sn–Ag–Cu/Cu(ENIG) sandwich solder joints", *Journal of Alloys and Compounds*, vol. 448, no. 1-2, pp. 177-184, 2008.

[32] R. Gagliano and M. Fine, "Growth of η phase scallops and whiskers in liquid tin-solid copper reaction couples", *JOM Journal of the Minerals, Metals and Materials Society*, vol. 53, no. 6, pp. 33-38, 2001.

[33] M. Reid, J. Punch, M. Collins and C. Ryan, "Effect of Ag Content on the Microstructures of Sn-Ag-Cu Based Solder Alloys", *Soldering & Surface Mount Technology*, vol. 20, no. 4, pp. 3-8, 2008.

[34] J.-M. Song, J.-J. Lin, C.-F. Huang and H.-Y. Chuang, "Crystallization, morphology and distribution of Ag_3Sn in Sn–Ag–Cu alloys and their influence on the vibration fracture properties", *Materials Science and Engineering: A*, vol. 466, no. 1–2, pp. 9-17, 2007.

[35] K. Zeng and K.N. Tu, "Six cases of reliability study of Pb-free solder joints in electronic packaging technology", *Materials Science and Engineering: R: Reports*, vol. 38, no. 2, pp. 55-105, 2002.

[36] C.T. Sims, N.S. Stoloff and W.C. Hagel, "*Book Superalloys II*", John Wiley & Sons, New York, 1987, pp. 39 – 261.

[37] M. Reid, M.J. Pomeroy and J.S. Robinson, "Microstructural instability in coated single crystal superalloys", *Journal of Materials Processing Technology*, vol. 153–154, no. pp. 660-665, 2004.

[38] H.K. Kim, H.K. Liou and K.N. Tu, "Three-dimensional morphology of a very rough interface formed in the soldering reaction between eutectic SnPb and Cu", *Applied Physics Letters*, vol. 66, no. 18, pp. 2337-2339, 1995.

[39] H.K. Kim and K.N. Tu, "Kinetic analysis of the soldering reaction between eutectic SnPb alloy and Cu accompanied by ripening", *Physical Review B*, vol. 53, no. 23, pp. 16027-16034, 1996.

[40] A.A. Lin, H.K. Kim, K.N. Tu and P.A. Totta, "Spalling of Cu_6Sn_5 spheroids in the soldering reaction of eutectic SnPb on Cr/Cu/Au thin films ", *Journal of Applied Physics*, vol. 80, no. pp. 2774–2779, 1996.

[41] S. Bader, W. Gust and H. Hieber, "Rapid formation of intermetallic compounds interdiffusion in the Cu-Sn and Ni-Sn systems", *Acta Metallurgica et Materialia*, vol. 43, no. 1, pp. 329-337, 1995.

[42] S. Choi, J.P. Lucas, K.N. Subramanian and T.R. Bieler, "Formation and growth of interfacial intermetallic layers in eutectic Sn-Ag solder and its composite solder joints", *Journal of Materials Science: Materials in Electronics*, vol. 11, no. 6, pp. 497-502, 2000.

[43] P.L. Tu, Y.C. Chan, K.C. Hung and J.K.L. Lai, "Growth kinetics of intermetallic compounds in chip scale package solder joint", *Scripta Materialia*, vol. 44, no. 2, pp. 317-323, 2001.

[44] S. Kang, R. Rai and S. Purushothaman, "Interfacial reactions during soldering with lead-tin eutectic and lead (Pb)-free, tin-rich solders", *Journal of Electronic Materials*, vol. 25, no. 7, pp. 1113-1120, 1996.

[45] M. Schaefer, R. Fournelle and J. Liang, "Theory for intermetallic phase growth between cu and liquid Sn-Pb solder based on grain boundary diffusion control", *Journal of Electronic Materials*, vol. 27, no. 11, pp. 1167-1176, 1998.

[46] C. Shin, Y. Baik and J. Huh, "Effects of microstructural evolution and intermetallic layer growth on shear strength of ball-grid-array Sn-Cu solder joints", *Journal of Electronic Materials*, vol. 30, no. 10, pp. 1323-1331, 2001.

[47] M. Islam, Y. Chan, M. Rizvi and W. Jillek, "Investigations of interfacial reactions of Sn-Zn based and Sn-Ag-Cu lead-free solder alloys as replacement for Sn-Pb solder", *Journal of alloys and compounds*, vol. 400, no. 1, pp. 136-144, 2005.

[48] B.-J. Lee, N.M. Hwang and H.M. Lee, "Prediction of interface reaction products between Cu and various solder alloys by thermodynamic calculation", *Acta Materialia*, vol. 45, no. 5, pp. 1867-1874, 1997.

[49] R.A. Lord and A. Umantsev, "Early stages of soldering reactions ", *Journal of Applied Physics*, vol. 98, no. pp. 063525, 2005.

[50] J. Görlich, G. Schmitz and K.N. Tu, "On the mechanism of the binary Cu/Sn solder reaction ", *Applied Physics Letters*, vol. 86, no. 5, pp. 053106, 2005.

[51] S. Choi, T. Bieler, J. Lucas and K. Subramanian, "Characterization of the growth of intermetallic interfacial layers of Sn-Ag and Sn-Pb eutectic solders and their composite solders on Cu substrate during isothermal long-term aging", *Journal of Electronic Materials*, vol. 28, no. 11, pp. 1209-1215, 1999.

[52] W. Choi and H. Lee, "Effect of soldering and aging time on interfacial microstructure and growth of intermetallic compounds between Sn-3.5Ag solder alloy and Cu substrate", *Journal of Electronic Materials*, vol. 29, no. 10, pp. 1207-1213, 2000.

[53] F. Gao, T. Takemoto and H. Nishikawa, "Effects of Co and Ni addition on reactive diffusion between Sn–3.5Ag solder and Cu during soldering and annealing", *Materials Science and Engineering: A*, vol. 420, no. 1–2, pp. 39-46, 2006.

[54] P.T. Vianco, "An overview of surface finishes and their role in printed circuit board solderability and solder joint performance", *Circuit World*, vol. 25, no. 1, pp. 6-24, 1999.

[55] A. Sunwoo, J. Morris and G. Lucey, "The growth of Cu-Sn intermetallics at a pretinned copper-solder interface", *Metallurgical and Materials Transactions A*, vol. 23, no. 4, pp. 1323-1332, 1992.

[56] H. Reynolds and J. Morris, "The role of Cu-Sn intermetallics in wettability degradation", *Journal of Electronic Materials*, vol. 24, no. 10, pp. 1429-1434, 1995.

[57] R.E. Pratt, E.I. Stromswold and D.J. Quesnel, "Effect of solid state intermetallic growth on the fracture toughness of Cu/63Sn-37Pb solder joints", *IEEE Trans. CPMT-A*, vol. 19, no. pp. 134-141, 1996.

[58] A. Paul, "*The kirkendall effect in solid state diffusion*", Eindhoven University of Technology, Ph.D thesis, 2004.

[59] K. Zeng, "Lead-free soldering: Materials science and solder joint reliability", *JOM Journal of the Minerals, Metals and Materials Society*, vol. 61, no. 6, pp. 28-28, 2009.

[60] I. Dutta, P. Kumar and G. Subbarayan, "Microstructural coarsening in Sn-Ag-based solders and its effects on mechanical properties", *JOM Journal of the Minerals, Metals and Materials Society*, vol. 61, no. 6, pp. 29-38, 2009.

[61] S.-w. Chen, C.-h. Wang, S.-k. Lin, C.-n. Chiu and C.-c. Chen, "Phase transformation and microstructural evolution in solder joints", *JOM Journal of the Minerals, Metals and Materials Society*, vol. 59, no. 1, pp. 39-43, 2007.

[62] D. Yu, C. Wu, C. Law, L. Wang and J. Lai, "Intermetallic compounds growth between Sn-3.5 Ag lead-free solder and Cu substrate by dipping method", *Journal of alloys and compounds*, vol. 392, no. 1, pp. 192-199, 2005.

[63] P. Tu, Y. Chan, K. Hung and J. Lai, "Growth kinetics of intermetallic compounds in chip scale package solder joint", *Scripta materialia*, vol. 44, no. 2, pp. 317-324, 2001.

[64] N. Mookam and K. Kanlayasiri, "Effect of soldering condition on formation of intermetallic phases developed between Sn–0.3Ag–0.7Cu low-silver lead-free solder and Cu substrate", *Journal of Alloys and Compounds*, vol. 509, no. 21, pp. 6276-6279, 2011.

[65] G.Y. Li and B.L. Chen, "Formation and growth kinetics of interfacial intermetallics in Pb-free solder joint", *Components and Packaging Technologies, IEEE Transactions on*, vol. 26, no. 3, pp. 651-658, 2003.

[66] A.C.K. So and Y.C. Chan, "Reliability studies of surface mount solder joints - effect of Cu-Sn intermetallic compounds", *Components, Packaging, and Manufacturing*

Technology, Part B: Advanced Packaging, IEEE Transactions on, vol. 19, no. 3, pp. 661-668, 1996.

[67] W. Peng, E. Monlevade and M.E. Marques, "Effect of thermal aging on the interfacial structure of SnAgCu solder joints on Cu", *Microelectronics Reliability*, vol. 47, no. 12, pp. 2161-2168, 2007.

Chapter 3: Results and discussion

3.1 Open Circuit Corrosion Study of Sn-9Zn Lead-Free Solder in Alkaline Solution

3.1.1 Introduction

A solder is a part of an electronic packaging that plays various crucial roles, such as electrical and mechanical connections [1-3]. One of the most famous lead (Pb)-free solders is Sn-9Zn. A wide range of reliability issues involving tensile strength, creep resistance and melting point have been addressed to ensure that the new Pb-free solders can replace Sn-Pb in assembly and application without major modifications [4-7].

The corrosion behaviors of Pb-free solders have been extensively studied [8-15]. Lin et al. [9] have reported that Al-Zn-Sn solders produce very dense corrosion product layers of oxides, chlorides and oxychlorides that contribute to passivation behavior in sodium chloride (NaCl) solution. Rosalbino et al. [14, 15] agree that compact corrosion products can be obtained as corrosion byproducts of solders in 0.1 M NaCl. Li et al. [8] also reveals that Pb-free solders exhibit better corrosion resistance than Sn-Pb in 3.5 wt % NaCl.

Alkaline-based batteries that utilize 6 M potassium hydroxide (KOH) as the electrolyte are commonly used to supply electrical power to devices. However, any excessive loading or unexpected leakage from the batteries may wet the solders on the electronic circuit. The existence of copper (Cu) as bonding pad can also possibly induce galvanic corrosion with Sn-9Zn solder in the presence of KOH. Although known to be corrosive, studies on the corrosion properties of solders in KOH solution are very limited.

In the present study, the open circuit potential and current of reflowed Sn-9Zn on Cu (Sn-9Zn/Cu) in 6 M KOH is studied. Morphological, elemental, phase and mechanical analyses are conducted to gain further understanding of the obtained potential and current behaviors.

3.1.2 Experimental

Sn and Zn were co-melted in the presence of nitrogen gas at 450 °C to produce Sn-9Zn solder alloy. Sn-9Zn plate was obtained by pressing the solidified solder with a hydraulic press, and punched to produce 5 mm-diameter solder pellets. The reflowing process of the Sn, Zn and Sn-9Zn solders on top of a 10 × 10 mm^2 Cu plate was performed at 250 °C for 10 s using a hotplate to produce Sn/Cu, Zn/Cu and Sn-9Zn/Cu. The sample was then cold-mounted with epoxy resin.

Sn/Cu, Zn/Cu and Sn-9Zn/Cu as the working electrodes versus Hg/HgO as the reference electrode were immersed in 6 M KOH for corrosion tests. Potential and current were recorded using a UT803 UNI-T multimeter equipped with data interface recording software. X-ray diffraction (XRD) was performed using a Bruker AXS D9 diffractometer to evaluate the structural changes. A field emission scanning electron microscopy (FESEM) system was used to characterize the morphological transformation. Alternatively, the elemental properties of the solder were studied by an energy dispersive X-ray (EDX) instrument coupled to a Zeiss Supra 35VP FESEM system.

For mechanical analysis, two Cu plates were used to create a Cu/Sn-9Zn/Cu butt joint with dimensions of 40.0 × 5.0 × 1.5 mm^3. A hot plate was used in the soldering process. The temperature was maintained at 250 °C for 10 s with the application of ZnCl-based flux. The

soldered joint was air cooled to solidify. Once cooled, the excess solder on the Cu plates were completely ground. The pull test was performed at a crosshead speed of 2 mm/min at room temperature to determine the tensile strength of the joint. Pre- and post-pull test images of the joint were taken by a Dinolite microscope to investigate the fracture surface further.

3.1.3 Results and Discussion

3.1.3.1 Corrosion potential and current analyses

The corrosion potential behaviors of Sn/Cu, Zn/Cu, and Sn-9Zn/Cu after immersion in 6 M KOH is presented in **Figure 1**. The control sample Sn/Cu shows a stable potential at -1050 mV, and Zn/Cu gives -1330 mV. On the contrary, Sn-9Zn/Cu undergoes two stages of potential change. Stage 1 demonstrates a sudden rise in corrosion potential from its initial potential point of -1330 to -1120 mV after 40 min. Stage 2 occurs after the completion of Stage 1. In Stage 2, the potential changes appear to be in a stable region, forming a long plateau of potential against time. The potential remains almost constant until the end of immersion.

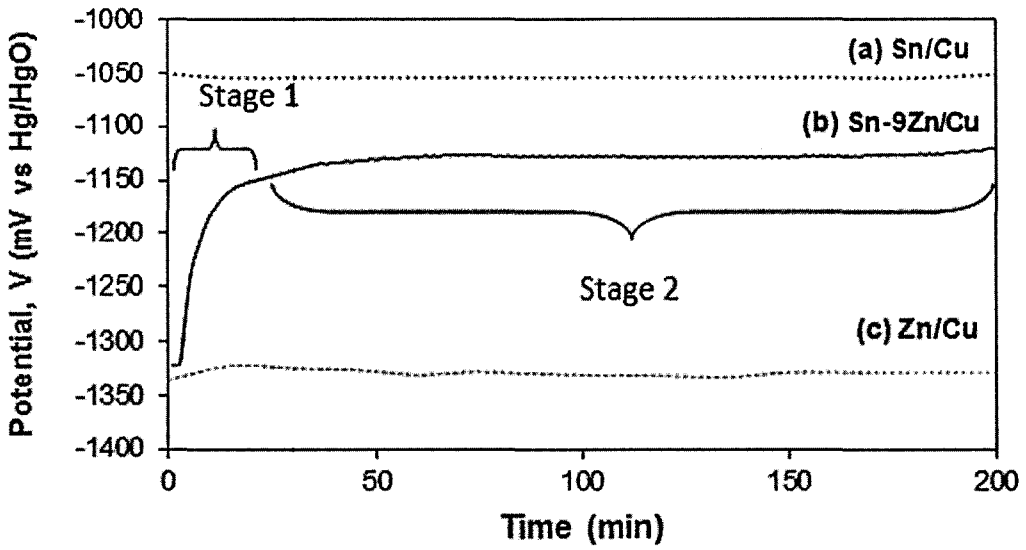

Figure 1: Corrosion potential plots of (a) Sn/Cu, (b) Sn-9Zn/Cu and (c) Zn/Cu against time in 6 M KOH

The value of the initial potential obtained for Sn-9Zn/Cu at -1330 mV is almost the same as the open circuit potential of Zn/Cu in 6 M KOH. Zn is the first to be dissolved in 6 M KOH because it is more active than Sn and Cu. The specific reaction of Zn removal from Sn-9Zn/Cu at the early stage leads to dealloying or dezincification. The preferential dissolution process of specific elements in an alloy compound has also been observed by Alfantzi et al. [16]. This dissolution process contributes to the initiation of potential in Stage 1, according to the reaction [17]:

$$Zn \rightarrow Zn^{2+} + 2e^{-} \qquad (1)$$

There is a large amount of OH^- ions in KOH electrolyte. As a result, the ions have higher ability to reach the solder alloy surface, contributing to the formation of ZnO [17]:

$$Zn^{2+} + 2\ OH^- \rightarrow Zn(OH)_2 \qquad (2)$$

$$Zn(OH)_2 \rightarrow ZnO + H_2O \qquad (3)$$

ZnO production and deposition causes Zn depletion and increased potential from -1330 mV to a much nobler value of -1120 mV. Once the solder surface is covered with ZnO, the contact between Zn and OH^- becomes difficult, leaving the potential to be saturated. Consequently, Stage 2 is allowed to start at a nobler potential value.

Given that Zn is the minor element in Sn-9Zn, Zn is quickly depleted or blocked by ZnO on the surface. Thus, Sn can be dissolved as the second most active material after Zn in this system. According to Alvarez et al. [18], Sn dissolves and passivates:

$$Sn + 2OH^- \rightarrow Sn(OH)_2 + 2e^- \qquad (4)$$

$$Sn(OH)_2 \rightarrow SnO + H_2O \qquad (5)$$

Subsequently, $Sn(OH)_4$ species form:

$$SnO + H_2O + 2OH^- \rightarrow Sn(OH)_4 + 2e^- \quad (6)$$

$$Sn(OH)_2 + 2OH^- \rightarrow Sn(OH)_4 + 2e^- \quad (7)$$

This species then dehydrates:

$$Sn(OH)_4 \rightarrow SnO_2 + 2H_2O \quad (8)$$

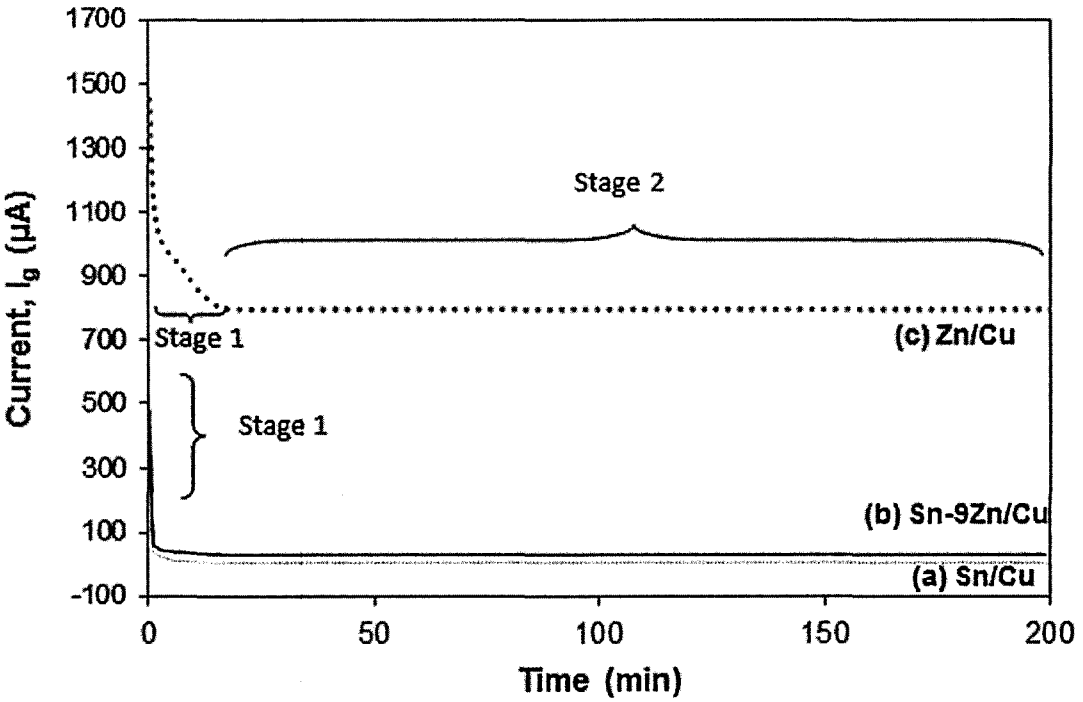

Figure 2: Corrosion current plots of (a) Sn/Cu, (b) Sn-9Zn/Cu and (c) Zn/Cu against time in 6 M KOH

Figure 2 shows the variations in the corrosion current (*i*) of Sn/Cu, Zn/Cu and Sn-9Zn/Cu in 6 M KOH solution. In general, all *i* profiles show sudden reductions immediately after immersion before forming steady plateaus. Zn gives the highest initial *i* at 1470 μA, which quickly drops to 1000 μA within only 5 min. This phenomenon is followed by a steady decrease for 20 min until reaching a stable *i* plateau at 800 μA. The starting current value for Sn-9Zn/Cu is 490 μA and *i* immediately plummets to ~10 μA. Within only 5 min, a steady plateau is formed and stabilized until the end of immersion. The *i* profile of Sn/Cu is strikingly similar to that of Sn-9Zn/Cu in 6 M KOH solution, except for a much lower initial *i* at 133.5 μA. The formation of a stable plateau of potential has also been achieved by other researchers [19, 20], who confirm that the formation of a surface corrosion product layer is attributed to Stage 2.

The fast reduction of *i* implies that Sn-9Zn alloy reverses its behavior upon contact with KOH. The passivation of alloys may contribute to this behavioral change. During the early stage of immersion, Sn-9Zn behaves anodically and Zn, as the most active material in the alloy, is the first to be oxidized. As a result of interaction with OH^- ions, the corrosion product ZnO is formed and deposited, thereby acting as a barrier for protecting Sn-9Zn from further reaction with OH^-. Accordingly, the surface of Sn-9Zn changes and becomes cathodic.

A large *i* signifies that the system undergoes high-magnitude corrosion [20, 21]. Zn/Cu gives the highest initial and stabilized *i* values in 6 M KOH solution. The position of the metal in the galvanic series plays a major contribution in corrosion. Zn/Cu is farther in this series compared with Sn-9Zn/Cu and Sn/Cu. Thus, a large value of *i* is produced because anode Zn is consumed rapidly in 6 M KOH. The small amount of Zn in Sn-9Zn allows Sn-9Zn/Cu to possess a slightly higher initial *i* than Sn/Cu. However, once Zn is depleted, *i* drops and the profile becomes identical with Sn/Cu.

3.1.3.2 Morphological, elemental and phase analyses

Figure 3a shows the FESEM image of Sn-9Zn alloy before the corrosion analysis. The microstructure of Sn-9Zn is as expected from an alloy of eutectic composition. The fine eutectic lamellar structure is found in the form of dark needle-like Zn-rich phases distributed in the matrix of Sn. After immersion in 6 M KOH (**Figure 3b**), the surface roughens. The deposition of corrosion products as a compound is believed to be the reason for this characteristic. This rough layer covers the entire surface. However, there are significant cracks on this layer.

EDX analysis was performed on the Sn-9Zn solder surface before and after immersion in 6 M KOH. Sn has the dominant percentage (91 wt %) in Sn-9Zn before immersion in the scanned area (**Figure 3a**). After immersion (**Figure 3b**), three elements, Sn, O and Zn, are detected. Sn still dominates the composition at 63 wt %, followed by O as the new element (22 wt %) and finally Zn (14 wt %). The detection of O forming the corrosion product compound with Sn and Zn confirms that OH^- reacts with the oxidized Sn and Zn during immersion in 6 M KOH. The corrosion products can either be SnO, SnO_2, ZnO or the combinations of all these oxides. There are observed cracks linked with one another on the surface of the rough corrosion product layer, suggesting that the layer formed is brittle and mechanically weak.

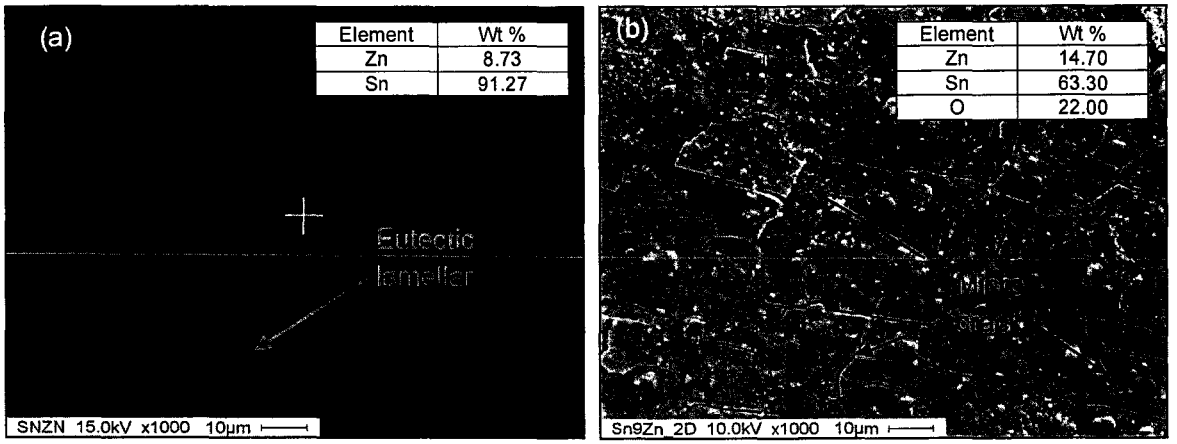

Figure 3: Microscopy and elemental analyses of Sn-9Zn (a) before and (b) after immersion in 6 M KOH

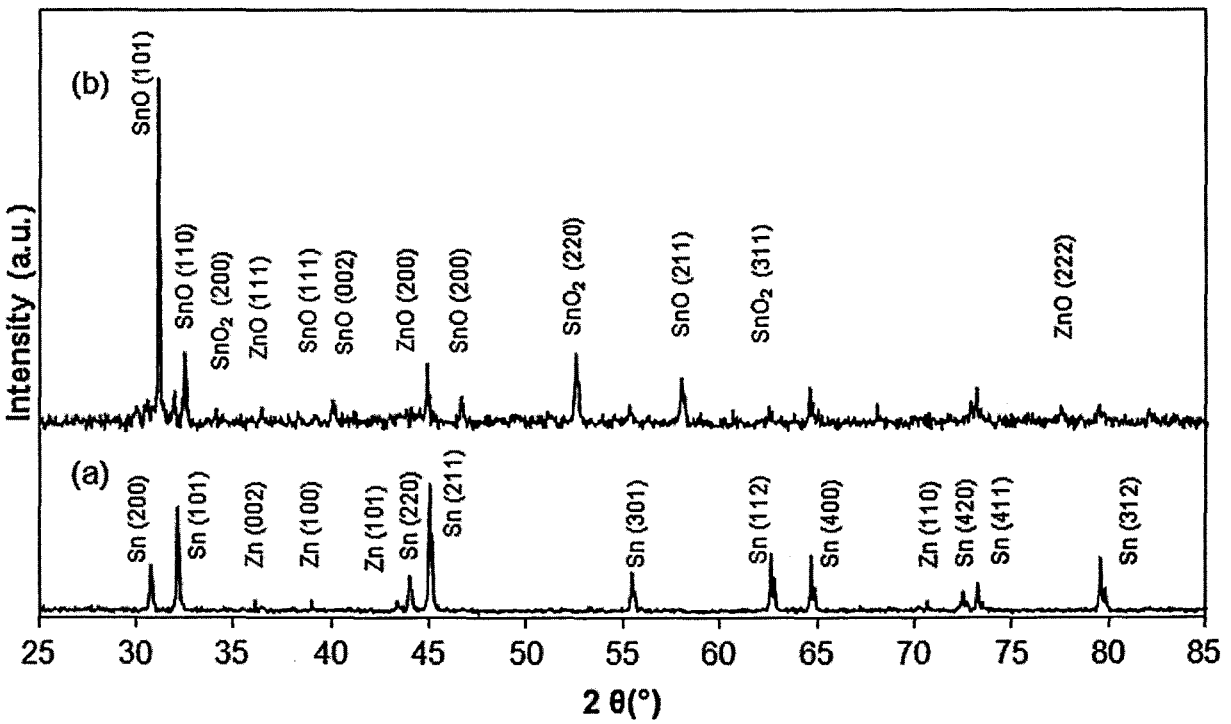

Figure 4: XRD patterns of Sn-9Zn (a) before and (b) after immersion in 6 M KOH

Figure 4 shows the XRD pattern of Sn-9Zn before and after immersion in 6 M KOH. Two phases are detected for Sn-9Zn solder before immersion, namely, those of Sn and Zn. This result is in accordance with that obtained from EDX analysis. Sn is matched with ICDD file no. 03-065-2631, whereas 01-087-0713 is for Zn. There are 10 different peaks of Sn observed, with Sn (211) as the most dominant at $2\theta = 44.91°$. On the other hand, only four peaks of Zn are found. Significant changes in the phases are observed after immersing Sn-9Zn in 6 M KOH. Three new phases of tin oxides, namely, SnO (ICDD 00-024-1342) and SnO_2 (ICDD 00-033-1374), are recorded. In contrast, the only zinc oxide is ZnO (ICDD 03-065-0682). Among the three new phases, SnO is the major oxide as evidenced by six different peaks and shows the highest intensity at 30.80° (101).

The original peaks of Sn and Zn are either decreased or diminished after coming into contact with 6 M KOH. The loss of intensities highlights that both original phases are either consumed to produce the new oxide phases as corrosion products or undetected as a result of being covered by the deposited rough corrosion product layer. Thus, the results of the corrosion potential and current analyses, as well as microstructural analysis are further validated.

3.1.3.3 Mechanical property analysis

The effect of KOH solution on the mechanical properties of Cu/Sn-9Zn/Cu butt joint is shown in **Figure 5**. The stress obviously increases linearly with increased load.

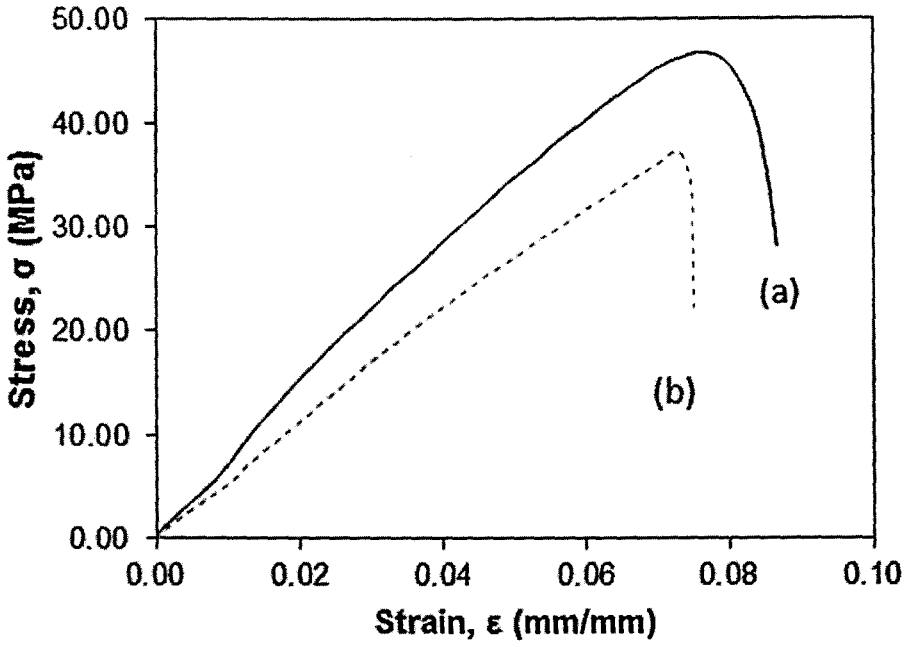

Figure 5: Stress-strain curves of Cu/Sn-9Zn/Cu butt joint (a) before and (b) after immersion in 6 M KOH

The ultimate tensile strength (UTS) of the as-prepared joint is 45 MPa and peaks at a strain value of 0.075. However, after immersion, the Cu/Sn-9Zn/Cu butt joint undergoes reduction in both UTS and strain. The UTS is reduced by 22% to 35 MPa after immersion. On the other hand, the strain at the UTS changes to 0.074. The stress-strain curves also reveal that the tensile stress value sharply drops after the peak compared with the as-prepared joint. This result indicates the lack of ductility of the joint after immersion.

Figure 6 shows the macrostructural images of as-prepared Cu/Sn-9Zn/Cu butt joint after immersion in 6 M KOH and after failure under tensile loading. The as-prepared joint (**Figure 6a**) reveals that the Cu plates are well attached to the shiny, grayish Sn-9Zn solder. After immersion

(**Figure 6b**), the solder are significantly darkened, enabling the boundaries between the Cu plates and Sn-9Zn to become clearer. The solder region also appears to be dull and has lost its original appearance before immersion. The post-tensile analysis image is shown in **Figure 6c**. The joint failure is due to the formation of crack through the solder region, implying that the interfaces of the joint are well connected. Small necking regions can be observed along the crack.

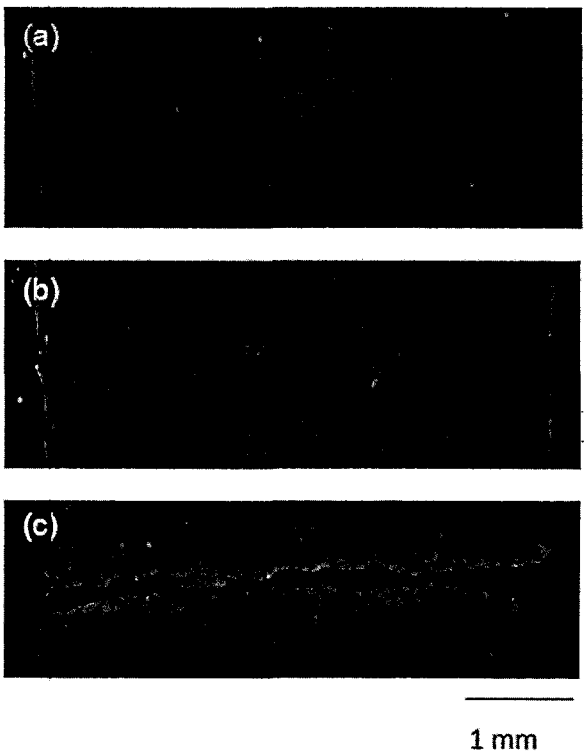

Figure 6: Macroscopic images of Cu/Sn-9Zn/Cu butt joint (a) before immersion in 6 M KOH, (b) after immersion in 6 M KOH and (c) after tensile test

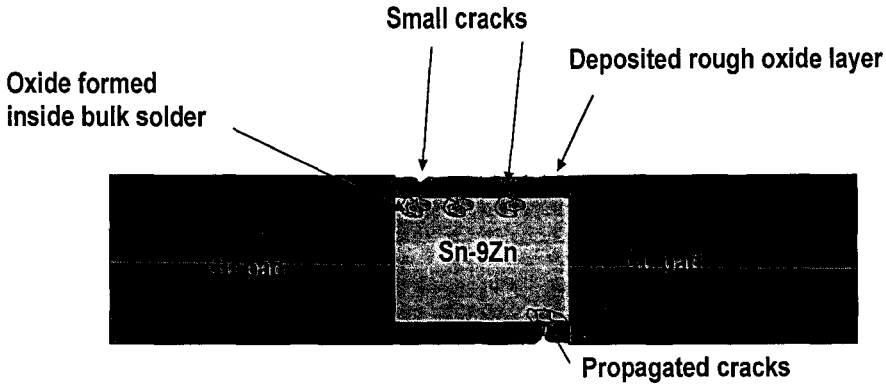

Figure 7: Schematic diagram of Cu/Sn-9Zn/Cu butt joint after immersion in 6 M KOH (side view)

Figure 7 shows the schematic diagram of Cu/Sn-9Zn/Cu butt joint after immersion in 6 M KOH. Sn and Zn from the bulk solder region are consumed to produce SnO, SnO_2 and ZnO, leading to the formation of small cracks. The oxides produced are co-deposited and forms a rough oxide layer on the solder surface. With the brittle nature of oxides replacing Sn and Zn, the mechanical integrity of the joint is weakened. The existence of linked cracks throughout the surface also allows further penetration of OH^- into the rough oxide layer, causing the cracks to propagate deeper in the bulk solder region and produce more undesirable brittle oxides. Accordingly, the strength of the joint is directly affected, causing UTS loss and sharply decreased tensile stress after UTS is achieved as load applied to the joint.

3.1.4 Summary

The corrosion potential and current of Sn-9Zn changes in two stages with increased immersion time in 6 M KOH. Complex oxides develop on the solder surface to stutter the

dissolution of active materials in the first stage. The formation of the corrosion product layer consequently produces the stable second stage. The stress-strain curve shows UTS loss after immersing the Cu/Sn-9Zn/Cu butt joint in 6 M KOH. This result shows that the reliability of the Sn-9Zn solder joint is significantly affected when in contact with KOH electrolyte in real-life applications. The formation of linked cracks as revealed by FESEM makes the oxides more brittle, allowing further penetration of OH^- on the solder surface and consequently weakening the joint strength.

3.1.5 References

1. M. Abtew, G. Selvaduray, *Mater. Sci. Eng. R-Rep.*, 27 (2000) 95-141.
2. Q.V. Bui, N.D. Nam, B.I. Noh, A. Kar, J.G. Kim, S.B. Jung, *Mater. Corros.*, 61 (2010) 30-33.
3. R.K. Shiue, L.W. Tsay, C.L. Lin, J.L. Ou, *Microelectron. Reliab.*, 43 (2003) 453-463.
4. T.-C. Chang, S.-M. Chou, M.-H. Hon, M.-C. Wang, *Mater. Sci. Eng. A- Struct. Mater. Prop. Microstruct. Process*, 429 (2006) 36-42.
5. T.-C. Chang, M.-H. Hon, M.-C. Wang, *J. Electron. Mater.*, 32 (2003) 516-522.
6. T.-C. Chang, J.-W. Wang, M.-C. Wang, M.-H. Hon, *J. Alloy. Compd.*, 422 (2006) 239-243.
7. M.N. Islam, Y.C. Chan, M.J. Rizvi, W. Jillek, *J. Alloy. Compd.*, 400 (2005) 136-144.
8. D. Li, P.P. Conway, C. Liu, *Corrosion Sci.*, 50 (2008) 995-1004.
9. K.-L. Lin, T.-P. Liu, *Mater. Chem. Phys.*, 56 (1998) 171-176.
10. U.S. Mohanty, K.-L. Lin, *Mater. Sci. Eng. A- Struct. Mater. Prop. Microstruct. Process*, 406 (2005) 34-42.

11. U.S. Mohanty, K.-L. Lin, *Corrosion Sci.*, 48 (2006) 662-678.

12. U.S. Mohanty, K.-L. Lin, *Appl. Surf. Sci.*, 252 (2006) 5907-5916.

13. U.S. Mohanty, K.-L. Lin, *Corrosion Sci.,* 50 (2008) 2437-2443.

14. F. Rosalbino, E. Angelini, G. Zanicchi, R. Carlini, R. Marazza, *Electrochim. Acta*, 54 (2009) 7231-7235.

15. F. Rosalbino, E. Angelini, G. Zanicchi, R. Marazza, *Mater. Chem. Phys.*, 109 (2008) 386-391.

16. A.M. Alfantazi, T.M. Ahmed, D. Tromans, *Mater. Des.*, 30 (2009) 2425-2430.

17. A.A. Mohamad, *J. Power Sources*, 159 (2006) 752-757.

18. P.E. Alvarez, S.B. Ribotta, M.E. Folquer, C.A. Gervasi, J.R. Vilche, *Corrosion Sci.,* 44 (2002) 49-65.

19. D. Mercier, M.G. Barthes-Labrousse, *Corrosion Sci.,* 51 (2009) 339-348.

20. N.A. Popovich, R. Govind, *J. Power Sources*, 112 (2002) 36-40.

21. N.M. Taher, A.S. Al Jabab, *Dent. Mater.,* 19 (2003) 54-59.

22. W. Xue, C. Wang, H. Tian, Y. Lai, *Surf. Coat. Technol.*, 201 (2007) 8695-8701.

3.2 Corrosion of Sn-3.0Ag-0.5Cu Thin Films on Cu Substrates in Alkaline Solution

3.2.1 Introduction

The drive for lead-free solders in the microelectronics industry presents a number of new reliability challenges, especially from failure due to corrosion. The progressive decrease in metal feature sizes has rendered bondwires, bondpads, and board-level interconnects increasingly susceptible to corrosion failure. Many times, the electronic components are exposed to different corrosive chemical and physical environments that involve ionic species, such as hydroxides, chlorides, hydrogen, sodium, potassium and carbonate ions. Although large endeavors and preventive methods have been performed to protect the solder joints from working environments, the joints continue to corrode due to the absorbed moisture and corrosive particles that are ubiquitous in the environment, even in a clean room, and these particles are notably difficult to exclude completely. Stringent measurements to decrease the ionic contamination in molding compounds and clean room chemicals have been practiced to reduce the corrosion potential [1].

The corrosion present in solder joints may change the microstructure of the corroded regions, which, in turn, decreases its mechanical properties by providing a crack initialization location [2]. However, the performance of Sn-3.0Ag-0.5Cu (SAC305) in alkaline solution has not been reported, although it is of significant importance as an electrolyte for the alkaline batteries used in automotive and electronic devices. Generally, potassium hydroxide (KOH) is preferable because its solutions are more conductive [3]. Because the alkaline battery is embedded in the electronic system, there is a risk of electrolyte leakage during its application. This leakage, in turn, causes the electrical circuit to be exposed to a corrosive KOH environment, and the leakage of the electrolyte could be catastrophic to the circuit.

Therefore, the corrosion behavior of the SAC305 thin film in KOH solution should be taken into account to achieve a better understanding of the issue. The present analysis employed a potentiodynamic polarization test to examine the corrosion and electrochemical behavior of SAC305 thin film solder alloy in 6 M KOH solution. In addition, the surface morphology, elemental composition and phase were determined to understand the corrosion and structure property relationships in thin films.

3.2.2 Experimental

A total mass of 0.3 g of SAC305 solder wire was weighed prior to thermal evaporation deposition. The deposition of SAC305 solder wire onto the Cu plate was performed using an Edward Autolab 306 automatic thermal evaporator. During the evaporation, a pressure of 3.4 x 10^{-5} torr and a voltage of 7 V was applied to enable the SAC305 to evaporate and deposit onto the Cu plate (as-deposited SAC305/Cu sample). The as-deposited SAC305 thin films on Cu plates were subsequently reflowed on a hot plate at 230, 240, 250, and 260 °C for 30 s to promote an interfacial reaction (as-reflowed SAC305/Cu sample).

Electrochemical measurement was carried out in a single compartment cell using a standard three-electrode configuration: Hg/HgO electrode as the reference electrode with a platinum electrode as the counter and samples as the working electrode. The surface area exposed to the test solution was 1.0 cm^2. This test was conducted in 6 M KOH solution at room temperature (25 °C). Autolab PGSTAT-30 GPES (Eco Chemie, B.V.) was used to control the potential. Potentiodynamic polarization curves were recorded in the potential range of -2.00 to +2.00 V vs. Hg/HgO reference electrode at a scan rate of 10 mV s^{-1} after allowing a steady-state potential to develop.

All of the samples were studied at the top and the cross-sectioned surface prior to and after the potentiodynamic polarization. A Bruker AXS D9 diffractometer was used for X-ray diffraction (XRD) characterization to identify the phases present. Field Emission Scanning Electron Microscopy (FESEM) using a Zeiss Supra^{TM} 35VP with energy dispersive X-ray (EDX) was used for microstructural and element compositional analysis, respectively.

3.2.3 Results and Discussion

3.2.3.1 Characterization at initial condition

Figure 1 and **2** show the top surface microstructures and XRD diffraction patterns of all the studied samples, respectively. Bare Cu (**Figure 1a**) exhibits a rather rough surface, owing to manual grinding, having sharp and intense peaks stemming from the Cu crystal phase (ICDD 01-085-1326) at 43.33°, 50.45° and 74.13° (**Figure 2a**). Meanwhile the as-deposited SAC305/Cu shows a bumped, continuous film (**Figure 1b**). The majority of the Braggs peaks are of β-Sn phase with Cu phase and slight traces of the Cu_6Sn_5 crystal phase (**Figure 2b**). Ag_3Sn phases (ICDD 00-044-1300) were also present in the as-deposited SAC305/Cu. However, owing to its low concentration, the Ag_3Sn reflections are too low to be observed in the XRD diffractogram. The peaks of β-Sn and Cu_6Sn_5 matched with the standard peaks of ICDD 00-004-0673 and ICDD 00-045-1488, respectively.

After solder reflow (**Figure 1c**), the microstructure changed into a layered, continuous film with reduced surface roughness. Additionally, EDX reveals the presence of O with 13.84 to 31.55 at% at the surface, indicating that oxidation had occurred during solidification. All of the as-reflowed SAC305/Cu at 230, 240, 250 and 260 °C (**Figure 2c-f**) displayed identical reflections. Notably, after solder reflow, most of the β-Sn phases diminished and reduced. In contrast, the Braggs peaks of Cu_6Sn_5 and Ag_3Sn became more evident. Moreover, new phases of

IMCs were formed and confirmed to be Cu_3Sn (ICDD 03-065-4653) and SnO (ICDD 00-006-0395).

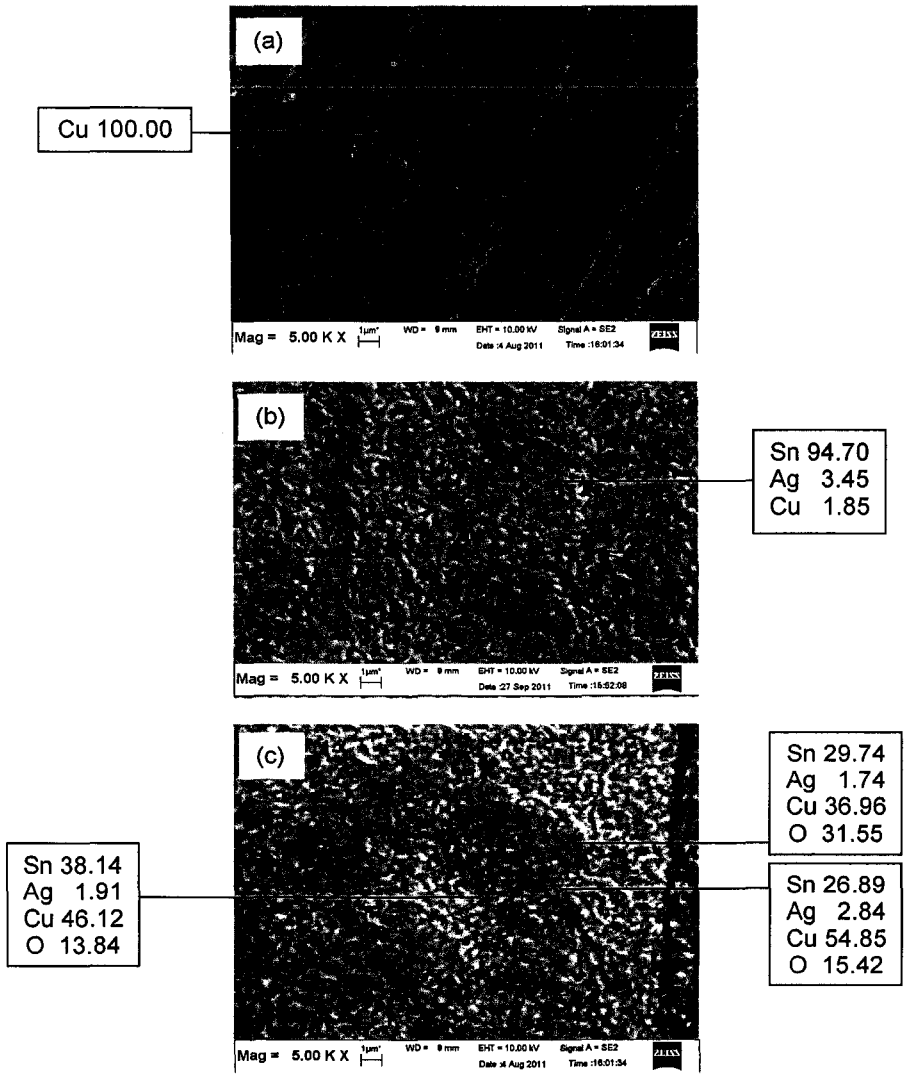

Figure 1: FESEM micrographs of the top surface of (a) bare Cu plate, (b) as-deposited SAC305/Cu (red arrows show the grain boundaries), and (c) as-reflowed SAC305/Cu at different reflow temperatures before the potentiodynamic polarization.

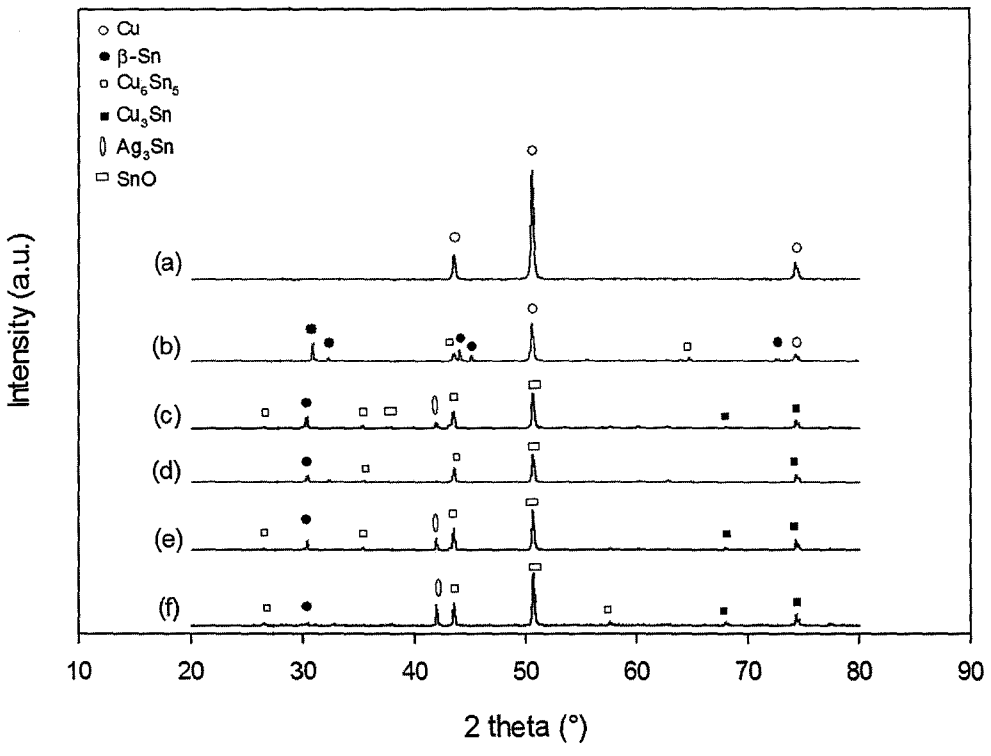

Figure 2: XRD patterns from the top surface of (a) bare Cu, (b) as-deposited SAC305/Cu, and as-reflowed SAC305/Cu at (c) 230, (d) 240, (e) 250 and (f) 260 °C for 30 s prior to the potentiodynamic polarization.

During deposition, the SAC305 atoms grow into grain-like structures. Next, these grains bump into each other and coalesce into a continuous form with a certain degree of surface roughness [1]. After solder reflow, the thin film appearance became smoother. It appears that the neighboring grains are merging with each other, which can be observed from the disappearing grain boundaries as arrowed in **Figure 1b**. XRD analysis revealed that solder reflow promotes the formation of Ag-Sn and Cu-Sn IMCs. Thus, the peak of Ag_3Sn became observable. The thin film solder contains limited Ag. This in turn resulted in insufficient material to form large structures. Moreover, the stable Ag_3Sn further restricts the solubility of Ag in the β-Sn phase.

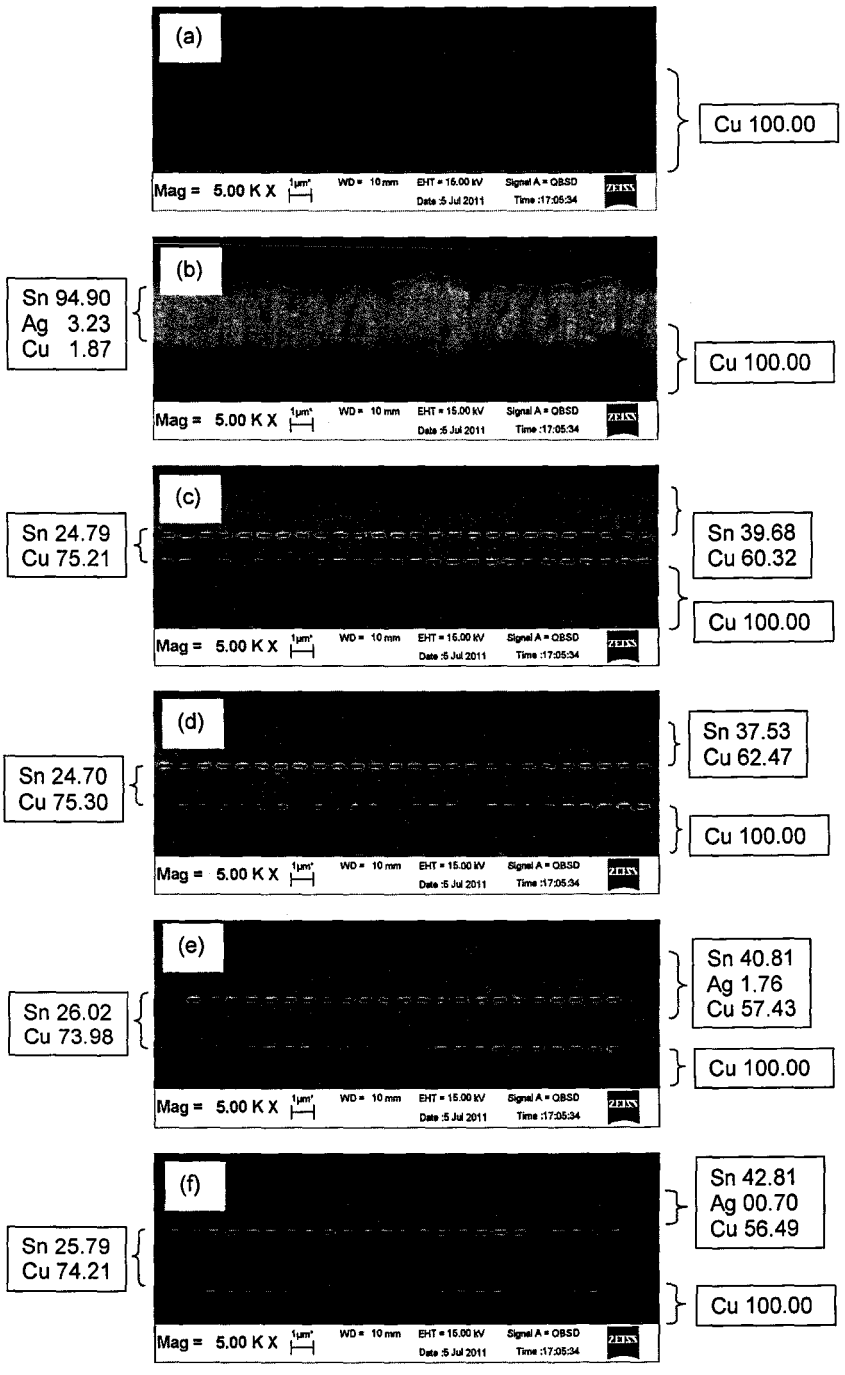

Figure 3: FESEM micrographs of the cross-sectional surface of (a) bare Cu plate, (b) as-deposited SAC305/Cu and as-reflowed SAC305/Cu at (c) 230, (d) 240, (e) 250 and (f) 260°C reflow temperatures before the potentiodynamic polarization.

The cross-sectional views of all samples prior to the potentiodynamic polarization measurement are also provided in **Figure 3**. **Figure 3a** shows that the bare Cu has a typical one-phase appearance, whereas the as-deposited SAC305 thin film (**Figure 3b**) comprises two layers. The top white layer is the SAC305 solid layer. This layer comprises loose SAC305 particles that adsorb physically to the Cu substrate. It is clear that the thickness of the deposited thin film is not uniform across the substrate.

After solder reflow, an interfacial reaction occurred. As shown in **Figure 3c-f**, two layers of IMCs formed. The top region is Cu_6Sn_5, and the layer beneath is Cu_3Sn. Cu_6Sn_5 has irregular thickness and a scallop-type structure, whereby the very thin Cu_3Sn has a more uniform thickness and a layer-like morphology. However, to some extent, it follows the topography of the adjacent Cu6Sn5 phase layer. EDX analysis determined that the composition of Cu_6Sn_5 consists of 39.68 at% Sn and 60.32 at% Cu. It was found to be depleted by 4-5 at% Sn compared with published literature values [4-7]. In contrast, Cu_3Sn has a composition of 24.79 at% Sn and 75.21 at% Cu. Obviously; the thin film SAC305 solder reacted completely with the excessive Cu substrate to form Cu_6Sn_5 during the reflow. The Cu_3Sn intermetallic layer was consistently increased as the temperature increased, while the Cu_6Sn_5 gradually decreased with increased reflow temperatures.

The formation of an IMC layer is mainly due to the diffusion of Cu atoms into the molten solder matrix during the reflow, as reported by Yoon et al. [8], who evaluated the interfacial reactions of Cu/eutectic Sn–Ag–Cu/Cu sandwich solder joints during isothermal aging at 150 °C. The dissolved Cu atoms precipitated to form IMCs in the solder matrix. Cu_6Sn_5 first forms during the wetting reaction between the liquid Sn and Cu. It is believed that Cu_6Sn_5 has a high rate of growth at the SAC305/Cu interface [9]. The formation depletes Sn. To a certain extent,

when the supply of Sn through the interfacial IMC is more restricted than the supply of Cu from the substrate, the Cu_6Sn_5 layer that formed initially will transform into Cu_3Sn [10]. Thus, the initial formation of a very thin layer of Cu_3Sn comes from the solid-state reaction between Cu_6Sn_5 and Cu in the reflowing process. Hence, it is expected that its thickness will be much smaller than that of Cu_6Sn_5.

3.2.3.2 Potentiodynamic Polarization Curves

Figure 4 compares the polarization curves for bare Cu, as-deposited SAC305/Cu and as-reflowed SAC305/Cu during immersion in 6 M KOH solution. It is expected that bare Cu has a different polarization curve compared with the other samples. However, as-deposited SAC305/Cu and as-reflowed SAC305/Cu have almost identical trends because they are composed of the same material. The Cu has a higher equilibrium potential than that of as-reflowed SAC305/Cu and as-deposited SAC305/Cu. The as-deposited SAC305 thin film contains a high content of Sn atoms, whereas Sn reacted rapidly with Cu to form Cu-Sn IMCs during the reflow. Thus, a significant shift of the equilibrium corrosion potential toward noble values occurred as the Cu amount increased. The corrosion current densities were obtained through the potentiodynamic polarization corrosion supplied by the Tafel method. Also, other corrosion-related parameters were subsequently summarized in **Table 1**.

The polarization curves are started with a similar cathodic region, ranging from -1.5 to -1.1 V vs. Hg/HgO. During polarization in KOH solution, the only possible cathodic reaction is the reduction of dissolved oxygen to form hydroxide (OH^-) ions:

$$O_2 + 2H_2O + 4e^- \rightarrow 4OH^- \qquad (1)$$

When the current density reaches about 10 m A cm^{-2}, many hydrogen bubbles evolve from the cathode due to hydrogen evolution on the cathode.

$$2H_2O + 2\,e^- \rightarrow H_2 + 2OH^- \qquad (2)$$

The turning point of the curve was represented at the beginning of anodic scan, which is also the start of the active region.

Although Cu is a noble metal, corrosion proceeds with the presence of dissolved oxygen. From -1.1 V vs. Hg/HgO, the current increases as potentials increases, Cu is in an active region. As the potential increases further to -0.4 V vs. Hg/HgO (peak I), formation of Cu (I) spesies to form Cu_2O as a film on the surface via the general reaction [11]:

$$2Cu + 2OH^- \rightarrow Cu_2O + H_2O + 2e^- \qquad (3)$$

Then, second oxidation of Cu occurs when the electrode potential rises to that required for dehydration to form Cu (II) species and formation of CuO at the interface in 6 M KOH (peak II) [12].

$$Cu \rightarrow Cu^{2+} + 2e^- \qquad (4)$$

$$Cu^{2+} + 2OH^- \rightarrow Cu(OH)_2 \leftrightarrow CuO + H_2O \qquad (5)$$

$$Cu + 2OH^- \rightarrow CuO + H_2O + 2e^- \qquad (6)$$

In the as-deposited SAC305/Cu case, in the active region, ranging from -1.1 to -1.0 V vs. Hg/HgO, electron transfer occurs followed by chemical reaction to form the final product potassium stannite (peak III).

$$Sn + 2OH^- \rightarrow Sn(OH)_2 + 2e^- \qquad (7)$$

$$Sn(OH)_2 + OH^- \rightarrow HSnO_2^- + H_2O \qquad (8)$$

At higher potential, the electrode is blocked by a solid film based on SnO (peak IV). First transition occurs when the blocked electrode potential rises to 0.2 V vs. Hg/HgO for formation of SnO_2 (peak V):

$$Sn + H_2O \rightarrow SnO + 2H^+ + 2e^- \quad (9)$$

$$SnO + 2OH^- \rightarrow SnO_2 + H_2O + 2e^- \quad (10)$$

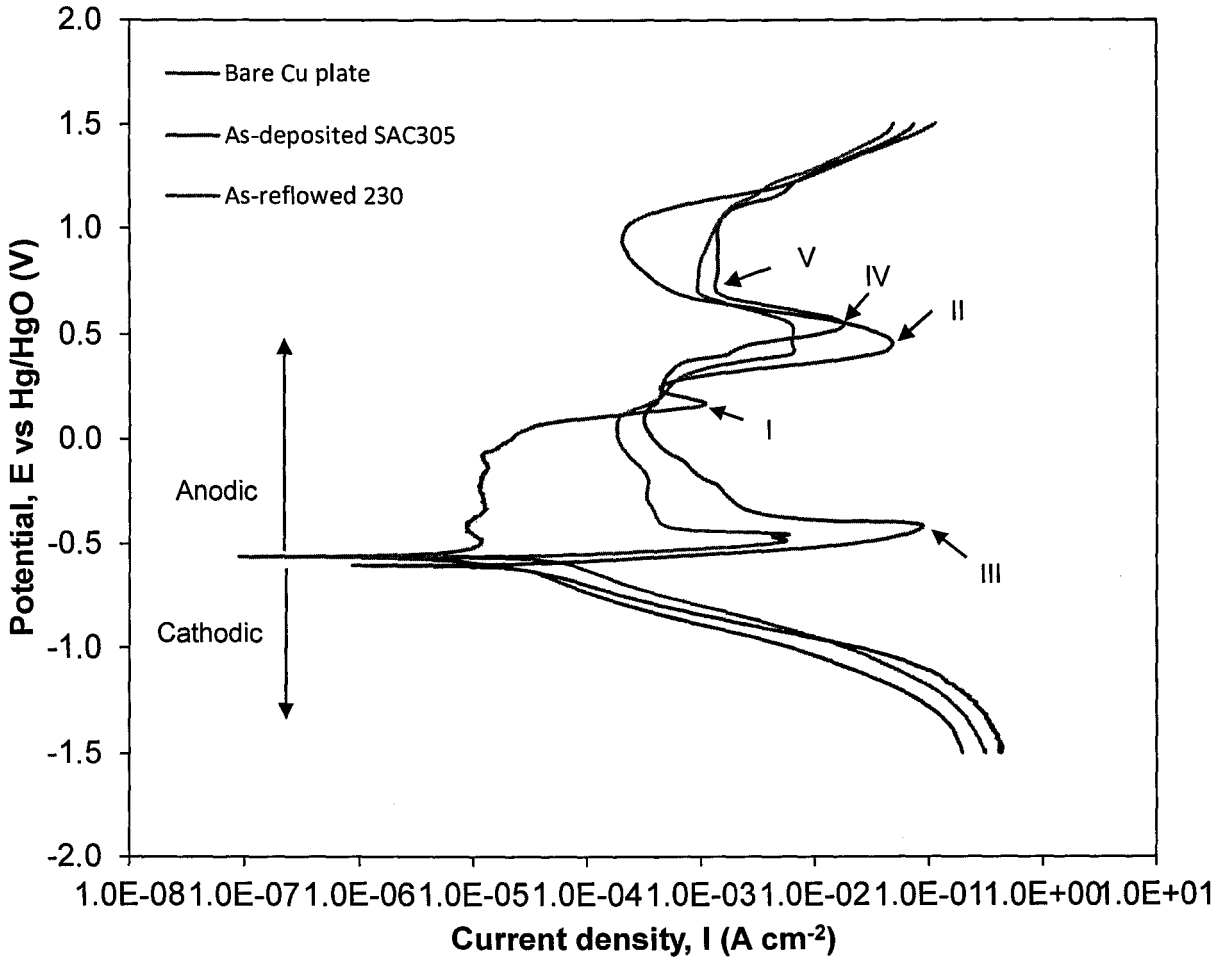

Figure 4: Potentiodynamic polarization curves of the bare Cu plate, the as-deposited SAC305/Cu and the as-reflowed SAC305/Cu after polarized in a 6 M KOH solution.

Table 1: Summary of the corrosion parameters of the bare Cu plate, as-deposited SAC305/Cu and as-reflowed SAC305/Cu.

Sample	E_{corr}, (V vs Hg/HgO)	i_{corr}, ($x10^{-5}$ A cm^{-2})	Pseudopassivation range, (V vs Hg/HgO)
Bare Cu plate	-1.062	0.009	–
As-deposited	-1.105	1.058	+0.00 – +0.50
As-reflowed 230°C	-1.111	2.396	+0.00 – +0.50
As-reflowed 240°C	-1.107	2.802	+0.00 – +0.50
As-reflowed 250°C	-1.094	2.044	+0.00 – +0.50
As-reflowed 260°C	-1.088	1.975	+0.00 – +0.50

Figure 5 shows the potentiodynamic polarization curves for all the studied as-reflowed SAC305/Cu in 6 M KOH. Obviously, all of the as-reflowed SAC305/Cu at 240, 250 and 260 °C displayed identical patterns of polarization curves to the one at 230 °C, demonstrating the behavior in the active, passive, pseudopassive and transpassive regions. The passivation current density is decreased as the reflow temperature increased, while the pseudopassivation domain for all of the as-reflowed SAC305/Cu falls in a comparable potential range. The Sn from the unreacted Sn and Cu_6Sn_5 phase dissolved by OH^- to form $Sn(OH)_2$ and $HSnO_2^-$ at -1.0 V vs. Hg/HgO. When the electrode reaches -0.1 V vs. Hg/HgO, active dissolution of Cu from Cu_6Sn_5 phase occurs, resulting in the formation of CuO film. Consumption of OH^- ions increases the

concentration of water molecules at the interface, causes the dissolution of Sn to form SnO at higher potential. Formation of SnO_2 and CuO occur when the potential rises to 0.2 and 0.5 V vs. Hg/HgO, respectively.

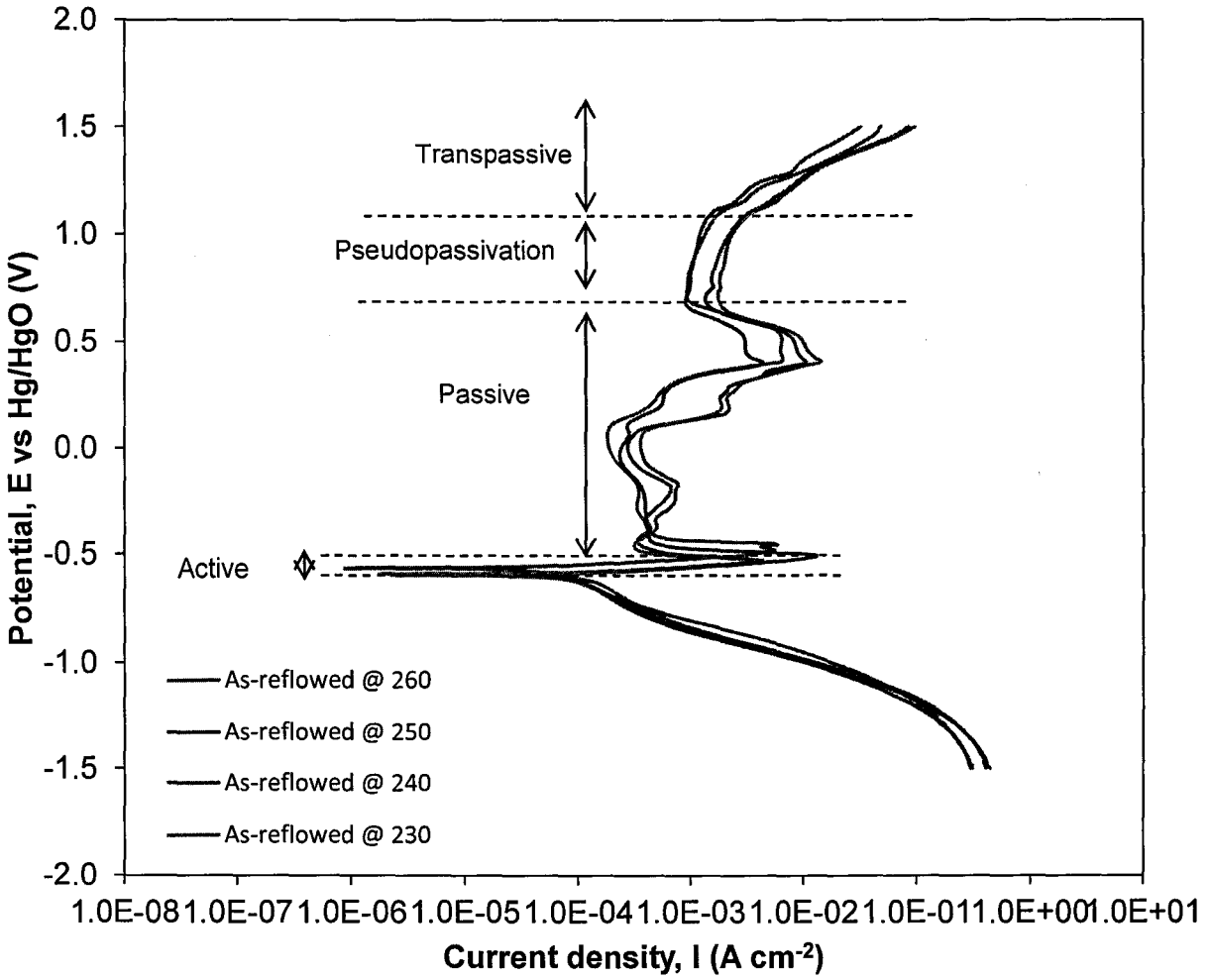

Figure 5: Potentiodynamic polarization curves of the as-reflowed SAC305/Cu at reflow temperatures of 230, 240, 250 and 260 °C, after polarized in a 6 M KOH solution.

The active dissolution of Sn can be explained by the potential difference that exists within the SAC305 solder alloy. As seen in **Table 2**, Sn is the most active metal. Thus, Sn acts as an anode in the alloy and preferentially dissolves in the corrosive conditions.

Table 2: Electrode potentials of elements of solder [2, 15].

Element	Reaction	Electrode potential (V)
Silver	$Ag^{2+} + e^- = Ag$	+ 0.7996
Copper	$Cu^+ + e^- = Cu$	+ 0.5210
	$Cu^{2+} + 2e^- = Cu$	+ 0.3419
Tin	$Sn^{2+} + 2e^- = Sn$	- 0.1375

3.2.3.3 Microstructure and structure of corrosion products

The surface morphology and structural properties of all of the samples at the end of the polarization is illustrated in **Figure 6** and **7**, respectively. **Figure 6a** infers the corroded surface of bare Cu. The surface appears to be rough. The cratering surface of Cu consists of 89.15 at% Cu and 10.75 at% O, which is in good agreement with the experimental reflection that slight traces of CuO phase (ICDD 01-078-0428) at 53.54° and 61.76° (**Figure 7a**). Regarding the as-deposited SAC305/Cu (**Fig. 6b**), it is observed that some of the SAC305 granule bumps had been washed away, exposing the base Cu region underneath. These observations are tally with the XRD data that indicate that the upper layer may be related to the formation of SnO and SnO_2, while the layer underneath is formed by CuO (**Figure 7b**).

Nevertheless, in terms of the microstructure of as-reflowed SAC305/Cu, the surfaces contain pits and a porous structure. For a parallel degree of corrosion, the corroded surface changed and revealed the rounded top region of the groove-like scallop (**Figure 6c**) to a clearer

three-dimensional image of hexagonal-base/spherical-cap geometric model of scalloped Cu_6Sn_5 with triple junction grain boundary sites (**Figure 6d**) followed by the corrosion of layered Cu_3Sn structures (**Figure 6e-f**).

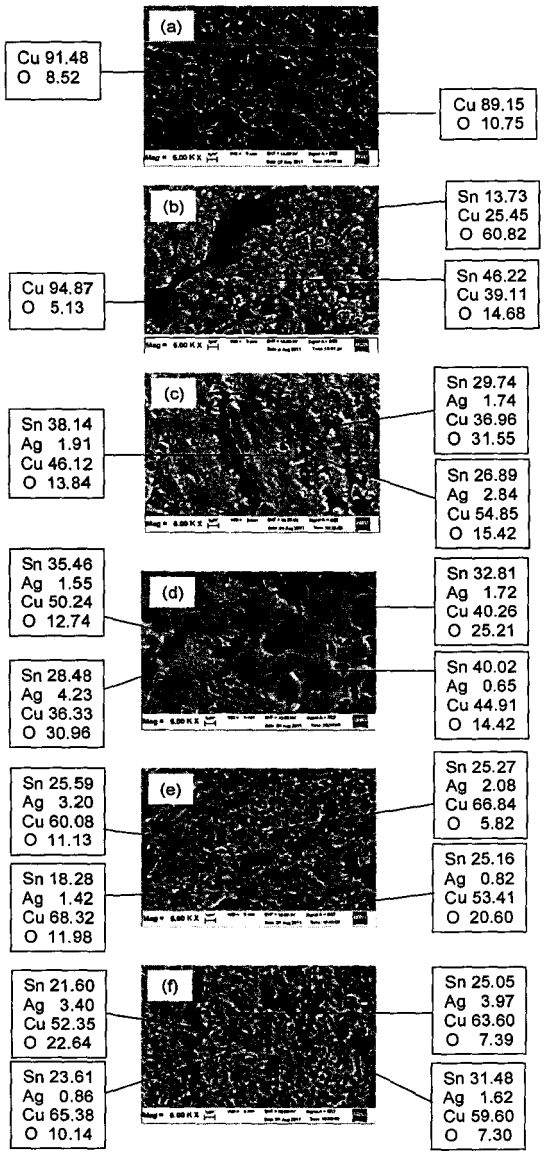

Figure 6: FESEM micrographs of the corroded top surface of (a) bare Cu plate and (b) as-deposited SAC305/Cu, and the as-reflowed SAC305/Cu at reflow temperatures of (c) 230, (d) 240, (e) 250 and (f) 260 °C after the potentiodynamic polarization in 6 M KOH.

As observed, by comparing the microstructures, the corrosion attack becomes less accentuated when it reaches the Cu_3Sn surface. These corroded surface morphologies are aligned with the polarization curves showing that the corrosion resistance of SAC305/Cu increased more with higher solder reflow temperatures than with lower temperatures. The corrosion resistance of Cu_3Sn is better than that of Cu_6Sn_5 because of its higher Cu content [13].

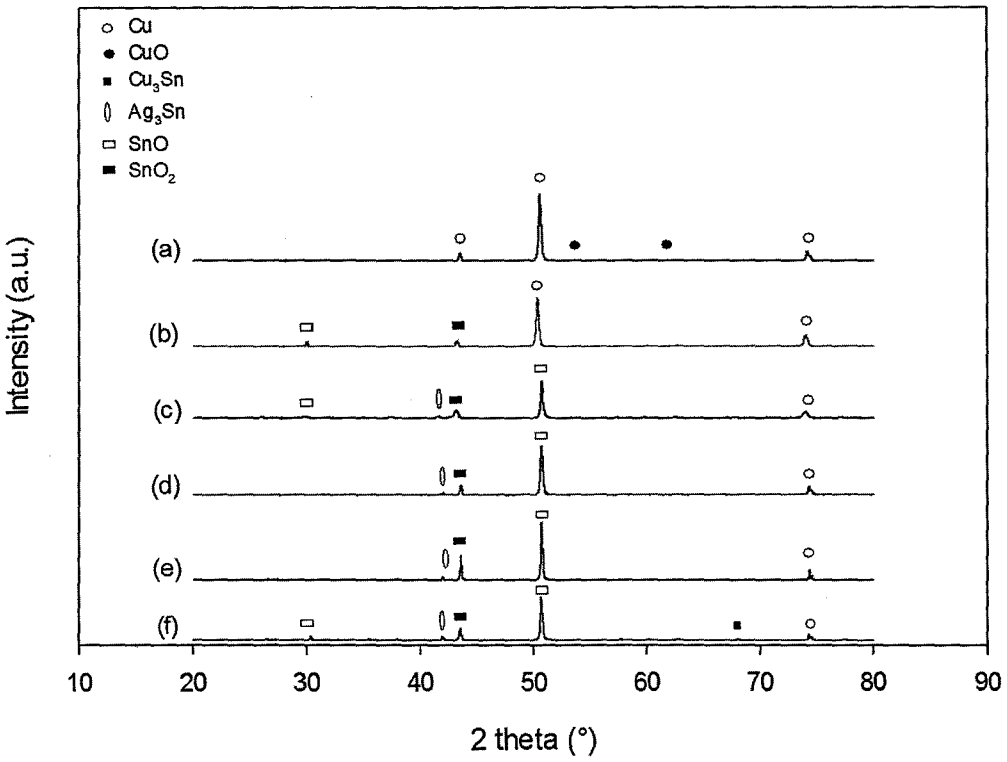

Figure 7: XRD patterns from the top surface of (a) bare Cu, (b) as-deposited SAC305, and as-reflowed SAC305/Cu at (c) 230, (d) 240, (e) 250 and (f) 260 °C for 30 s after the potentiodynamic polarization in 6 M KOH.

The surfaces are covered by oxides and are mainly composed of Sn and O. These oxides are identified as SnO and SnO_2 (**Figure 7c-f**). The presence of SnO and SnO_2 phases in the XRD analysis had confirmed the formation of both passive films during the passivation and pseudopassivation stages in the anodic polarization curve. Also, the Cu-Sn and Ag-Sn

intermetallics are retained after the polarization. The low Ag content found at the corroded surface indicates that Ag was not involved in the corrosion. Ag_3Sn is retained and does not dissolve during the KOH immersion. This compound exhibits cathodic behavior, thereby promoting the dissolution of the β-Sn and Cu-Sn phases.

This finding is in accordance with the study performed by Rosalbino et al. [14], which suggests that the Ag_3Sn and Cu_6Sn_5 phases are protected by the Sn-rich phase and remain unattacked on the surface after polarization in aerated 0.1 NaCl solution. Consequently, they exhibit cathode behavior, thereby promoting the dissolution of the Sn phase.

Figure 8 shows the cross-sectional micrographs of all of the corroded samples after immersion in 6 M KOH. A very thin layer of oxide film formed on the corroded surface of the bare Cu (**Fig. 8a**). The corrosion attack localized at the exposed surface area without penetrating into the bulk Cu area. **Figure 8b** reveals that a portion of the as-deposited SAC305/Cu has been removed, exposing the Cu underneath. The exposed Cu region and the as-deposited SAC305/Cu are subsequently attacked by the KOH solution to form an oxide passive layer on top. Similarly, the surface of all as-reflowed SAC305/Cu is covered with a very thin layer of SnO. Concerning the as-reflowed SAC305/Cu (**Figure 8c-d**), it is clear that corrosion occurred at the top Cu_6Sn_5 layer with the formation of pores, while corrosion reached the underneath Cu_3Sn layer when there is no more protection from the top Cu_6Sn_5 (**Figure 8e-f**).

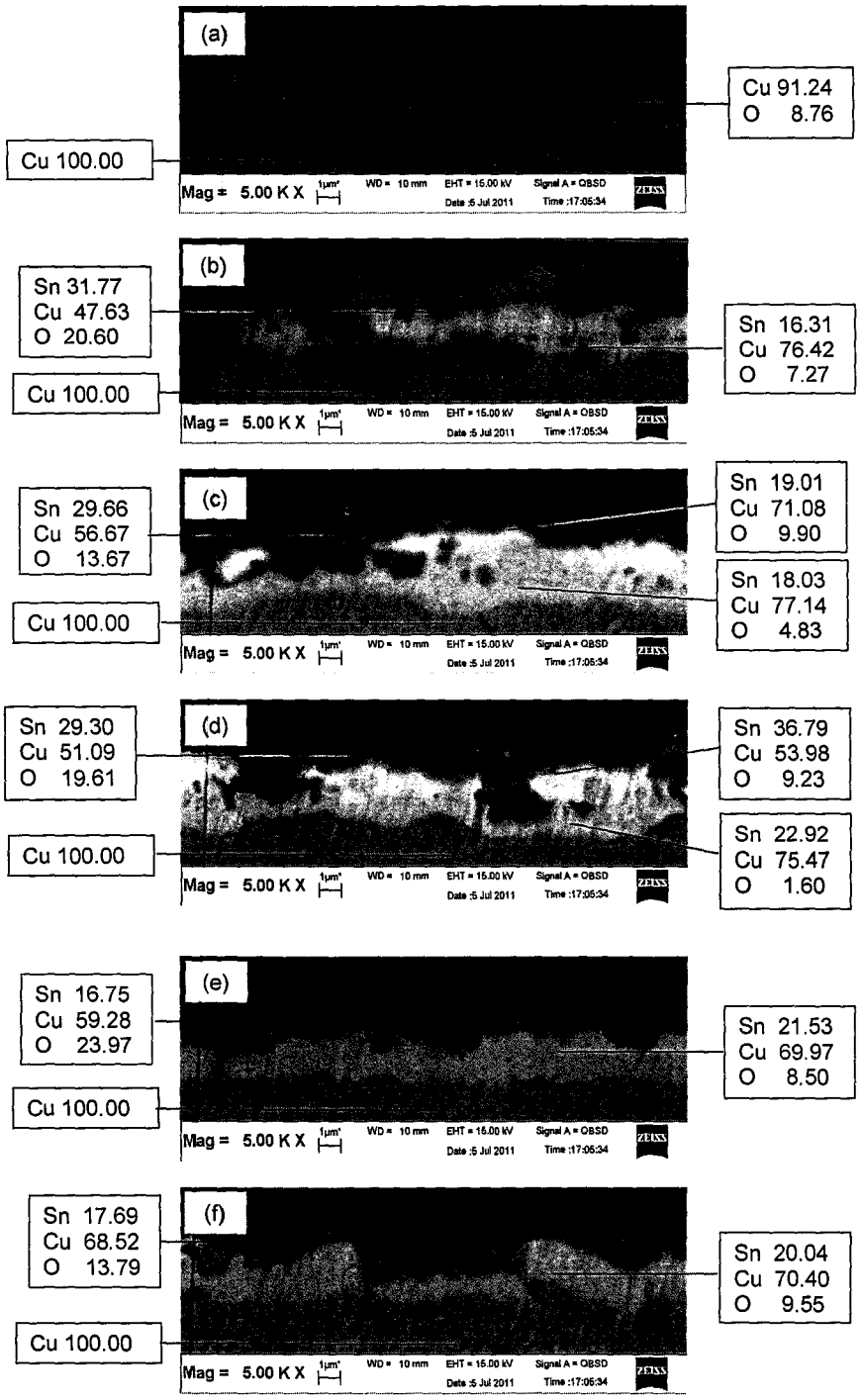

Figure 8: FESEM micrographs of the cross-sectional surface of (a) bare Cu plate, (b) as-deposited SAC305/Cu and as-reflowed SAC305/Cu at (c) 230, (d) 240, (e) 250 and (f) 260 °C reflow temperatures after the potentiodynamic polarization.

3.2.3.4 Corrosion Mechanism of Thin Films

The corrosion phenomenon of SAC305 thin films is illustrated in **Figure 9**. Initially, the SAC305 thin film is physically deposited onto the Cu substrate after the evaporation (**Figure 9a**). During polarization, some of the SAC305 granule bumps directly leached into the KOH solution. Simultaneously, the remaining Sn and the exposed Cu base reacted with the OH^- ions from the KOH solution. Hence, a deposition attack of the solder surface to form an oxide layer occurred (**Figure 9b**).

For as-reflowed SAC305/Cu, most of the Sn had reacted to form Cu-Sn IMCs during solder reflow. As-reflowed SAC305/Cu at a lower reflow temperature range produced a thick Cu_6Sn_5 layer and a thin Cu_3Sn layer beneath, as inferred in **Figure 9c**. During polarization, the small amount of unreacted Sn phase probably dissolved into the solution, while a fraction of Sn^{2+} deposits onto the Cu_6Sn_5 surface to form passivity and pits. Somehow, the corrosion attacked on the outermost interfacial Cu_6Sn_5 IMC when there is no more Sn remaining. Because the Cu_6Sn_5 IMC layer is thick, most of the OH^- reaction occurred at this layer without affecting the Cu_3Sn layer underneath (**Figure 9d**).

In contrast, as-reflowed SAC305/Cu at a higher reflow temperature range was composed of thin Cu_6Sn_5 and thick Cu_3Sn structures (**Figure 9e**). The different thicknesses of both interfacial Cu-Sn IMCs result in different morphologies of the corroded surface. As observed, corrosion promoted into the inner Cu_3Sn after the thin Cu_6Sn_5 layer is mostly attacked during polarization (**Figure 9f**).

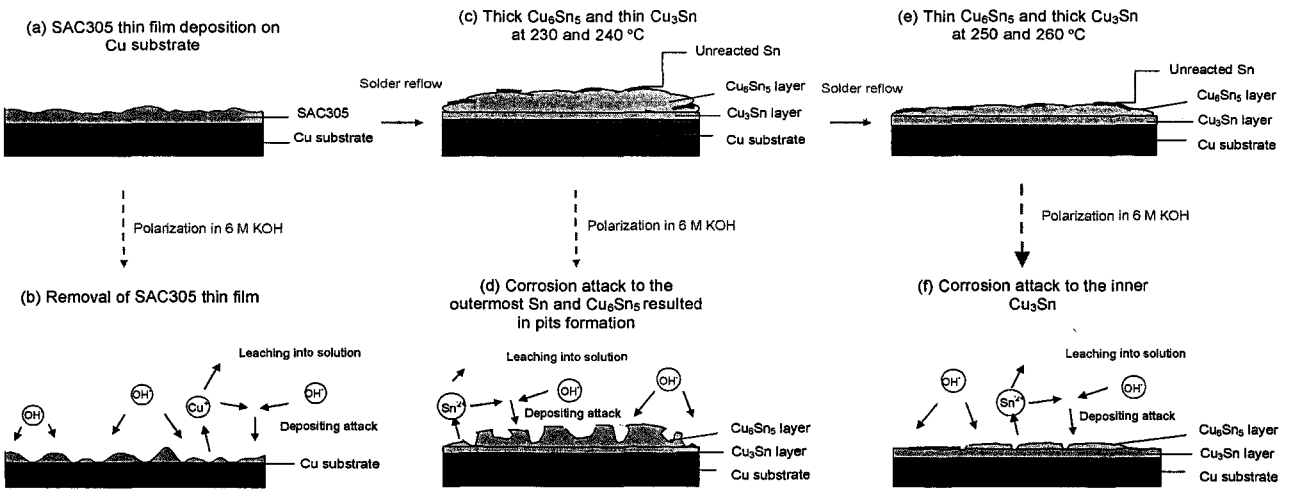

Figure 9: Corrosion mechanism of (a) as-deposited SAC305/Cu and as-reflowed SAC305/Cu at temperatures of (b) 230 and (c) 260 °C.

3.2.4 Summary

Bare Cu is found to possess the best corrosion resistance, while the as-deposited SAC305 has the lowest corrosion resistance. Bare Cu conforms to the well-known duplex structure of a Cu_2O/CuO and $Cu(OH)_2$ layer. For as-deposited SAC305/Cu, the corroded surface contains a very thin layer of oxide attributed to the dissolution of a low concentration of the Sn phase. Therefore, the corrosion products mainly consisted of SnO and SnO_2, which was represented in the passivation and pseudopassivation regions of the curve. The variation in solder reflow temperature resulted in different thicknesses of Cu-Sn IMCs at the interface. This difference, in turn, revealed different morphology during the tests. As-reflowed SAC305/Cu with an exposed Cu_3Sn layer exhibited better corrosion resistance than did Cu_6Sn_5. In thin film SAC305, the cathodic behavior of the phases present can be described by the declining sequence of Cu_3Sn > Cu_6Sn_5 > Sn.

3.2.5 References

1. Ulrich, R.K. and W.D. Brown, *Advanced electronic packaging.* 2nd ed. IEEE Press Series on Microelectronic System, ed. S.K. Tewksbury. 2006, United States of America: John Wiley & Sons, Inc.
2. Fubin, S. and S.W.R. Lee. *Corrosion of Sn-Ag-Cu lead-free solders and the corresponding effects on board level solder joint reliability.* in *Electronic Components and Technology Conference, 2006. Proceedings. 56th.* 2006.
3. *Solid state ionics for batteries*, T. Minami, et al., Editors. 2005, Springer-Verlag Tokyo: Hicom, Japan.
4. K.N, T., *Cu/Sn interfacial reactions: thin-film case versus bulk case.* Materials Chemistry and Physics, 1996. **46**(2–3): p. 217-223.
5. Inaba, M., et al., *Effects of Fe, Ni and Sn on reaction diffussion at solder/Cu-base-alloys interface.* Journal of the Japan Institute of Metals, 1984. **48**: p. 863-870.
6. Kay, P.J. and C.A. Mackay, *The Growth of Intermetallic Compounds on Common Basis Materials Coated with Tin and Tin-lead Alloys.* Transactions of the Institute of Metal Finishing, 1976. **54**: p. 68-74.
7. Kim, K.S., S.H. Huh, and K. Suganuma, *Effects of cooling speed on microstructure and tensile properties of Sn–Ag–Cu alloys.* Materials Science and Engineering: A, 2002. **333**(1-2): p. 106-114.
8. Yoon, J.-W. and S.-B. Jung, *Effect of surface finish on interfacial reactions of Cu/Sn–Ag–Cu/Cu(ENIG) sandwich solder joints.* Journal of Alloys and Compounds, 2008. **448**(1-2): p. 177-184.

9. Tu, K.N. and K. Zeng, *Tin–lead (SnPb) solder reaction in flip chip technology.* Materials Science and Engineering: R: Reports, 2001. **34**(1): p. 1-58.

10. Islam, M., A. Sharif, and Y. Chan, *Effect of volume in interfacial reaction between eutectic Sn-3.5% Ag-0.5% Cu solder and Cu metallization in microelectronic packaging.* Journal of Electronic Materials, 2005. **34**(2): p. 143-149.

11. Strehblow, H.H. and U. Collisi, *The formation of Cu2O layers on Cu and their electrochemical and photoelectrochemical properties.* Journal of Electroanalytical Chemistry, 1990. **284**: p. 385-401.

12. Brisard, G.M., et al., *Application of probe beam deflection to study the electrooxidation of copper in alkaline media.* Electrochimica Acta, 1995. **40**(7): p. 859-865.

13. Tsao, L.C., *Corrosion Characterization of Sn37Pb Solders and With Cu Substrate Soldering Reaction in 3.5wt.% NaCl Solution*, in *International Conference on Electronic Packaging Technology & High Density Packaging*. 2009. p. 1164-1166.

14. Rosalbino, F., et al., *Corrosion behaviour assessment of lead-free Sn–Ag–M (M=In, Bi, Cu) solder alloys.* Materials Chemistry and Physics, 2008. **109**(2-3): p. 386-391.

15. Jones, D.A., *Principles and Prevention of Corrosion.* 1992, New York: Macmillan.

3.3 Corrosion behaviour of Sn-3.0Ag-0.5Cu Lead-Free Solder in Potassium Hydroxide Electrolyte

3.3.1 Introduction

Sn-Ag-Cu solders have been widely used in electronic industries as promising replacements for Sn-Pb solders. Corrosion of Sn-Ag-Cu mostly contributed to the exposure of corrosive media and moisture absorption in application. However, the susceptibility of Sn-Ag-Cu to corrosion is one of main issue needs to be solved. Moreover, insufficient information is available on the corrosion properties of these lead-free solders.

At present, the corrosion behaviour of the Sn-Ag-Cu solders is mainly studied using sodium chloride (NaCl) electrolyte to simulate the seawater condition. The authors in all of these studies [1-5] employed the potentiodynamic polarisation test to qualify the corrosion behaviour of these lead-free solders. Li et al. [1] investigated the corrosion resistance of Sn-Pb and several candidates of the lead-free solders in 3.5 wt. % NaCl electrolyte through potentiodynamic polarisation. Results showed that lead-free solders have better corrosion resistance than that of the Sn-Pb solders. This phenomenon was because of the lower passivation current density and lower corrosion current density obtained by the lead-free solder after the passivation film breakdown, which signified a more stable passivation film on the surface. Rosalbino et al.[2] investigated the corrosion behaviour of Sn–3Ag–3Cu (at. %) alloy in 0.1 M NaCl electrolyte using the similar corrosion test, and compared the results with that of the Sn-3.0Ag-0.5Cu (SAC305) solder. The Sn-3Ag-3Cu alloy showed a passivation process, whereas no passive behaviour was observed for the SAC305 alloy. The Sn-3Ag-3Cu alloy has lower pseudopassivation current density and a larger pseudopassivation range compared with that of

the SAC305 alloy. This observation revealed that the corrosion resistance of Sn-3Ag-3Cu is somewhat better than that of SAC305 alloy.

However, no current data in literature exist on the corrosion properties of SAC305 in alkaline environment. Alkaline solution is widely used in batteries as electrolyte. Given that batteries are is included inside different devices and in contact with electrical circuits, the leakage of electrolyte could be catastrophic to the circuit. Thus, the corrosion and electrochemical behaviour of SAC305 solder alloy in 6 M potasium hydroxide (KOH) electrolytes was studied in the current paper through the potentiodynamic polarisation analysis. Surface morphology, elemental composition, and phase compositional analyses were also conducted to assist in the interpretation of the obtained polarisation curves.

3.3.2 Experimental

The SAC305 solder wire (Kester 48) was placed onto the Cu plate and reflowed at 230 °C for 60 s using a hot plate. **Figure 1** illustrates the formation of the SAC305 solder layer on Cu substrate during solder reflow. The common metallographic practices of grinding and polishing were used to prepare the samples after the reflow process. The morphologies of the samples were studied at the top and the cross-sectioned surface. An etchant of alcoholic ferric chloride solution was used to reveal the microstructures. Bruker AXS D9 diffractometer was used for X-ray diffraction (XRD) characterisation to identify the phases of SAC305 solder after the reflow process. Zeiss Supra^{TM} 35VP field Emission Scanning Electron Microscopy (FESEM) with energy dispersive X-ray (EDX) was used to determine the microstructure and elemental composition of the SAC305 solder before and after the reflow process.

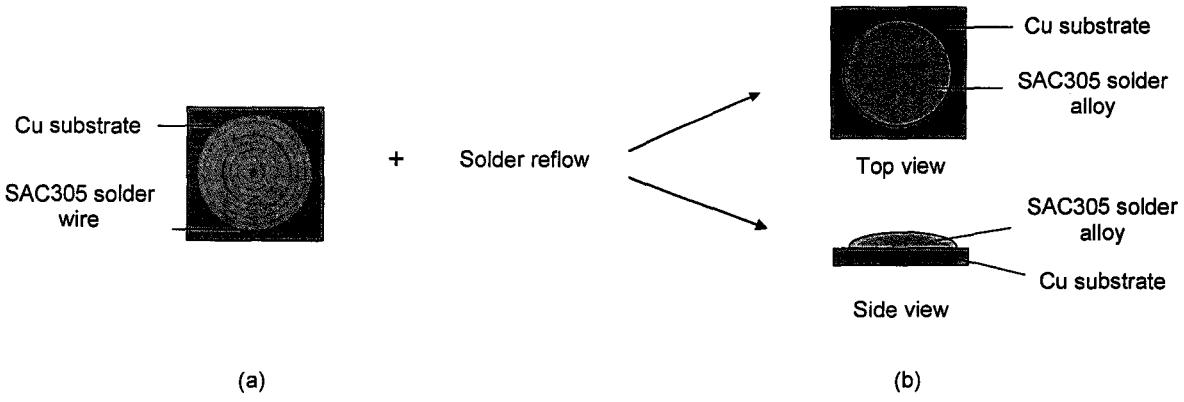

Figure 1: SAC305 solder on the Cu substrate during the solder reflow process. (a) SAC305 solder wire coiled at its initial state and (b) SAC305 solder alloy changed into a button-shaped mound after solidification as the final state.

Electrochemical measurement was carried out in a single compartment cell using a standard three-electrode configuration: Hg/HgO electrode was used as the reference electrode, a platinum electrode was used as the counter, and as-reflowed SAC305 was used as the working electrode. The surface area exposed to the test solution was 1.0 cm^2. The test was conducted in a 6 M KOH solution at room temperature. Autolab PGSTAT-30 GPES (Eco Chemie, B.V.) was the electrochemical interface used to control the potential. Potentiodynamic polarisation curves were recorded in the potential range of - 2.00 to + 2.00 V vs. Hg/HgO reference electrode at a scan rate of 1.67 x 10^{-4} V s^{-1}, after allowing a steady-state potential to develop. The corroded samples were then re-examined under FESEM and XRD for microstructural and elemental composition analysis, as well as phase determination for the complex interpretation of the polarisation scans.

3.3.3 Results and discussion

3.3.3.1 Polarisation Analysis

Figure 2 shows the polarisation curve of the as-reflowed SAC305 immersed in a 6 M KOH electrolyte. The cathodic branch started from a potential value of -2.0 V vs. Hg/HgO and ended at a value of approximately -1.1 V vs. Hg/HgO. The corrosion current density in this range decreased as the potential is made more positive. The turning point of the curve represents the beginning of the anodic scan. Since the KOH solution is exposed to the atmosphere it contains dissolved oxygen. Hence, the cathodic reaction involved the reduction of dissolved oxygen (Eq. 1), whereas the anodic reaction involved the dissolution of Sn (Eq. 2).

Cathodic reaction : $O_2 + 2H_2O + 4e^- \rightarrow 4OH^-$ (1)

Anodic reaction : $Sn + nH_2O \rightarrow Sn^{2+}.nH_2O + 2e^-$ (2)

Mohran et al. [6] who studied the anodic polarisation of pure Sn in 0.5 M oxalic acid found that the charge transfer reaction in the first active dissolution (Eq. 2) was then followed by the formation of Sn^{4+} species according to :

$$Sn^{2+} \rightarrow Sn^{4+} + 2e^- \quad (3)$$

The active dissolution of Sn can be explained by the potential difference existing among the alloy. **Table 1** shows that the electrode potential of Ag and Cu are much higher compared to that of Sn. Thus, Sn was considered as the most active among these metals. As a result, Sn acts as an anode in the alloy and therefore more easily dissolves in corrosive conditions.

The current density in the active region (-1.1 to -0.5 V vs. Hg/HgO) started to increase rapidly, which corresponds to the hydroxide (OH^-) ion-stimulated active dissolution of Sn to form a hydrous product ($SnOH_2$) as reported by Cheng *et al.* [4]. The intersection point of the cathodic slope and anodic slope in the active region is the highlight of the analysis as the

corresponding potential is the corrosion potential (E_{corr}) while the current is termed corrosion current density (i_{corr}). The corrosion potential (E_{corr}) and corrosion current density (i_{corr}) obtained from the sample was – 1.108 V vs. Hg/HgO and 1.795 x 10^{-4} A cm^{-2}, respectively. The sample exhibited a passivation process ranging from of -0.5 V vs. Hg/HgO to 0.0 V vs. Hg/HgO. The passivation was probably due to the formation of SnO from $SnOH_2$. The formation of SnO on the surface of Sn–Ag–Cu solder joint in de-ionized water has also been reported [7]. The integrated reactions of the $SnOH_2$ and SnO_2 formation are given by [8]:

$$Sn + 2OH^- \rightarrow Sn(OH)_2 + 2e^- \quad (4)$$

$$Sn(OH)_2 \rightarrow SnO + H_2O \quad (5)$$

Table 1: Electrode potentials of solder elements.

Element	Reaction	Electrode potential (V)
Silver	$Ag^{2+} + e^- = Ag$	+ 0.7996
Copper	$Cu^+ + e^- = Cu$	+ 0.5210
	$Cu^{2+} + 2e^- = Cu$	+ 0.3419
Tin	$Sn^{2+} + 2e^- = Sn$	- 0.1375

The breakdown of the passive film caused the polarisation curve to increase its current density when the anodic potentials exceed 0.0 V to 0.2 V vs. Hg/HgO. Thus, the passive film on the surface would no longer protect the underlying solder, causing it to be attacked by corrosive media. However, the dissolution of the newly exposed Sn is somehow restricted compared to that in the active region. After which, the current densities decreased gradually from 0.2 V to 0.5 V vs. Hg/HgO as the passive film recovered by the formation of the second corrosion product.

Further scanning in the anodic direction (from 0.5 V to 1.0 V vs. Hg/HgO), depicted that the current remains independent of potential, thereby indicating the onset of a pseudopassivation reaction. The pseudopassivation region is ascribed to the formation of the second corrosion product film, which is most likely SnO_2. The formation of the second SnO_2 passive film is caused by the formation and transformation of more SnO and $Sn(OH)_2$ into the $Sn(OH)_4$, as a result of increasing corrosion. The rapid phase transformation occurs during the dehydration of $Sn(OH)_4$ into the SnO_2. All these generation mechanisms could be described as follows: **[8]**

Formation of $Sn(OH)_4$: $SnO + H_2O + 2OH^- \rightarrow Sn(OH)_4 + 2e^-$ (6)

$Sn(OH)_2 + 2OH^- \rightarrow Sn(OH)_4 + 2e^-$ (7)

Dehydration : $Sn(OH)_4 \rightarrow SnO_2 + H_2O$ (8)

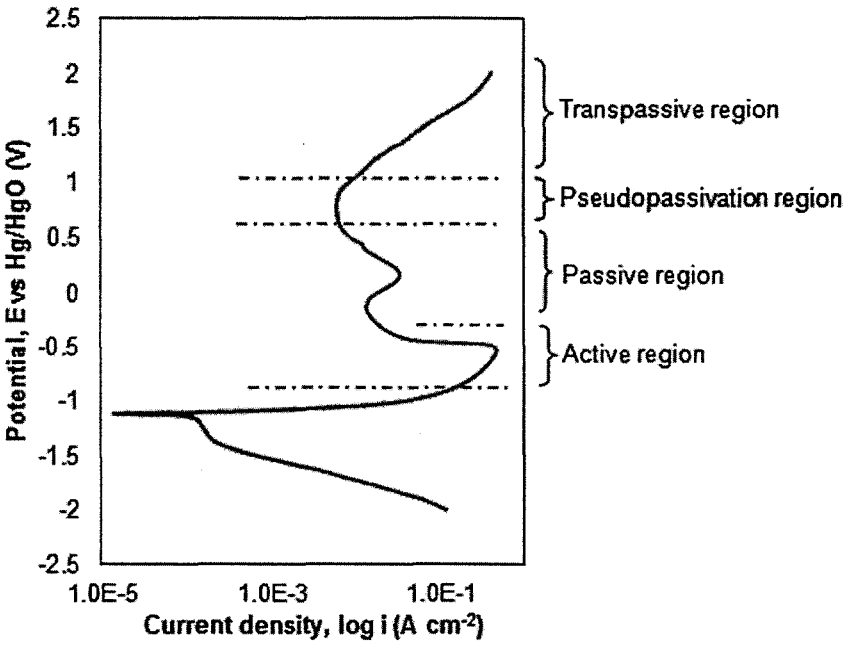

Figure 2: Potentiodynamic polarisation curve for an as-reflowed SAC305 sample in 6 M KOH solution.

This result is consistent with the anodic behaviour of Sn in sodium stannate solution investigated by El Rahim [9] who preceded that primary active dissolution of Sn yielded in $Sn(OH)_2$ and/or SnO formation by a dissolution-precipitation mechanism. Further oxidation during the second stage leads to the formation of $Sn(OH)_4$ and/or SnO_2 film. In contrast, Rosalbino *et al.*[3] who studied the potentiodynamic polarisation of Sn-Ag-Cu solders in aerated 0.1 M NaCl reported the SnO formed during passivation process. Furthermore, corrosion product constituted by tin oxychlorides are present at the corroded surface after the test. Additonally, Cotton and Wilkinson [10] revealed that the breakdown of SnO passive film in NaCl was due to the active dissolution of Sn by the Cl^- ions.

Further penetration of OH^- into the SAC305 solder is limited by the presence of SnO_2 layer, thus, enhancing the corrosion resistance of SAC305. The gradual increase in current density from 1.0 V vs. Hg/HgO in the transpassive region was due to the breakdown of the porous passive film.

3.3.3.2 Structural Analysis

Figure 3 presents the XRD patterns of as-reflowed SAC305 before and after the potentiodynamic polarisation test. The XRD patterns initially revealed the presence of β-Sn (ICDD 00-004-0673), slight traces of epsilon-Ag_3Sn (ICDD 00-044-1300), and η-Cu_6Sn_5 (ICDD 00-045-1488) crystal phases. However, two new phases were formed at latter part of the polarisation test, namely SnO and SnO_2. The peaks of SnO and SnO_2 matched with the standard peaks of (ICDD 00-006-0395) and (ICDD 00-041-1445), respectively. The SnO phases are detected at 47.81° and 50.76°, whereas that of the SnO_2 was at 64.71°. The presence of SnO and

SnO_2 phases in the XRD analysis confirmed the formation of both passive films during the passivation and pseudopassivation stages, as suggested in the anodic polarisation analysis.

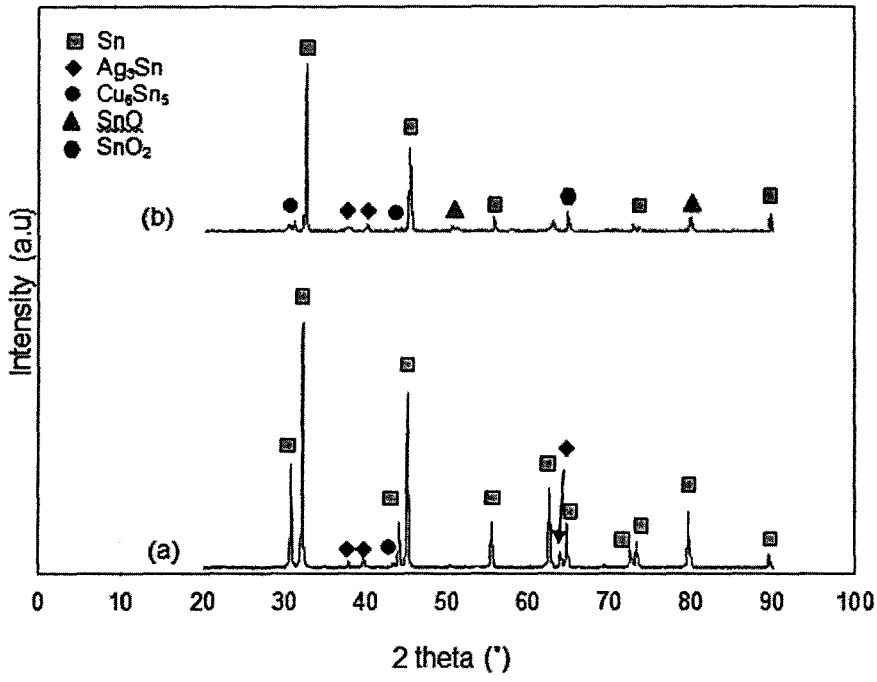

Figure 3: XRD pattern of the as-reflowed SAC305/Cu, (a) before and (b) after the potentiodynamic polarisation test in 6 M KOH.

Some of the major constituent of β-Sn phase at 30.64°, 64.56°, and 79.47° completely diminished after polarisation, whereas the intensities for the Sn plane at 32.04°, 44.91°, and 55.33° were significantly reduced. The absence of the true surface product of $Sn(OH)_4$ in the XRD patterns was evidently hydrous oxide, which has been accepted generally due to dehydration to yield a more stable film of SnO_2 [11]. However, this observation has been included in the earlier reaction scheme to explain that it was formed as a product of the transformation sequence of the film formed on the Sn surface.

3.3.3.3 Morphology Analysis

The FESEM image of SAC305/Cu before the polarisation test is depicted in **Figure 4**. The sample exhibits a three-phase appearance. The bulk phase was β-Sn with low solubility of Cu and Ag, which is in agreement with the study by Hwang [12]. The black crystals embedded in the β-Sn matrix with 44.83 at. % Sn and 55.17 at. % Cu signifies the η-Cu_6Sn_5 intermetallics **[13]**. In addition, acicular structures composed of 43.58 at. % Sn and 52.44 at. % Ag showed up as epsilon-Ag_3Sn intermetallics. However, the composition of epsilon-Ag_3Sn shown in the EDX analysis demonstrated different values from other studies **[14, 15]**. This is the experimental error due to overlap of the interaction volume of the electron beam and the production of EDS X-rays from more than one phase. However, the formation of the intermetallics was observed in the XRD pattern (**Figure 3**).

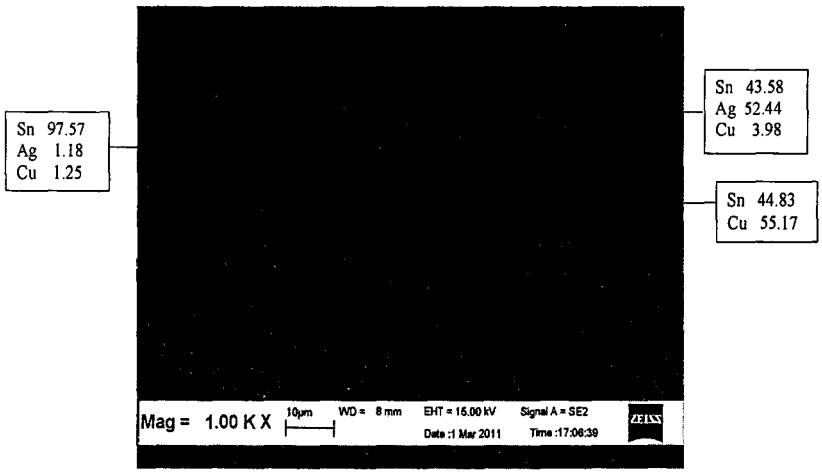

Figure 4: FESEM micrograph on the surface of as-reflowed SAC305 with element compositional analysis in atomic percentage (at. %).

Figure 5 illustrates the surface morphology of the as-reflowed SAC305 at the end of the polarisation. Several pits, cracks, and porous-like structure spread over the corroded surface were observed. The EDX results revealed that the corrosion products are mainly composed of Sn and

O, and identified as SnO and SnO_2. The current experimental result is in good agreement with previous XRD patterns, showing that some Sn planes are rapidly diminished with others, changing into SnO and SnO_2 peaks.

Furthermore, the EDX analysis indicated the presence of Cu and/or Ag-containing tin oxide corrosion product on the surface of the corroded sample. The structure of epsilon-Ag_3Sn and η-Cu_6Sn_5 are retained, and was not dissolve during the KOH immersion. These IMC phases are nobler than the β-Sn phase, and exhibit cathode behaviour, thus, promoting the dissolution of the β-Sn phase. On the other hand, the β-Sn phase is an anode, which reacts with OH^- ions, causing the formation of passive oxide film and pits. The oxide layer can prevent Sn from dissolving into the solution to a certain extent. However, various defects existed in the oxide layer, offering reaction conditions and locations for the dissolution of Sn. For example, the high applied voltage results in the formation of cracks in this layer.

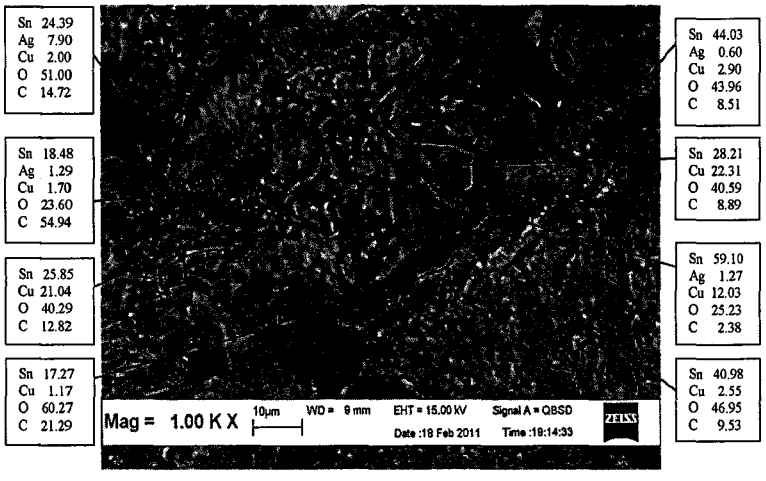

Figure 5: FESEM micrograph on the surface of as-reflowed SAC305 after the potentiodynamic polarisation test in 6 M KOH solution. The elemental compositions are in at. %.

Figure 6 depicts the cross-sectional views of the as-reflowed SAC305 analysed at the surface and interface region before and after the polarisation test. The morphology at the bulk

surface (**Figure 6a**) consists of the light-grey matrix of β-Sn where η-Cu_6Sn_5 appeared as black crystals and epsilon-Ag_3Sn as grey crystals with needle shape. **Figure 6b**, which was taken at the interface region, has a typical η-Cu_6Sn_5 scallop-type layer. The spalling of η-Cu_6Sn_5 also occurred owing to high concentration of Sn. Some relatively large and long η-Cu_6Sn_5 formed in the solder matrix and on the top of the scallops. The presence of Ag in the SAC305/Cu interface is minimal and an epsilon-Ag_3Sn platelet was found.

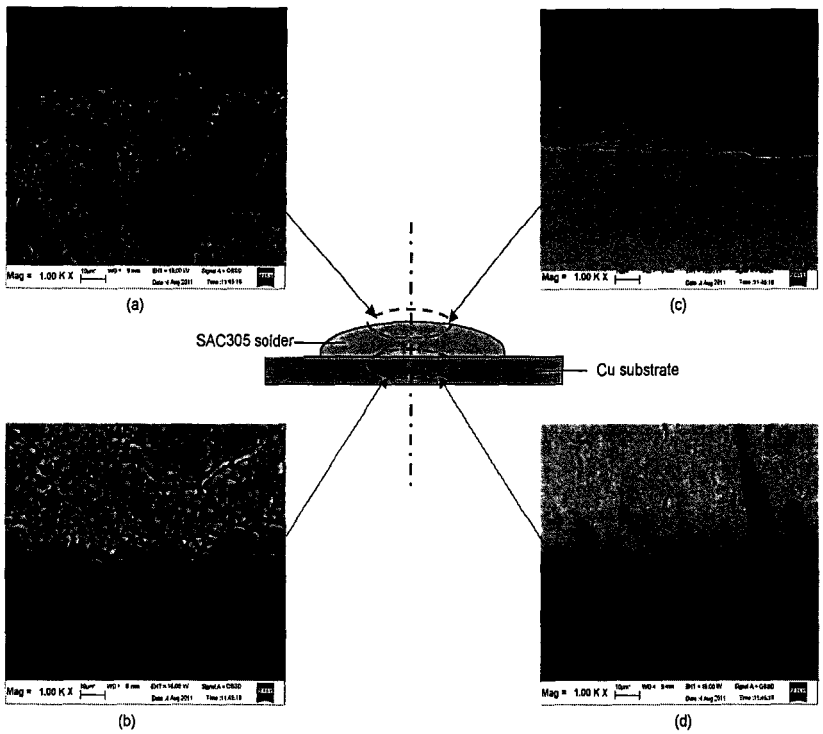

Figure 6: Schematic diagram with FESEM images of the as-reflowed SAC305/Cu, with (a) and (b) are captured before the polarisation test, whereas (c) and (d) are observed after the polarisation test in 6 M KOH solution.

A layer of corrosion product was formed at the surface of the sample after the polarisation test (**Figure 6c**). As discussed earlier, the phases formed are SnO and SnO_2, which are attributed to the active dissolution of the β-Sn phase. In the current work, corrosion only

occurred at the exposed surface region instead of being promoted in the solder joint. This phenomenon is evident from the scallop structure of the η-Cu_6Sn_5 phase, which remained unattacked after the test in **Figure 6d**.

The scallop type of η-Cu_6Sn_5 formed during the reflow treatment. In addition, the formation of relatively large IMCs was related to the dissolution of the Cu substrate into the molten SAC305 during the reflow process; followed by the precipitation of the dissolved Cu as large η-Cu_6Sn_5 IMCs in the solder matrix. This phenomenon is in accordance with the finding of Yoon and Jung [16] on the interfacial reaction of Cu/Sn-3.5Ag-0.7Cu/Cu(ENIG) sandwich solder joints during isothermal aging at 150 °C for 1000 h. On the other hand, the low Ag content found at the SAC305/Cu interface manifests that Ag was not actively involved in the formation of the IMC at the interface. The solubility of Ag in Sn is limited due to the more stable epsilon-Ag_3Sn and heterogeneous nucleation of both phases occurs when the cooling temperature reaches below the eutectic tie-line [17].

3.3.4 Summary

The polarisation showed that the SAC305 solder was seriously attacked in 6 M potassium hydroxide by the dissolution of Sn in the active potential region. Further scanning in the anodic direction revealed the formation of SnO during the first stage of Sn passivation. Then, breakdown of primary passive film occurred and caused pitting corrosion at the SAC305 solder underneath. Spontaneously, the passive film was recovered of by forming second corrosion product of SnO_2 in the pseudopassivation region. Therefore, the corrosion products mainly comprised SnO and SnO_2. The corrosion products present at the surface is tin oxide, which co-

exists with β-Sn, ε-Ag_3Sn, and η-Cu_6Sn_5 phases. This phenomenon showed that epsilon-Ag_3Sn and η-Cu_6Sn_5 are retained and are not dissolved during the KOH immersion. These IMC phases are nobler and exhibit cathodic character, hence, promoting the dissolution of the β-Sn phase.

3.3.5 References

1. Li, D., P.P. Conway, and C. Liu, *Corrosion characterization of tin–lead and lead free solders in 3.5 wt.% NaCl solution.* Corros. Sci., 2008. **50**: p. 995-1004.
2. Rosalbino, F., et al., *Electrochemical corrosion study of Sn–3Ag–3Cu solder alloy in NaCl solution.* Electrochim. Acta, 2009. **54**: p. 7231-7235.
3. Rosalbino, F., et al., *Corrosion behaviour assessment of lead-free Sn–Ag–M (M = In, Bi, Cu) solder alloys.* Mater. Chem. Phys., 2008. **109**: p. 386-391.
4. Cheng, C.Q., et al., *Leaching of heavy metal elements in solder alloys.* Corros. Sci., 2011. **53**: p. 1738-1747.
5. Wu, B.Y., Y.C. Chan, and M.O. Alam, *Electrochemical corrosion study of Pb-free solders.* J. Mater. Res., 2006. **21**: p. 62.
6. Mohran, H., A.-R. El-Sayed, and H. Abd El-Lateef, *Anodic behavior of tin, indium, and tin–indium alloys in oxalic acid solution.* Journal of Solid State Electrochemistry, 2009. **13**(8): p. 1279-1290.
7. Chang, H., et al., *Generation of Tin(II) Oxide Crystals on Lead-Free Solder Joints in Deionized Water.* Journal of Electronic Materials, 2009. **38**(10): p. 2170-2178.
8. Alvarez, P.E., et al., *Potentiodynamic behavior of tin in different buffer solutions.* Corros. Sci., 2002. **44**: p. 49-65.

9. El Rahim, S.S.A., A. El Sayed, and A.A. El Samahi, *Electrochemical behaviour of the tin anode in alkaline-stannate plating baths.* Surface and coatings Technology, 1986. **27**(3): p. 205-217.

10. Cotton, F.A. and G. Wilkinson, *Advanced Inorganic Chemistry*. 1972, London: Wiley.

11. Gervasi, C.A., et al., *Electrochemical studies on the anodic behavior of tin in citrate buffer solutions.* Journal of Electroanalytical Chemistry, 2010. **639**(1-2): p. 141-146.

12. Hwang, J.S., *Environmentally-Friendly Electronics: Lead Free Technology*. 2001: Electrochemical Publications, Ltd, Isle of Man.

13. Kim, K.S., S.H. Huh, and K. Suganuma, *Effects of cooling speed on microstructure and tensile properties of Sn-Ag-Cu alloys.* Mater. Sci. Eng. A, 2002. **333**: p. 106-114.

14. Abtew, M. and G. Selvaduray, *Lead Free Solders in Microelectronics.* Mater. Sci. Eng. R, 2000. **27**: p. 95-141.

15. Reid, M., et al., *Effect of Ag Content on the Microstructures of Sn-Ag-Cu Based Solder Alloys*, in *Soldering & Surface Mount Technology*. 2008, Emerald Group Publishing Limited. p. 3-8.

16. Yoon, J.W. and S.B. Jung, *Effect of surface finish on interfacial reactions of Cu/Sn–Ag–Cu/Cu(ENIG) sandwich solder joints.* J. Alloys Compd, 2008. **448**: p. 177-184.

17. Sidhu, R.S., et al., *On the Nature of the Interface between Ag3Sn Intermetallics and Sn in Sn-3.5Ag Solder Alloys.* J. Electron. Mater., 2007. **36**: p. 1615.

3.4 Interfacial Reaction of a Sn-3.0Ag-0.5Cu Thin Film during Solder Reflow

3.4.1 Introduction

Sn-Ag-Cu lead-free solders have been extensively studied in recent years as substitute materials for use in electronic, automotive, maritime, and aerospace applications. Lead-free solders have been employed in solder ball, solder alloy, solder paste, and solder wire [1-5]. Solders are used at the different interconnection levels of the electronic packaging hierarchy. The interconnection technology has progressed from conventional automated wire and tape bonding to area-array packaging (e.g. flip chip) owing to package miniaturization. In flip chip bonding, a solder serves as a die bonding material via the solder bumping process. For this purpose, evaporation is one of the common methods for depositing solder alloys onto the chip bondpads [6]. The emerging flip chip technology has resulted in solder joint reliability concerns in cases where more complicated interfacial reactions are employed.

The solder joint strength is controlled by selecting the land pattern design and ensuring good metallurgical bonding via intermetallic compound (IMC) formation. The reliability of solder joints is mainly dependent on the interfacial IMC layer [7]. A thin, continuous and uniform IMC layer is essential for good bonding. However, because of their inherent brittle nature and the tendency to generate structural defects, a thick IMC layer at the solder/conductor metal interface may fracture the solder joints [8]. Under certain conditions, it is essential to determine what thickness of solders is sufficient. Manko [9] reported that the formation of IMC with thickness of 1–2 μm between the solder and UBM is considered an indicator of good metallurgical bond and wetting.

It has been extensively documented [1, 2, 4, 5, 10-14] that Cu_3Sn and Cu_6Sn_5 IMCs formed at the interface region of bulk Sn-Ag-Cu solder and Cu substrate during soldering. For instances,

interfacial Cu_3Sn and Cu_6Sn_5 IMCs are formed between some Sn-based solder alloys and a Cu under-bump metallization (UBM) [15, 16] and also between organic solderability preservative (OSP) finished Cu bond-pads [5]. Subsequent heat treatment causes continued growth of the IMCs [1, 14].

However, a subtle and unstudied aspect of these intermetallics on the thin film characteristics of Sn-Ag-Cu lead-free solders is limited. Small solder volumes saturate more quickly with Cu, thus accelerating the precipitation of IMC [7, 17]. Previous work [18] confirmed that subsequent thermal treatments of thin solder coatings on Cu base substrates changed the surface character of the solder. The actual surface may have regions of Cu_6Sn_5 and/or Cu_3Sn which directly exposed to the environment. Consequently, the shelf life owing to solderability of components having such surfaces might be affected by the reactivity of the exposed IMCs with the environment. Hence, the reactivity of thin film characteristics need to be considered to get ready for rapidly growing trend towards electronic product miniaturization and the increasing demand for reliability.

Thus, the present work presents results obtained by investigating the interfacial reaction of a Sn-3.0Ag-0.5Cu (SAC305) thin film on a Cu substrate. The microstructural analysis and phase characterisation were performed to open the possibility for much more detailed insight into the structure of the SAC305 film on Cu substrate and mechanistic details of the IMC formation.

3.4.2 Experimental

A 10 mm × 10 mm Cu plate was metallographically prepared by grinding with progressively finer grades of silica carbide paper to remove the oxide layer. The plate was cleaned with acetone to eliminate the grease. A total mass of 0.3 g of Sn-3.0Ag-0.5Cu (SAC305, Kester)

solder wire was measured. The deposition of SAC305 solder wire onto the Cu plate was performed using an Edward Autolab 306 automatic thermal evaporator, as depicted in **Figure 1**. The evaporation was conducted with a pressure of 3.4×10^{-5} torr and voltage of 7 V. The specimens after evaporation will be referred to as "as-deposited SAC305/Cu".

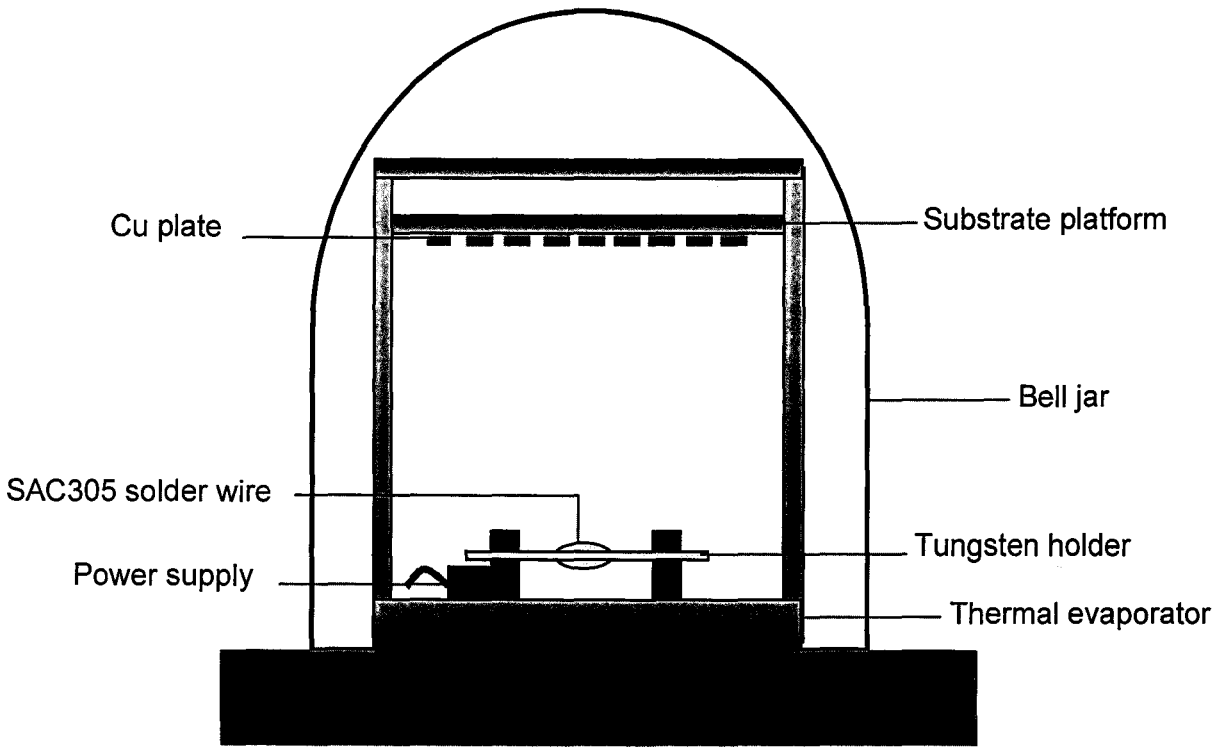

Figure 1: Sketch of the thermal evaporator for SAC305 solder wire deposition on Cu plate

The as-deposited SAC305/Cu was reflowed on a hot plate at ambient air environment at 230, 240, 250, and 260 °C for 30 s to promote interfacial reaction. For a temperature of 230 °C, the solder reflow was conducted for 5, 10, 15 and 20 s. No flux was applied during solder reflow. After solder reflow the specimens will hereafter be referred to as "as-reflowed SAC305/Cu". The as-reflowed SAC305/Cu were mounted and vertically sectioned for cross-sectional surface views. The as-reflowed SAC305/Cu was subjected to grinding, 0.05 μm alumina polishing, and soap polishing to remove contaminants on the surface. Ultrasonic cleaning in ethanol was

performed to remove excessive impurities. The as-reflowed SAC305/Cu was then etched with alcoholic ferric chloride to obtain better contrast on the metallography.

To investigate the interfacial reaction, the as-deposited SAC305/Cu and as-reflowed SAC305/Cu were examined and studied using field emission scanning electron microscopy (FESEM; Zeiss Supra^{TM} 35VP) and energy dispersive X-ray (EDX) for microstructural analysis and chemical composition determination, respectively. A Bruker D8 Advance diffractometer was used for X-ray diffraction (XRD) for phase determination. The IMC thickness was measured in several selected areas of the FESEM micrographs of each sample.

3.4.3 Results and discussion

3.4.3.1 Surface Appearance

Figure 2 shows the top surface of the samples at different microstructural states. **Figure 2a** displays a typical reddish-orange surface of Cu prior to thermal evaporation. The top surface of the bare Cu plate is covered with a silvery SAC305 thin film after evaporation (**Figure 2b**). After solder reflow from 230 to 260 °C, discoloration and oxidation occurred. Subsequently, the surface of the SAC305 thin film turned into a dull greyish colour (**Figure 2c**).

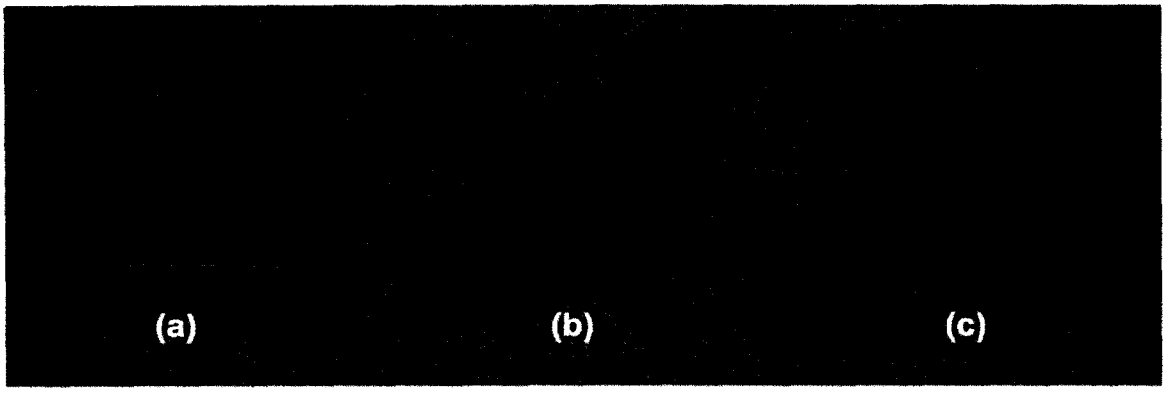

Figure 2: (a) Pure bare Cu substrate, (b) as-deposited SAC305, and (c) as-reflowed SAC305/Cu at 230 °C for 30 s

The discoloration of the SAC305 thin film is due to the susceptibility of Sn to oxidation. Hung et al. [19] concluded that the solidification surfaces of Sn-3.5Ag and Sn-3.5Ag-2.0Cu alloy thin films, after melting Sn alloy at 310 °C, were mostly composed of SnO and SnO_2. The authors also added that Sn alloys are highly susceptible to oxidation in air, which is attributed to the increased concentration of Sn^{2+} and O at sites near the solidified thin film surface. In addition, the Gibbs free energy of oxide formation (Table I) indicates that SnO_2 formation is the most favourable. Most of the O and Sn atoms reacted to form the oxidative film SnO_x. This finding indicates that O reacted with the Sn melt to produce the oxidative film SnO_x during solidification.

Table 1. Standard free energy of oxide formation (per gram atom O basis) [35, 36]

Compound	$\Delta G^0_{f,T}$ (kJ/g atom O)			
	298 K	400 K	500 K	600 K
SnO_2	- 260.2	- 249.7	- 239.7	- 228.8
Ag_2O	- 10.5	- 3.8	2.5	8.8
CuO	-129.4	- 119.7	- 111.0	- 101.7

3.4.3.2 Phase Determination

The XRD patterns of the samples from the top surface are compared in **Figure 3**. The bare Cu sample (**Figure 3a**) reveals sharp and intense peaks stemming from the Cu crystal phase (ICDD 01-085-1326) at 43.33°, 50.45°, and 74.13°. The pure SAC305 solder wire displayed β-Sn reflections, together with a minor peak of ή-Cu_6Sn_5 at 31.58° (**Figure 3b**). The peaks of β-Sn and ή-Cu_6Sn_5 matched the standard peaks of ICDD 00-004-0673 and ICDD 00-045-1488, respectively. Ag_3Sn phases (ICDD 00-044-1300) are also observed in the pure SAC305 solder

wire. However, owing to its low concentration, the Ag_3Sn reflections are too low to be observed. The inserted plots in Figure 3 show the presence of slight traces of Ag_3Sn at the 2θ values, ranging from 42 to 46° and from 69 to 75°. Likewise, the as-deposited SAC305/Cu thin film (**Figure 3c**) is found to consist of its major constituents, namely, β-Sn phase, Cu phase, and slight traces of ή-Cu_6Sn_5 and Ag_3Sn crystal phases. The overall intensity of the SAC305 solder wire is much lower than that of the as-deposited SAC thin film, presumably contributing to its narrower surface area of diffraction.

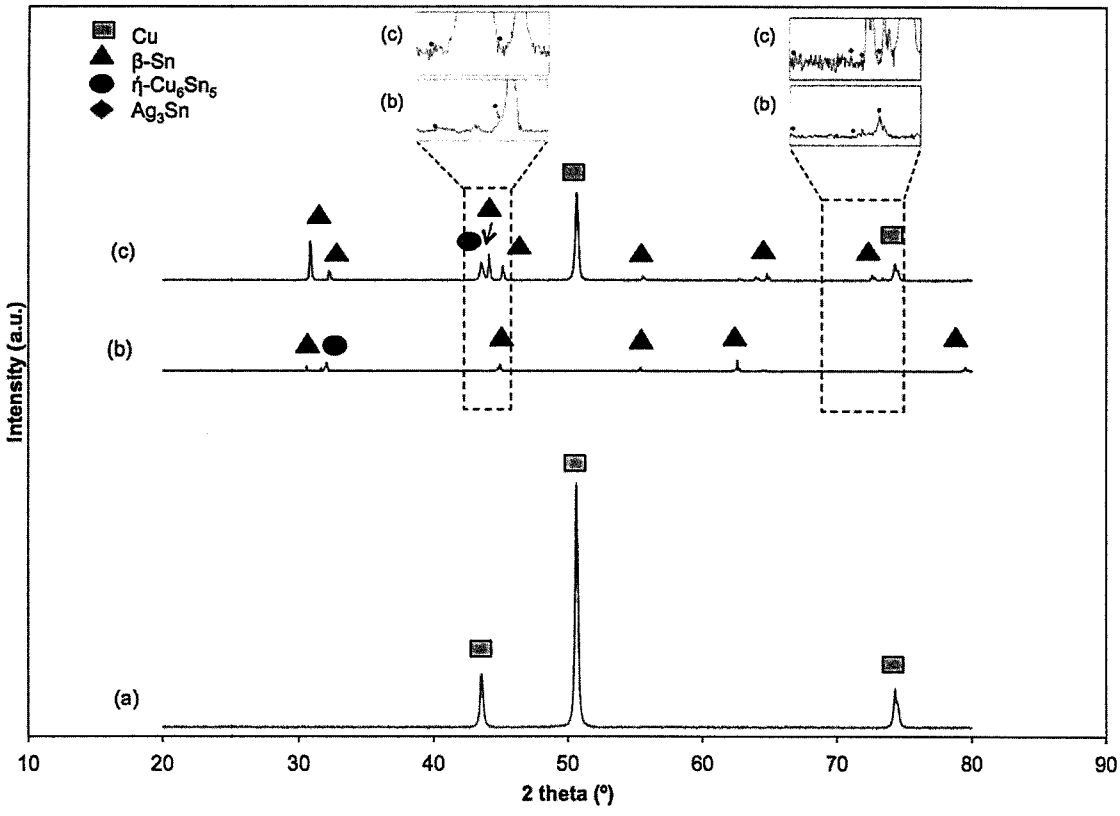

Figure 3: XRD patterns from the top surface of (a) bare Cu, (b) pure SAC305 solder wire, and (c) as-deposited SAC305

Figure 4 shows the XRD patterns from the top surface of all as-reflowed SAC305/Cu samples. Notably, after solder reflow at 230 °C, most of the β-Sn phases diminished, except for

the phase represented at 30.64° (**Figure 4a**). In contrast, the diffraction peaks of ή-Cu_6Sn_5 became more evident. New phases of IMCs are formed and confirmed as η-Cu_6Sn_5 (ICDD 00-002-0713), ε-Cu_3Sn (ICDD 03-065-4653), Ag_3Sn, and SnO (ICDD 00-006-0395). All as-reflowed SAC305/Cu samples at 240, 250, and 260 °C (Figures 4b to 4d) displayed identical reflections to the sample at 230 °C, demonstrating the presence of Ag_3Sn, Cu-Sn IMCs, and SnO. The XRD analysis revealed that solder reflow promoted the formation of Ag-Sn and Cu-Sn IMCs. Thus the peak of Ag_3Sn became observable, though the small peak of Ag_3Sn may be due to the formation of fine Ag_3Sn platelets. There is a limited supply of Ag from the thin film solder. The low concentration of Ag resulted in insufficient material to form large structures. The dissolved Ag formed Ag_3Sn with Sn. The stable Ag_3Sn further restricted the solubility of Ag in the β-Sn phase [3].

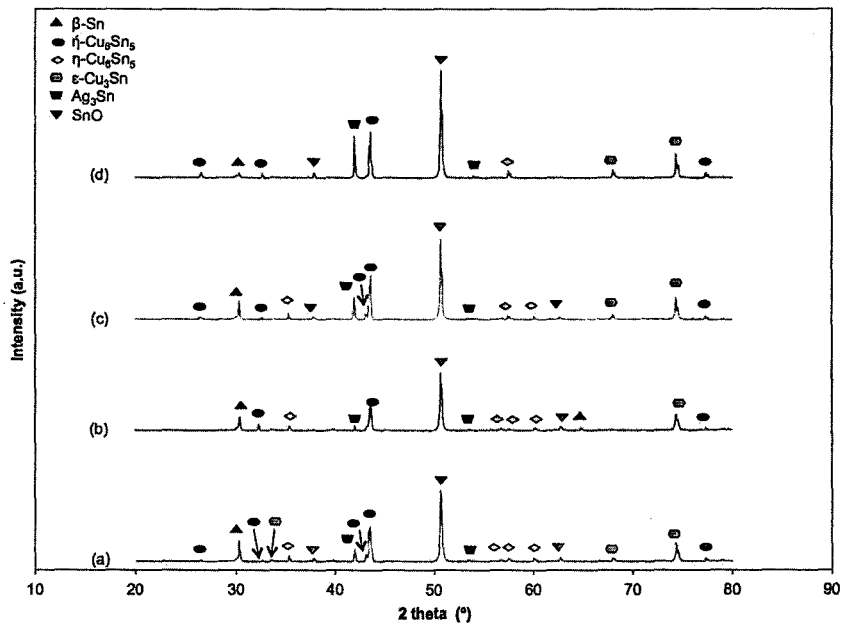

Figure 4: XRD patterns from the top surface of as-reflowed SAC305/Cu at reflow temperatures of (a) 230, (b) 240, (c) 250, and (d) 260 °C for 30 s

In this case, the formation of Ag_3Sn is favourable because the Ag content is greater than 2.5 mass% [2]. Pietriková et al. [20] also concluded that thermal hysteresis occurred between melting and solidification, which leads to the formation and crystallization of the Ag_3Sn phase as a result of further cooling. Notably, the general solidification behaviour of a ternary eutectic system follows [21, 22]:

$$L \rightarrow \beta\text{-Sn} + Ag_3Sn \qquad (1)$$

$$L \rightarrow \beta\text{-Sn} + Ag_3Sn + Cu_6Sn_5 \qquad (2)$$

In the present work, in all as-reflowed SAC305/Cu samples, Cu_3Sn is revealed as ε-Cu_3Sn, possessing an orthorhombic lattice structure. Monoclinic $\acute{\eta}$-Cu_6Sn_5 and hexagonal η-Cu_6Sn_5 coexist for all as-reflowed SAC305/Cu. Generally, below about 350 °C, Cu_6Sn_5 and Cu_3Sn are the main reaction products [23], whereas η-Cu_6Sn_5 is the IMC found at high temperatures. However, the appearance of the $\acute{\eta}$-Cu_6Sn_5 intermetallic phase, which is the low-temperature (< 186 °C) Cu_6Sn_5 phase, indicated that η-Cu_6Sn_5 did transform into $\acute{\eta}$-Cu_6Sn_5 during the cooling period of the soldered joint. The presence of SnO in the as-reflowed SAC305/Cu proved that the oxidation behaviour caused the dull-greyish colour of the sample surface, which is also in good agreement with Hung et al. [19].

The XRD patterns of the as-reflowed SAC305/Cu from a cross-sectional axis are shown in **Figure 5**. There are sharp and intense reflections of $\acute{\eta}$-Cu_6Sn_5, η-Cu_6Sn_5, and Cu_3Sn phases at 43.28°, 43.47°, and 50.85°, respectively. The minor peak of the Cu crystal phase at 74.13° is clearly visible, which decreased with increased reflow temperature. The relative intensity of the Cu_3Sn phase is lower than that of Cu_6Sn_5. Compared with the one from the top surface, only the Cu and IMC phases of Cu-Sn are present. This finding emphasises that the unreacted Sn remained in the top region because of its smaller density compared with Cu_6Sn_5 [12].

Consequently, Cu_6Sn_5 gradually precipitated at the interfacial region and rejoined to form a layer.

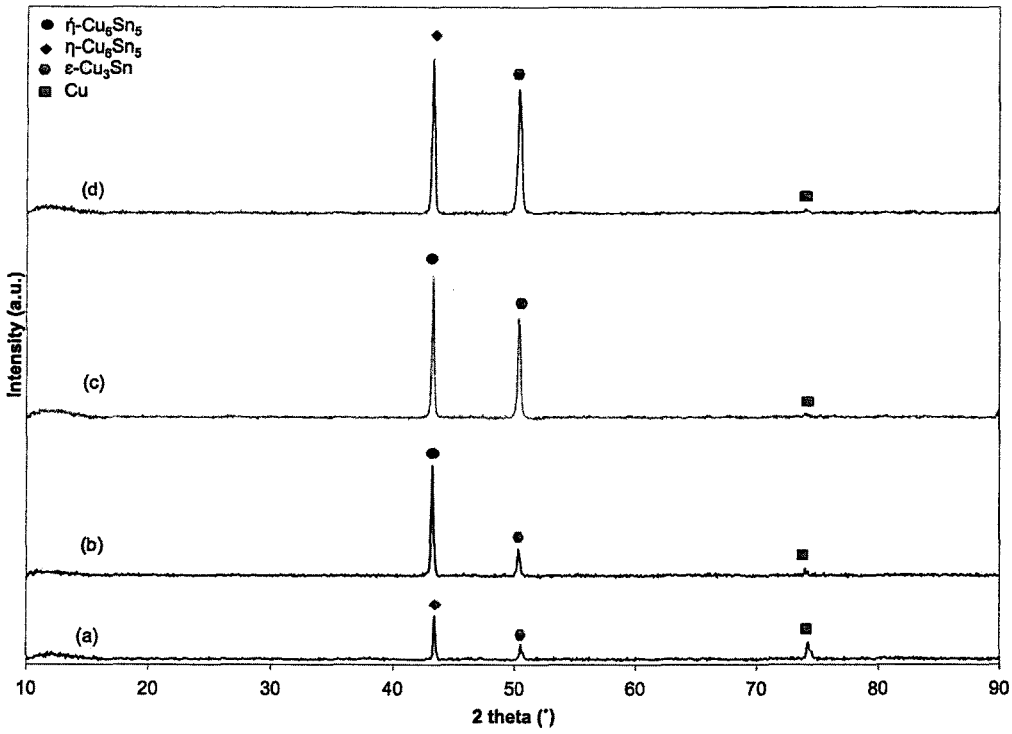

Figure 5: XRD patterns of the cross-sectional area of as-reflowed SAC305/Cu at reflow temperatures of (a) 230, (b) 240, (c) 250, and (d) 260 °C for 30 s

3.4.3.3 Morphology Evolution

Figure 6 shows a cross-sectional view of the as-deposited SAC305 thin film. The top white layer is the SAC305 solid layer, with a composition of 96.47 wt % Sn, 2.98 wt % Ag and 0.55 wt % Cu. These results indicate that no composition change occurred after evaporation. This layer is comprised of loose SAC305 particles that were physically adsorbed onto the Cu substrate. Thus it is easily removed, even under small polishing loads. The as-deposited SAC305 thin film had an average thickness of 2.0 ± 0.2 μm. The thickness of the deposited thin film was evidently not uniform across the substrate, though it was acceptable because the Cu substrates

remained static throughout the evaporation [24]. Thermal evaporation sources can be treated as a point source. Thus, it is clear that the deposited film will not be uniform across the substrate.

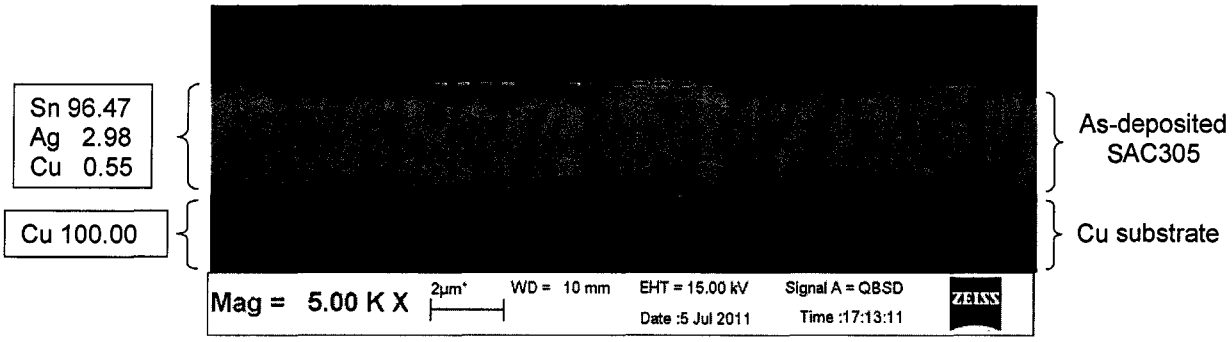

Figure 6: FESEM micrograph of the cross-sectional view of the as-deposited SAC305 thin film. The compositions (wt %) were obtained by EDX analysis.

The cross-sectional FESEM images of as-reflowed SAC305/Cu are shown in **Figure 7**. Under these conditions, two continuous IMC layers started to form at the solder joints region. The top region is Cu_6Sn_5, and the layer beneath is Cu_3Sn. Physically Cu_6Sn_5 is thick and irregular in thickness, whereas a thin band of Cu_3Sn is more uniform in thickness and is more planar; however it does, to some extent, follow the topography of the adjacent Cu_6Sn_5 phase layer. No spalling or flaking of the IMCs is observed at the low concentration of Sn in the thin film. EDX analysis revealed that the composition of Cu_6Sn_5 is 39.68 at.% Sn and 60.32 at.% Cu. Cu_6Sn_5 was determined to be depleted by 4 at.% to 5 at.% Sn, compared with values in the literature [25-28]. In contrast, Cu_3Sn has a composition of 24.79 at.% Sn and 75.21 at.% Cu. Obviously, the thin film SAC305 solder completely reacted with the excessive Cu substrate to form Cu_6Sn_5 during the reflow.

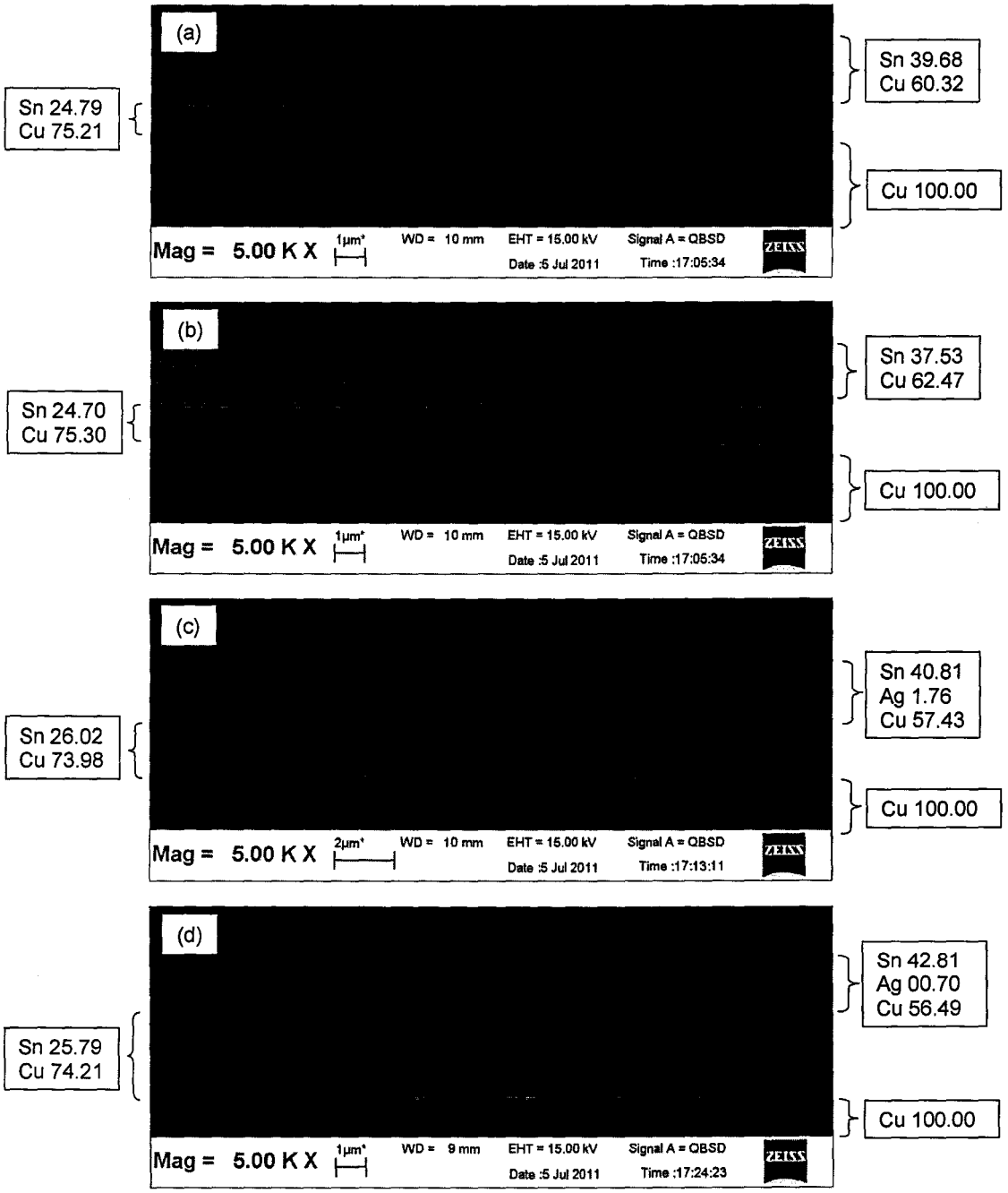

Figure 7: FESEM micrographs of SAC305/Cu as-reflowed joints at reflow temperatures of (a) 230, (b) 240, (c) 250, and (d) 260 °C for 30 s with alcoholic ferric chloride etching. The compositions (at.%) were obtained by EDX analysis

The effect of solder reflow times on the interfacial Cu-Sn IMCs was also being studied, as displayed in **Figure 8**. Similarly, it can be seen that each solder joint consists of three colonies: Cu_6Sn_5, Cu_3Sn and Cu substrate. A very thin Cu_3Sn layer with a thickness of 0.19 um emerges between the Cu_6Sn_5 and Cu substrate (Fig. 8a). This shows that Cu_3Sn is present, even after short solder reflow time of 5 s. After soldering for longer times (Figs. 8b–d), the Cu_3Sn IMC layer is much thicker, though it only comprises a small fraction of the total intermetallic layer. It can be seen that the Cu_3Sn layer expanded rapidly by shifting the Cu_3Sn/Cu_6Sn_5 interface towards the Cu_6Sn_5.

In general, for all the as-reflowed specimens studied, the morphology of the Cu_6Sn_5 layer is continuous, as opposed to a scalloped, overlapping structure, as reported elsewhere [1, 10, 12, 13, 29]. The most probable explanation is that the small Sn supply from the SAC305 thin film restricts the growth of Cu_6Sn_5 into a scalloped structure. In accordance with the assumptions for the physical growth model, the first requirement is the establishment of a continuous intermetallic layer. Once a continuous layer is well defined, additional growth occurred by diffusion of the reacting species (Sn and/or Cu) through the intermetallic layer [30].

The formation of the IMC layer is mainly due to the diffusion of Cu atoms into the molten solder matrix during the reflow [5]. However, the growth of the IMC layer is predominantly owed to the interdiffusion of the relevant components across the IMC layer. Moreover, the interdiffusion in thin films is much faster than in bulk materials, as a result of a high density of defects, such as vacancies, dislocations and interfaces [31]. The dissolved Cu atoms precipitated to form IMCs in the solder matrix. Cu_6Sn_5 first formed during the wetting reaction between liquid Sn and Cu. Cu_6Sn_5 is believed to have a high rate of growth at the SAC305/Cu interface [15], and this formation depletes Sn.

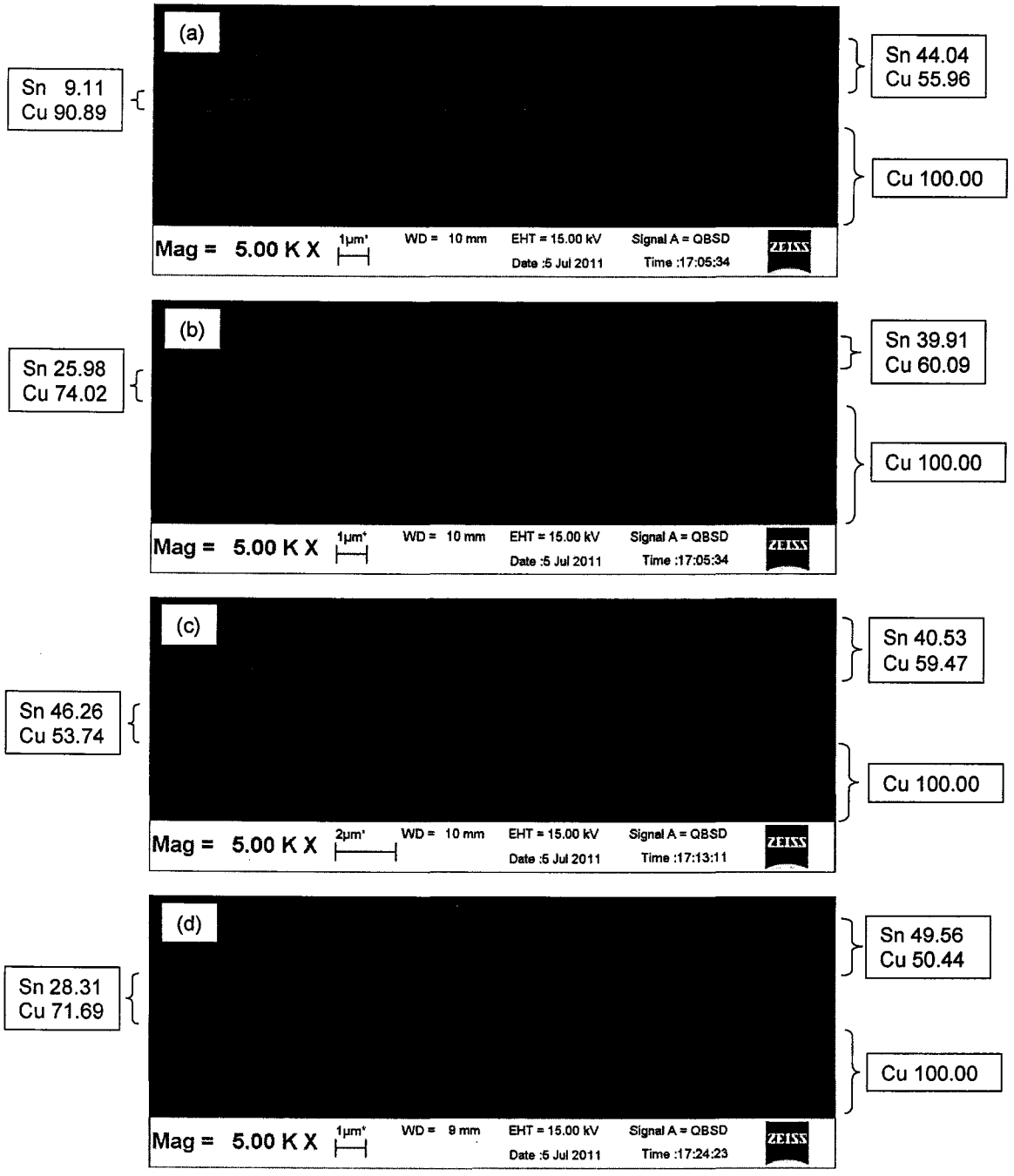

Figure 8: FESEM micrographs of the SAC305/Cu as-reflowed joints at constant reflow temperatures of 230 °C for (a) 5, (b) 10, (c) 15 and (d) 20 s with alcoholic ferric chloride etching. The compositions (at.%) are obtained by EDX analysis

To a certain extent, when the supply of Sn through the interfacial IMC is more restricted than the supply of Cu from the substrate, the Cu_6Sn_5 layer that is initially formed subsequently transforms into Cu_3Sn [4]. Thus the initial formation of the very thin layer of Cu_3Sn resulted from the solid-state reaction between Cu_6Sn_5 and Cu in the reflowing process. Thus the thickness of Cu_3Sn is expected to be much less than that of Cu_6Sn_5. The cross-sectional morphology and EDX results supported the observations from XRD data.

3.4.3.4 Effect of Solder Reflow Temperature and Time

Figure 9 compares the thicknesses of the IMC layers formed at the interfacial region as a function of the reflow temperatures. The Cu_3Sn intermetallic layer consistently increased with increased temperature, whereas Cu_6Sn_5 gradually decreased with increased reflow temperature. These results correlate well with the cross-sectional XRD patterns of as-reflowed SAC305/Cu (**Figure 5**), where the Cu_3Sn peak is obvious with respect to Cu_6Sn_5 reflection with increased reflow temperature.

Figure 10 graphically shows the relationship between the IMC layer thickness and reflow time. Likewise, at a certain reflow temperature, the thickness of the IMC layers found at the interfacial zone tended to increase with soldering time. Based on the study done by Yu and Wang [12], the increase in reflow time enables the IMCs layer to grow quickly due to the precipitation effect of the Cu_6Sn_5. It is recalled that Cu_6Sn_5 could develop into Cu_3Sn when the supply of Sn is limited. So the thickness of Cu_3Sn increases as the Cu_6Sn_5 layer decreases, despite the fact that in general Cu_6Sn_5 grows with solder time.

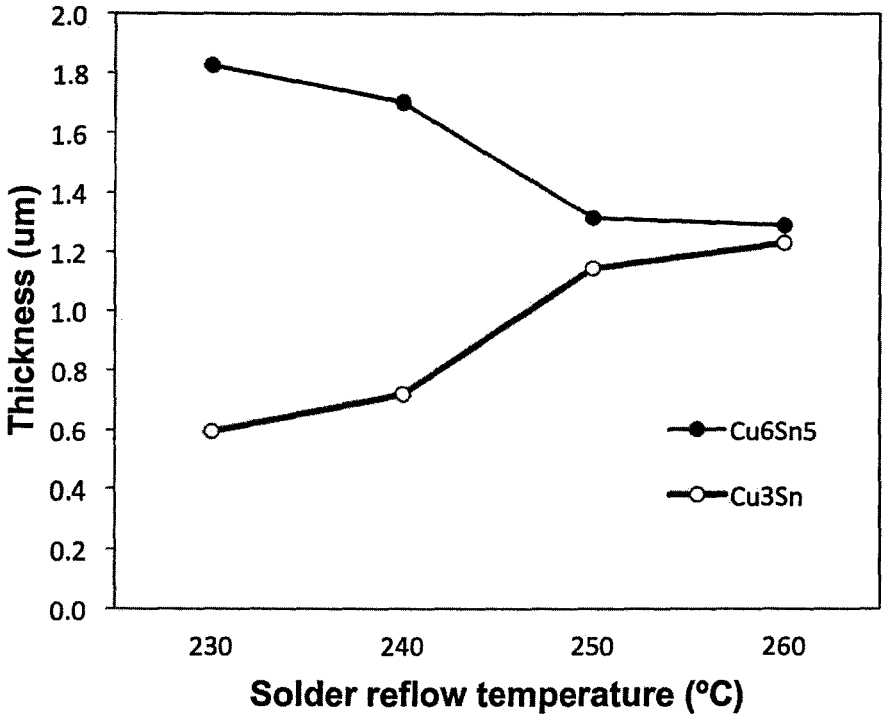

Figure 9: Thickness of Cu-Sn IMCs as a function of reflow temperature with a constant time of 30 s

These results provide evidence that the interfacial Cu_3Sn layer is growing at the expense of Cu_6Sn_5, according to the reaction of $Cu_6Sn_5 + 9Cu \rightarrow 5Cu_3Sn$ [32]. Moreover, it can be seen that the thickness growth of Cu_3Sn follows a linear equation. According to material kinetics, linear growth indicates that the formation of the interfacial Cu–Sn IMC layer is an interfacial reaction-controlled process [33].

The increase in the Cu_3Sn IMC layer results from the diffusion and reaction type growth during the soldering process [16]. The growth of Cu_3Sn consists of several steps: the dissolution of Cu from the Cu pad, the diffusion of Cu and Sn through the existing Cu_3Sn layer, and the conversion of Cu_6Sn_5 into Cu_3Sn at the Cu_6Sn_5/Cu_3Sn interface and the reaction of Sn with Cu at the Cu/Cu_3Sn interface [34]. Conversely, Cu_6Sn_5 is formed by the dissolution of Cu, followed by a chemical reaction [16], and its growth is restricted by the Cu_3Sn layer because the amount of

free Cu atoms that can diffuse to the Cu_6Sn_5 is very small. Therefore, Cu_3Sn grows rapidly with temperature, consuming Cu_6Sn_5 at the interface of Cu_3Sn/Cu_6Sn_5.

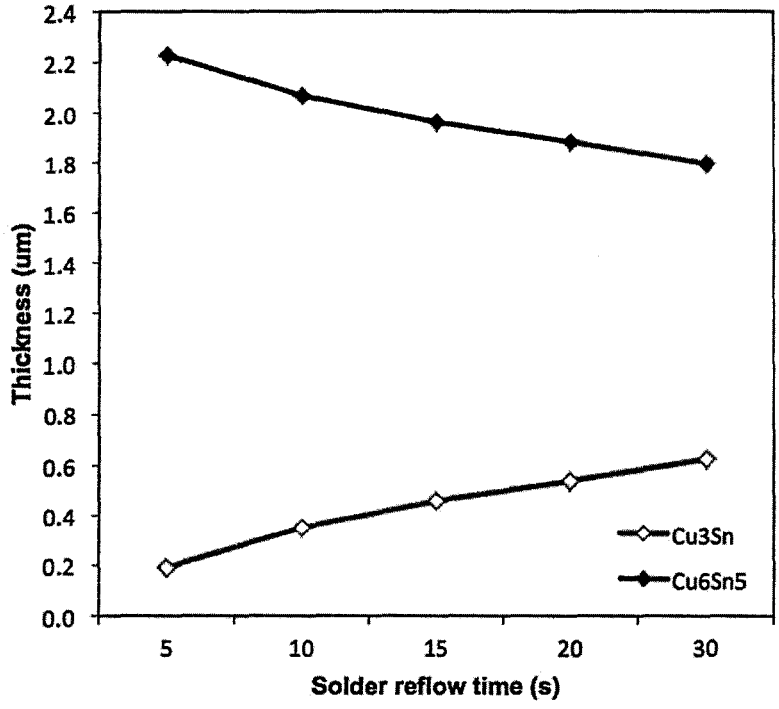

Figure 10: IMC layer thickness versus reflow time at a reflow temperature of 230 °C

3.4.4 Summary

In this study, the SAC305 thin film was deposited on Cu substrate through thermal evaporation technique. Practically, the as-deposited SAC305 thin film revealed the same composition as in solder wire. The SAC305 comprised of loose SAC305 particles that were physically adsorbed onto the Cu substrate. The as-deposited SAC305/Cu was reflowed in temperature range of 230-260 °C. The surface appearance of the as-deposited SAC305 thin film turned from silvery into a dull grayish color after solder reflow.

A fast interdifussion in SAC305/Cu during solder reflow leads to the formation of Cu_6Sn_5 and Cu_3Sn at the interfacial zone. Cu_6Sn_5 is located almost exclusively in the volume, whereas

Cu_3Sn appeared as a thin uniform layer structure beneath Cu_6Sn_5. Cu_6Sn_5 is thick and irregular in thickness, whereas a thin band of Cu_3Sn is more uniform in thickness and is more planar. The Cu_3Sn intermetallic layer consistently increased with increasing temperature. In contrast, the Cu_6Sn_5 layer gradually decreased with increasing reflow temperature. Hence, it is reasonable to assume that the interfacial Cu_3Sn layer grew at the expense of Cu_6Sn_5. Conversely, the growth of Cu_6Sn_5 is restricted by the Cu_3Sn layer within 2.0 μm of the SAC305 thin film.

Besides, the effect of solder reflow times on the interfacial Cu-Sn intermetallic compounds (IMCs) also being studied. Similarly, it can be seen that each solder joint consists of three colonies: Cu_6Sn_5, Cu_3Sn and Cu substrate. A very thin Cu_3Sn layer emerges between the Cu_6Sn_5 and Cu substrate. Cu_3Sn is present even after short solder reflow time and become thicker with increased reflow times. It can be seen that the Cu_3Sn layer expanded rapidly by shifting the Cu_3Sn/Cu_6Sn_5 interface towards the Cu_6Sn_5.

3.4.5 References

1. Liu, P., P. Yao, and J. Liu, *Effects of multiple reflows on interfacial reaction and shear strength of SnAgCu and SnPb solder joints with different PCB surface finishes.* Journal of Alloys and Compounds, 2009. **470**(1-2): p. 188-194.
2. Liu, C.-Y., et al., *Thermal behavior and microstructure of the intermetallic compounds formed at the Sn–3Ag–0.5Cu/Cu interface after soldering and isothermal aging.* Journal of Crystal Growth, 2006. **290**(1): p. 103-110.
3. Reid, M., et al., *Effect of Ag Content on the Microstructures of Sn-Ag-Cu Based Solder Alloys*, in *Soldering & Surface Mount Technology*. 2008, Emerald Group Publishing Limited. p. 3-8.
4. Islam, M.N., et al., *Investigations of interfacial reactions of Sn–Zn based and Sn–Ag–Cu lead-free solder alloys as replacement for Sn–Pb solder.* Journal of Alloys and Compounds, 2005. **400**(1-2): p. 136-144.

5. Yoon, J.-W. and S.-B. Jung, *Effect of surface finish on interfacial reactions of Cu/Sn–Ag–Cu/Cu(ENIG) sandwich solder joints.* Journal of Alloys and Compounds, 2008. **448**(1-2): p. 177-184.

6. Qin, Y., G.D. Wilcox, and C. Liu, *Electrodeposition and characterisation of Sn–Ag–Cu solder alloys for flip-chip interconnection.* Electrochimica Acta, 2010. **56**(1): p. 183-192.

7. Jang, G.-Y., J.-W. Lee, and J.-G. Duh, *The nanoindentation characteristics of Cu_6Sn_5, Cu_3Sn, and Ni_3Sn_4 intermetallic compounds in the solder bump.* Journal of Electronic Materials, 2004. **33**(10): p. 1103-1110.

8. Nai, S.M.L., J. Wei, and M. Gupta, *Interfacial intermetallic growth and shear strength of lead-free composite solder joints.* Journal of Alloys and Compounds, 2009. **473**(1–2): p. 100-106.

9. Manko, H.H., *Solders and Soldering.* 2001: McGraw-Hill.

10. Kim, K.S., S.H. Huh, and K. Suganuma, *Effects of intermetallic compounds on properties of Sn–Ag–Cu lead-free soldered joints.* Journal of Alloys and Compounds, 2003. **352**(1-2): p. 226-236.

11. Gong, J., et al., *Initial formation of CuSn intermetallic compounds between molten SnAgCu solder and Cu substrate.* Scripta Materialia, 2009. **60**(5): p. 333-335.

12. Yu, D.Q. and L. Wang, *The growth and roughness evolution of intermetallic compounds of Sn–Ag–Cu/Cu interface during soldering reaction.* Journal of Alloys and Compounds, 2008. **458**(1-2): p. 542-547.

13. Yoon, J.-W., et al., *Wettability and interfacial reactions of Sn–Ag–Cu/Cu and Sn–Ag–Ni/Cu solder joints.* Journal of Alloys and Compounds, 2009. **486**(1–2): p. 142-147.

14. Mookam, N. and K. Kanlayasiri, *Effect of soldering condition on formation of intermetallic phases developed between Sn–0.3Ag–0.7Cu low-silver lead-free solder and Cu substrate.* Journal of Alloys and Compounds, 2011. **509**(21): p. 6276-6279.

15. Tu, K.N. and K. Zeng, *Tin–lead (SnPb) solder reaction in flip chip technology.* Materials Science and Engineering: R: Reports, 2001. **34**(1): p. 1-58.

16. Laurila, T., V. Vuorinen, and J.K. Kivilahti, *Interfacial reactions between lead-free solders and common base materials.* Materials Science and Engineering: R: Reports, 2005. **49**(1-2): p. 1-60.

17. Frear, D. and P. Vianco, *Intermetallic growth and mechanical behavior of low and high melting temperature solder alloys.* Metallurgical and Materials Transactions A, 1994. **25**(7): p. 1509-1523.

18. Bennett, J.E., T.M. Paskowski, and H.E. Bair. *Solution to a solderability problem by combining metallography and thermal analysis.* in *Proceedings of tenth Northe American Thermal Analysis Society conference*. 1980. Boston, Massachusetts.

19. Hung, F.-Y., et al., *A study of the thin film on the surface of Sn–3.5Ag/Sn–3.5Ag–2.0Cu lead-free alloy.* Journal of Alloys and Compounds, 2006. **415**(1-2): p. 85-92.

20. Pietriková, A., J. Bednarčík, and J. Ďurišin, *In situ investigation of SnAgCu solder alloy microstructure.* Journal of Alloys and Compounds, 2011. **509**(5): p. 1550-1553.

21. Smallman, R.E. and R.J. Bishop, *Modern Physical Metallurgy and Materials Engineering*. 6th ed. 1999, Oxford: Butterworth-Heinemann.

22. Moon, K., et al., *Experimental and thermodynamic assessment of Sn-Ag-Cu solder alloys.* Journal of Electronic Materials, 2000. **29**(10): p. 1122-1136.

23. Massalski, T.B. and H. Okamoto, *Binary Alloy Phase Diagrams*. 2nd ed. 1990: ASM International.

24. Ulrich, R.K. and W.D. Brown, *Advanced electronic packaging*. 2nd ed. IEEE Press Series on Microelectronic System, ed. S.K. Tewksbury. 2006, United States of America: John Wiley & Sons, Inc.

25. Tu, K.N., *Cu/Sn interfacial reactions: thin-film case versus bulk case.* Materials Chemistry and Physics, 1996. **46**(2-3): p. 217-223.

26. Kim, K.S., S.H. Huh, and K. Suganuma, *Effects of cooling speed on microstructure and tensile properties of Sn–Ag–Cu alloys.* Materials Science and Engineering: A, 2002. **333**(1-2): p. 106-114.

27. Inaba, M., et al., *Effects of Fe, Ni and Sn on reaction diffussion at solder/Cu-base-alloys interface.* Journal of the Japan Institute of Metals, 1984. **48**: p. 863-870.

28. Kay, P.J. and C.A. Mackay, *The Growth of Intermetallic Compounds on Common Basis Materials Coated with Tin and Tin-lead Alloy.* Transactions of the Institute of Metal Finishing, 1976. **54**: p. 68-74.

29. Wang, F.-J., Z.-S. Yu, and K. Qi, *Intermetallic compound formation at Sn–3.0Ag–0.5Cu–1.0Zn lead-free solder alloy/Cu interface during as-soldered and as-aged conditions.* Journal of Alloys and Compounds, 2007. **438**(1–2): p. 110-115.

30. Schaefer, M., R. Fournelle, and J. Liang, *Theory for intermetallic phase growth between cu and liquid Sn-Pb solder based on grain boundary diffusion control.* Journal of Electronic Materials, 1998. **27**(11): p. 1167-1176.

31. Wronkowska, A.A., et al., *Structural analysis of In/Ag, In/Cu and In/Pd thin films on tungsten by ellipsometric, XRD and AES methods.* Applied Surface Science, 2008. **254**(14): p. 4401-4407.

32. Gao, F., T. Takemoto, and H. Nishikawa, *Effects of Co and Ni addition on reactive diffusion between Sn–3.5Ag solder and Cu during soldering and annealing.* Materials Science and Engineering: A, 2006. **420**(1–2): p. 39-46.

33. So, A.C.K. and Y.C. Chan, *Reliability studies of surface mount solder joints - effect of Cu-Sn intermetallic compounds.* Components, Packaging, and Manufacturing Technology, Part B: Advanced Packaging, IEEE Transactions on, 1996. **19**(3): p. 661-668.

34. Peng, W., E. Monlevade, and M.E. Marques, *Effect of thermal aging on the interfacial structure of SnAgCu solder joints on Cu.* Microelectronics Reliability, 2007. **47**(12): p. 2161-2168.

35. Abtew, M. and G. Selvaduray, *Lead-free Solders in Microelectronics.* Materials Science and Engineering: R: Reports, 2000. **27**(5-6): p. 95-141.

36. Zhang, S., Y. Zhang, and H. Wang, *Effect of oxide thickness of solder powders on the coalescence of SnAgCu lead-free solder pastes.* Journal of Alloys and Compounds, 2009. **487**(1-2): p. 682-686.

4. Conclusions

Various investigations on the development of lead-free solders have been widely studied to ensure that this new generation of solders are reliable while being environment-friendly. Amongst the most attractive lead-free solder compositions, tin-zinc (Sn-9Zn) and tin-silver-copper (Sn-Ag-Cu; SAC) solders shows high potential to be used in electronic industries. However, overall properties of these solders are needed to be carefully studied to fully optimized the promising potentials.

The Sn-9Zn solder is known to owns low melting temperature. However, due to the poor corrosion resistance, this solder needed further attention of improvements. The preferential dissolutions of Zn from Sn-9Zn solder in 6 M KOH is the main concern for this alloy. Besides that, small cracks that inhibited the passivation oxide of this binary solder produce poor resistant from further corrosion. Thus, the penetration of corrosive ions through the cracks formation weakened its joint strength.

On the other hand, SAC solders are widely renowned for its excellent mechanical properties and considerably good corrosion resistant. In 6 M KOH, the corrosion resistance of the as reflowed SAC/Cu solder was enhanced by the formation of intermetallic compound (IMC) at the interface of the as deposited SAC/Cu solder. Besides that, the existence of Cu_3Sn on the interface of SAC/Cu was shown to have better corrosion resistance compared with the presence of Cu_6Sn_5. Moreover, the formation of tin oxides of SnO and SnO_2 produced from the dissolution of Sn produces pseudopassivation layer that further improved the overall corrosion properties of SAC/Cu solder. Additionally, it was also confirmed that, the increased in reflow

temperature also increases the amount of Cu_3Sn at the expense of Cu_6Sn_5 for the bulk SAC solder. Thus, this contributed to the excellent corrosion resistance of SAC solder in 6 M KOH.